AFOSR-TR- 91 0788

TRANSFORM METHODS FOR PRECISION NONLINEAR WAVE MODELS OF FLEXIBLE SPACE STRUCTURES

FINAL REPORT

AFOSR CONTRACT: 49620-89-C-0082

PRA
Photon Research Associates, Inc.
Cambridge Division
1033 Massachusetts Avenue
Cambridge, MA 02138

(2)

TRANSFORM METHODS FOR PRECISION NONLINEAR WAVE MODELS OF FLEXIBLE SPACE STRUCTURES

FINAL REPORT

AFOSR CONTRACT: 49620-89-C-0082

Victor D. Lupi, Hon M. Chun, and James D. Turner

Photon Research Associates, Inc.
1033 Massachusetts Avenue
Cambridge, MA 02138

August 1991

SECURITY CLASSIFICATION OF THIS PAGE

REPORT DOCUMENTATION PAGE

Form Approved OMB No. 0704-0188

1a. REPORT SECURITY CLASSIFICATION: UNCLASSIFIED	1b. RESTRICTIVE MARKINGS
2a. SECURITY CLASSIFICATION AUTHORITY	3. DISTRIBUTION/AVAILABILITY OF REPORT: Approved for public release; distribution unlimited
2b. DECLASSIFICATION/DOWNGRADING SCHEDULE	
4. PERFORMING ORGANIZATION REPORT NUMBER(S)	5. MONITORING ORGANIZATION REPORT NUMBER(S)
6a. NAME OF PERFORMING ORGANIZATION: Photon Research Assoc., Inc. / 6b. OFFICE SYMBOL (If applicable): CR	7a. NAME OF MONITORING ORGANIZATION: Air Force Office of Scientific Research
6c. ADDRESS (City, State, and ZIP Code): 1033 Massachusetts Avenue, Cambridge, MA 02138	7b. ADDRESS (City, State, and ZIP Code): Bldg 410, Bolling AFB, Washington, DC 20332
8a. NAME OF FUNDING/SPONSORING ORGANIZATION: AFOSR / 8b. OFFICE SYMBOL (If applicable): NA	9. PROCUREMENT INSTRUMENT IDENTIFICATION NUMBER: F49620-89-C-0082
8c. ADDRESS (City, State, and ZIP Code): Bldg 410, Bolling AFB, Washington, DC 20332	10. SOURCE OF FUNDING NUMBERS: PROGRAM ELEMENT NO. 61102F / PROJECT NO. 2302 / TASK NO. B1 / WORK UNIT ACCESSION NO.

11. TITLE (Include Security Classification)
Transform Methods for Precision Nonlinear Wave Models of Flexible Space Structures (U)

12. PERSONAL AUTHOR(S)
Victor Lupi, Hon Chun, James Turner

13a. TYPE OF REPORT	13b. TIME COVERED	14. DATE OF REPORT (Year, Month, Day)	15. PAGE COUNT
Final Technical Report	FROM 6/90 TO 6/91	1990, 8, 20	167

16. SUPPLEMENTARY NOTATION

17. COSATI CODES			18. SUBJECT TERMS (Continue on reverse if necessary and identify by block number)
FIELD	GROUP	SUB-GROUP	

19. ABSTRACT (Continue on reverse if necessary and identify by block number)

This final report describes the results of the second year of work on a two year project. Several extensions to the Transform Element Method (TEM) described in the first year are presented, including: high frequency Mindlin-Herrmann rods and Timoshenko beams and two-dimensional elements for membranes, plates, and plane stress. Extensions are presented for solving open-loop control problems that use three-dimensional space frame TEM models, where the residual structural energy can be penalized via a rigorous integral constraint throughout the structural domain. Closed-loop extensions are presented for solving distributed control problems for one-dimensional elements (e.g., Bernoulli-Euler beams). New solution algorithms are discussed for solving the nonlinear functional matrix Riccati integro-partial differential equations that define the feedback control kernels. A formulation is presented for developing frequency-dependent multibody dynamics in terms of an order(N) recursive solution algorithm.

20. DISTRIBUTION/AVAILABILITY OF ABSTRACT: ☐ UNCLASSIFIED/UNLIMITED ☐ SAME AS RPT. ☒ DTIC USERS	21. ABSTRACT SECURITY CLASSIFICATION (U)
22a. NAME OF RESPONSIBLE INDIVIDUAL: Dr. Spencer T. Wu	22b. TELEPHONE (Include Area Code): (202) 767-6960 / 22c. OFFICE SYMBOL: NA

DD Form 1473, JUN 86 — Previous editions are obsolete. — SECURITY CLASSIFICATION OF THIS PAGE

(U)

ABSTRACT

This report summarizes recent efforts to utilize mathematically exact structural models for structural analysis and control design. The models developed remain exact at all frequencies, unlike modal models derived from finite element analysis. As a result, control designs based on these exact models are less susceptible to spillover and instability.

Two types of exact modelling techniques are presented. In the first (called Transform Element Modelling), the Laplace transform is utilized to express the equation describing the dynamics behavior of the structural element in the frequency-domain. This leads to mathematically exact dynamic stiffness matrices, which can be assembled to form an exact global structural model. The TEM methodology is shown to be superior to traditional finite element techniques in terms of both numerical accuracy and computation speed. Based on this approach, an open-loop optimal control algorithm for small angle slews of flexible structures is developed. The algorithm is applied to two structural models (a simple mass/appendage structure and the SCOLE structural model) and succeeds in minimizing the post-maneuver residual kinetic energy. The issue of closed-loop control using the TEM methodology is also addressed.

The second modelling technique presented (called the direct approach) deals with the original partial differential equations describing the dynamics of the structural elements, expressed in the time-domain. An extended state-space representation is used to develop a distributed control theory for simple, one-dimensional systems. The control theory is applied to a Bernoulli-Eular beam, and the feedback gains are determined for various control and deformation penalties. The results are validated with both discrete structural models and analytical results for a beam of infinite length.

A hybrid control design, which takes advantage of the favorable properties of both modelling methods is proposed. In this design, the distributed controller exerts low-authority control to achieve active damping augmentation. The TEM-based controller exerts high-authority control, and is designed to meet the performance specifications for the structural system.

ACKNOWLEDGEMENTS

The authors wish to thank Dr. D.J. Wilcox for his advice on implementation of the inverse Laplace transform algorithm. Some of the calculations required for this research were performed on the MIT CRAY 2 supercomputer. This work has been sponsored by the AFOSR, under contract 49620-89-C-0082.

TABLE OF CONTENTS

LIST OF FIGURES

LIST OF TABLES

NOMENCLATURE

ROMAN SYMBOLS

a	radius of rod of circular cross section
a	vector of arbitrary coefficients for TEM interpolation functions
A	cross section area for general beam element
B_x	matrix linear spatial differential operator for control input
c	stress wave propagation velocity
c	vector of undetermined coefficients for open-loop control inputs
C	closed contour in the complex plane
C	connectivity matrix for TEM assembly
D_{xy}	dual operator to L_{xy}
D	finite difference matrix operator for second derivative
D_x	matrix linear spatial differential operator for disturbance input
E	modulus of elasticity
E	internal energy of deformation of structural element
f	generalized distributed forcing input
f	vector of basis functions for open-loop control inputs
$\tilde{f}$	net forcing due to initial conditions and distributed forces
f_1,f_2	normalized distributed feedback gain kernels for infinite beam
F	internal force resultant for axial rod
F	matrix of basis functions for open-loop control inputs
g	generic function of time
G	shear modulus
G	dynamic flexibility matrix for TEM analysis
G_c	compensator transfer function matrix
I	moment of inertia of cross section for general beam element
j	imaginary unit
J	cost functional
J_a	augmented cost functional
k	generalized stiffness or mass parameter
k_1,k_2	distributed feedback gain kernels for finite beam
K	dynamic stiffness matrix for TEM analysis
L	structural element length

L_x	scalar linear differential operator
$\tilde{L}_x$	scalar linear differential operator
L_{xy}	linear spatial differential operator in two dimensions
$\mathbf{L}_x$	matrix linear spatial differential operator
L^{-1}	inverse Laplace transform operator
m	mass per unit length for general beam element
m	distributed curvature input
M	internal moment resultant for beam element
n	distributed disturbance input vector
N	number of frequency samples used in inverse Laplace transform algorithm
N	mesh discretization grid size for distributed control solution
p	distributed control costate vector
P_x	distributed control Riccati operator matrix
q	generalized TEM boundary force vector
q_d	net effect of distributed forcing and initial conditions on q
q_c	control boundary forces
Q	distributed control state penalty weighting matrix
r	distributed control effort penalty weighting
R	weighting matrix for open-loop optimal control
s	complex frequency
S	internal shear resultant for beam element
S	distributed control Riccati function matrix
t	time (independant variable)
t_f	open-loop optimal maneuver terminal time
T	simulation time for inverse Laplace transform algorithm
u_x,u_y	in-plane deformations for two-dimensional element
u	structural state vector in TEM formulation
u	distributed control input vector
u_p	effect of distributed forcing and initial conditions on u
v	generalized displacement
v_H	homogeneous solution vector in TEM formulation
v_p	Green's function in TEM formulation
w	generalized boundary displacement vector
w	disturbance input vector
W	primary N'th root of unity
W	quadratic cost matrix for optimal open-loop maneuvers

x	spatial coordinate (independant variable)
x	distributed state vector
y	dummy variable of integration
y	vector of outputs of interest
Y	response matrix to basis function inputs for optimal open-loop control problem
z	dummy variable of integration
z	performance measure
Z	primary 2N'th root of unity

GREEK SYMBOLS

α	offset of Bromwich contour from imaginary axis
β	normalized inverse mass density
δ	Dirac delta function
ε	components of strain tensor
Φ	dynamic stress function for TEM formulation
Γ	interpolation matrix for TEM formulation
η	normalized bending stiffness
Φ	matrix relating u to a in TEM formulation
λ	Lame constant
λ	Lagrange multiplier vector
ν	Poisson's ratio
θ	bending rotation of cross section of beam element
Θ	geometric matrix for TEM formulation
ρ	mass density
σ	components of normal stress
τ	shear stress
ω	radian frequency
$\Delta\omega$	frequency interval
Ξ	internal energy matrix in TEM formulation
Ψ	matrix relating w to a in TEM formulation
$\bar{\Psi}$	matrix relating q to a in TEM formulation
ζ	spatial frequency variable
∇^2	Laplacian operator

ANNOTATIONS

$\dot{(\,)}$	differentiation with respect to time
$\bar{(\,)}$	temporal Laplace transform
$\hat{(\,)}$	spatial Fourier transform
$(\,)^T$	transpose
$(\,)^*$	complex conjugate
$(\,)^*$	adjoint operator
$\delta(\,)$	first variation
$(\,)_i$	index for a vector quantity
$(\,)_{ij}$	index for a matrix quantity
$(\,)_u$	control component
$(\,)_n$	disturbance component
$(\,)_U$	potential energy component
$(\,)_T$	kinetic energy component
$(\,)_d$	dimensional form of variable
$(\,)_0$	initial condition
$(\,)^i$	element indentifier
${}^I(\,)$	inertial reference frame
$(\,)^{(i)}$	boundary point identifier
$(\,)^G$	global coordinates

1 INTRODUCTION

This report summarizes the research performed under AFOSR contract 49620-89-C-0082, "Transform Methods for Precision Nonlinear Wave Models of Flexible Space Structures." The work has focused, primarily, on exact modelling and control of flexible structures. Two modelling approaches have been developed, each of which has motivated a structural control methodology in a natural way. The Transform Element Modelling (TEM) approach uses the Laplace transform to obtain exact, frequency-domain structural element models. An assembly procedure is then used to create an exact global model. Several open-loop control algorithms have been developed based on the TEM models generated. The direct PDE approach deals specifically with the underlying time-domain partial differential equation describing the structural behavior. This methodology leads to a distributed control theory, which is analogous to traditional state-space control. These two control algorithms are alternatives to conventional structural control approaches. They are designed to alleviate the problems associated with control-structure interaction, as described in the next section.

1.1 The Control-Structure Interaction (CSI) Problem

The requirements for many military and civilian structures applications both in space and on earth call for the use of large, high performance, lightweight structures. In most cases, the structural weight must be kept as small as possible to avoid excessive transport costs. However, the flexibility associated with large, lightweight structures increases the likelihood of troublesome structural behavior. The vibrational modes generally begin at low frequency, and are excited by disturbances. Potential sources of these disturbances include rotating machinery for terrestrial applications and attitude control, antenna retargeting and payload shifting for space applications. Often, the structure, disturbance and control bandwidths are close or overlapping, causing undesirable vibration to propagate through the structure. This situation is described in Fig. 1-1. In systems with stringent pointing requirements (such as space-based telescopes, interferometers, lasers, etc.), this can severly degrade performance. Similarly, for systems requiring pilot isolation

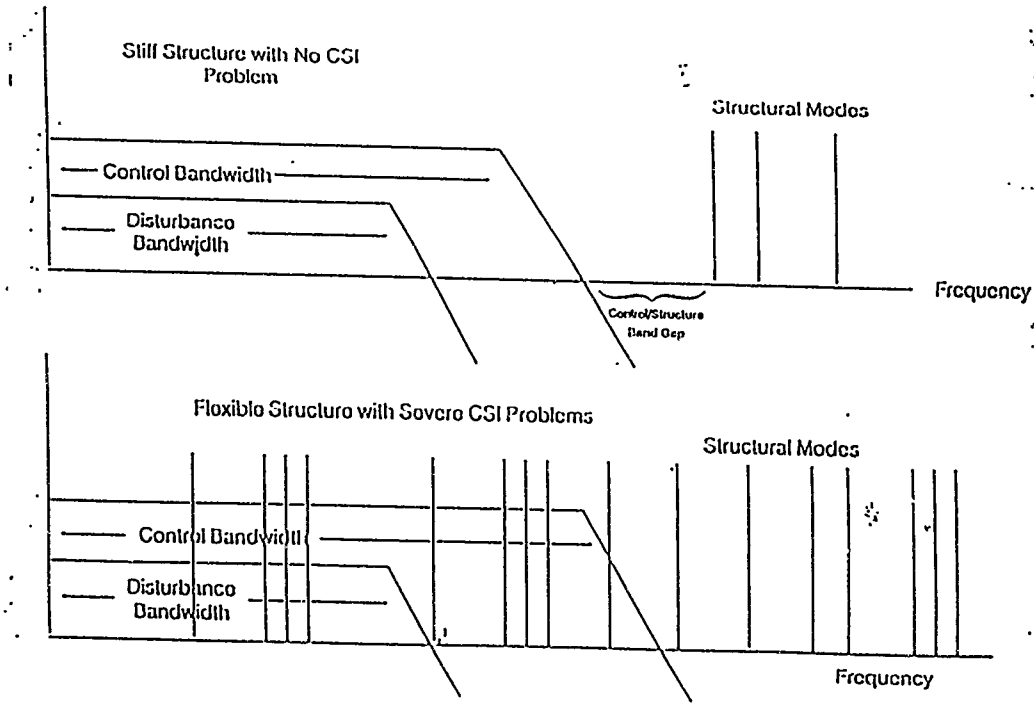

Fig. 1-1: Description of the CSI problem. Interaction occurs when the structural modes lie within the bandwidth of the control system and disturbances.

or flutter control, performance degradation occurs if unwanted vibration is present. When these problems arise, some sort of vibration suppression, either active or passive, is required.

Passive damping techniques alone are usually insufficient to meet performance requirements. In order to achieve significant modal damping (on the order of 50%, say), an unacceptably large mass of damping material must be added to the structure. As a general rule, passive damping can only provide about 5% to 10% damping for a 5% increase in structural mass (See, for example, Plunkett (1970)). Consequently, these techniques provide low levels of vibration suppression and are well suited for addressing steady-state disturbances arising from on-board or environmental sources. Active control techniques are required for suppressing transient behavior and large, disturbance-induced structural responses.

Large, lightweight structures have three basic characteristics which make active control design difficult. First, the structures are difficult to model precisely. The structural dynamics mathematical models obtained from finite element techniques only approximately analyze high frequency behavior. Typically, only the first few modes are known to any degree of accuracy. As a result, the active control design must be extremely robust. Unfortunately, robustness often leads to very conservative designs which sacrifice performance for stability. Second, these structures are modally dense and lightly damped. This makes the closed-loop system extremely sensitive to parameter variations, and often leads to instability. Third, the underlying dynamics are of infinite order. As a result, traditional full-order linear quadratic regulator (LQR) and linear quadratic gaussian (LQG) control designs are not directly applicable to these types of systems.

These structural characteristics lead to a phenomenon described by Balas (1978) as "spillover," and can be explained as follows. In a typical control design procedure, the approximate finite element model is first truncated to include only those modes which are known to a good degree of accuracy. This becomes the evaluation model, against which various control designs are judged. Typically, the evaluation model is of too high an order to achieve an [illegible] order controller. As a result, a reduced order controller is designed, either directly from the evaluation model (Bernstein, 1986), or based on a further truncation of the evaluation model

(Kosut (1970), Yousuff (1984)). In either case, the action of the controller excites all the modes of the evaluation model to some degree. This is referred to as control spillover. Likewise, the sensors associated with the controller also respond to the modes truncated from the evaluation model, leading to observation spillover. Additional control and observation spillover occurs when the reduced order controller is applied to the actual infinite order structure.

1.2 The Need for Better Models and Control Designs

Currently, the methodology generally employed in most structural control problems is the High-Authority Controller/Low-Authority Controller (HAC/LAC) approach, described in Gupta (1981). This is a heirarchical control architecture that addresses many of the issues presented in the previous section. The design procedure usually involves three distinct procedures. In addition to developing the HAC and LAC active control systems, passive damping augmentation is usually designed. In many cases, prefiltering of command inputs is also required to minimize excitation of structural modes. The modal-based command shaping method developed by Singer (1990) is an example of the prefiltering concept.

A passive damping treatment is almost always required in the control design of infinite order, lightly damped systems. The closed-loop system is guaranteed to be unstable for undamped infinite order systems and any physically realizable controller (i.e., any controller with some amount of phase lag). This phenomenon is explained in Fig. 1-2. Furthermore, even slightly damped systems can be made unstable by increasing the gain of the controller sufficiently. As a result, passive damping is usually required for all high performance structures. For some applications, adequate passive damping may be inherently present in the structure, due to material friction, viscoelasticity, and/or joint hysteresis. High performance applications will likely require careful tailoring of the passive design in order to meet performance goals. By shifting the open-loop poles of the system into the left half-plane, passive damping has the added benefit of desensitizing the controller to modelling errors, thereby increasing robustness. Though attractive

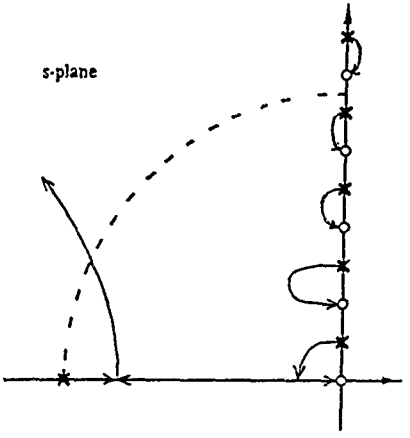

Fig. 1-2: Collocated rate feedback for an undamped system. The dynamics of the controller, represented here by a pole on the real axis, alter the angles of departure of the higher frequency loci. Instability first occurs in the locus with approximate radius corresponding to the radius of the first order pole of the controller.

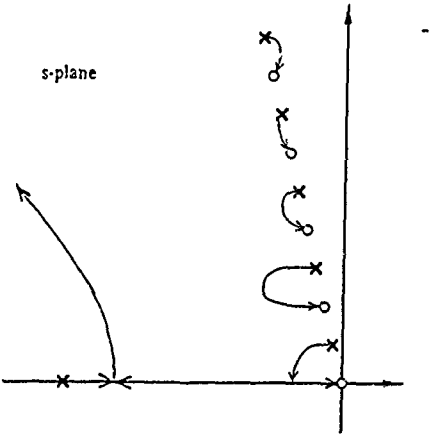

Fig. 1-3: Collocated rate feedback for a damped system. The passive damping, in this case, is sufficient to prevent instability, and the damping in the lower modes can be increased significantly. In an actual LAC design, many actuators and sensors are used, which enables greater damping of higher modes.

for practical and theoretical reasons, mass penalties place an upper limit to the amount of passive damping that can be implemented.

The LAC (also called active damping augmentation) is usually an *ad hoc* design, as the primary objective is to achieve robust control with a large number of simple controllers (Aubrun (1980)). Typically, collocated rate feedback is employed. The effect of this form of feedback on the modes of the structural system is shown in Fig. 1-3. The main objective of active damping augmentation is, as the name implies, to increase modal damping significantly, so that the HAC does not destabilize the system in the presence of modelling errors.

The primary design objectives are accomplished via the HAC. It is usually a dynamic compensator of high order, and utilizes information from sensors located throughout the structure. Multiple actuation is also commonplace. These actuators and sensors need not be distinct from those used in active damping augmentation. As the name implies, the HAC exerts high gain control on the structure, moving the closed-loop pole locations considerably.

The current state of the art in HAC/LAC design suffers from several serious deficiencies. The first and most important is the fidelity of the underlying structural model. The traditional finite element modelling approach is incapable of recovering the high frequency dynamics of the structure, unless an extremely fine discretization is utilized, which is usually computationally unacceptable. This limits the accuracy of the evaluation model and its utility in compensator design. Furthermore, modelling of damping mechanisms, such as viscoelasticity, is difficult to formulate in a finite element environment. The damping is usually assumed to be model, and the actual values for the damping ratios are determined quite arbitrarily.

Clearly, then, a more accurate structural modelling approach would be extremely beneficial. It particular, it is desirable to develop a modelling methodology that avoids modal truncation and spatial discretization altogether. This is the basis for Partial Differential Equation (PDE) modelling approaches. The equations describing the structure are kept intact, and remain mathematically exact at all frequencies. The issue of modelling error is then reduced to knowledge of the physical

parameters for the system and the actual choice of the mathematical representations of the structural elements.

Another limitation of the HAC/LAC methodology is in the active damping augmentation, which is, for the most part, *ad hoc*. Some systematic approaches have been developed, but have limited applicability. For example, MacMartin (1990) describes a method for minimizing the power imparted to the structure at an interface using H∞ techniques. However, only the near field effects are considered. Reflections of the disturbances at other boundaries of the structure are not modelled. This represents a worst case design, with the assumption that nothing is known about the structure except in the immediate vicinity of the controller. This approach is usually too conservative for practical applications. Miller (1991) uses a wave propagation approach to design controllers that absorb power at structural interfaces. Again, the lack of a far field model results in a conservative design. Furthermore, neither of these designs is applicable to applying control in the interior of a structural element. A more systematic LAC design methodology with less conservatism is clearly needed.

Current methods of designing the high-authority controller are typically overconservative, as the closed-loop systems designed from the truncated model tend to be sensitive to parameter uncertainty. Typically, only the first few modes are used in the design. The remaining modes are considered unreliable, and contribute to modelling error. A less conservative design (and therefore one with better nominal performance) would arise from an exact structural model, as the modelling errors are smaller and are more easily characterized.

The problems discussed above suggest that new modelling approaches may lead to new control design methodologies in a natural way. By using PDE models, mathematically exact representations of structural systems are available. Control designs based on these models will account for all modes of the structure, so that the design need not be overly conservative. The achievement of this design methodology would significantly enhance the overall performance of large, flexible structures in the presence of disturbances.

1.3 Summary of First Year Research

The research conducted in the first year of this program focused on developing exact structure models that preserve the wave-like characteristics of structural disturbance propagation. The primary emphasis was placed on developing the TEM methodology and validating it with several structural evaluation models. Of particular concern in the first year were numerical issues related to the accuracy of the model. For low and high frequencies, numerical overflow and roundoff errors occured when computing structural responses. These issues were resolved by using low- and high-frequency asymptotic approximations where required. Also developed was an open-loop, optimal control algorithm for linear and small angle slews of flexible structures. The details of these developments can be found in Lupi (1990), but are also presented in Chapters 2 and 4 for completeness. The application of the TEM approach to two-dimensional structural elements was also addressed. In Lupi (1991b), a plane stress element was developed that utilized a frequency-dependant version of the Airy stress function. The results of this study are also presented in Section 2.4.2.

1.4 Overview of Report

This report summarizes developments in structural modelling and control design from the past year as well as reviewing the previous year s research. Chapter 2 introduces the TEM methodology and its applications to structural analysis problems. The extension of the TEM approach to multibody systems is addressed in Chapter 3. Open-loop control designs, based on TEM models, are presented in Chapter 4. The extension to closed-loop control is also discussed. Chapter 5 develops the direct PDE modelling approach for one- and two-dimensional structural elements. The direct simulation of a simple one-dimensional system is also presented. The direct PDE modelling approach leads naturally to a distributed control theory, which is developed in Chapter 6. The possibility of a hybrid modelling approach for HAC/LAC control designs is discussed in Chapter 7. Finally, conclusions and recommendations are presented in Chapter 8.

2 THE TEM MODELLING APPROACH

In this chapter, we introduce the Transform Element Modelling (TEM) method of structural analysis. This approach begins with the partial differential equations describing the dynamics of the individual elements that describe the structure. The Laplace transform is then utilized to express these equations in the frequency-domain. Exact, frequency-dependant stiffness matrices, which relate a set of generalized forces to a set of generalized displacements at the element boundaries, are then derived. These stiffness matrices are then assembled to form a global model, in a manner similar to the traditional finite element assembly procedure. The advantages of this approach are described in Section 2.1. The procedure for converting frequency-domain data back into the time-domain is described in Section 2.2. The general theory for one-dimensional elements, and some simple representative examples, are presented in Section 2.3, while Section 2.4 applies the TEM methodology to two-dimensional structural element models. The assembly procedure is described in Section 2.5, and several applications of the TEM approach are presented in Section 2.6.

2.1 Advantages of the TEM Method

The TEM approach has several important advantages over the traditional Finite Element Method (FEM), as measured in terms of numerical accuracy and computational efficiency. The dynamics of the one-dimensional elements that comprise the structure to be analyzed are represented exactly in the TEM approach. This is made possible by the Laplace transform operation, which converts the time-domain partial differential equation of a structural element into a frequency-dependant ordinary differential equation. As a result, analytical general solutions to these equations are available for most common element models, such as Bernoulli-Euler and Timoshenko beams, and axial and torsional rods. More complicated elements can be handled by special numerical modelling approaches. This is in marked contrast to FEM modelling, where each element is divided into smaller subsections, each of which is constrained to deform with a finite number of degrees of freedom. The interpolation functions associated with the deformational

degrees of freedom satisfy the underlying differential equation exactly for the static case, but only approximate the exact solution the dynamic case. Consequently, for dynamics problems, the FEM analysis can only yield approximate results. Conversely, the TEM approach, which utilizes frequency-dependent (generally transcendental) interpolation functions, is mathematically exact at all frequencies. Furthermore, since only one mathematical element is required for each physical structural element, the TEM approach is far superior to the FEM methodology in terms of computational speed.

For two-dimensional structural elements, general exact solutions are not available, but the TEM methodology makes it possible to approximate the solutions in terms of finite series of displacement functions. Each of these functions satisfies the underlying differential equation in the interior of the element exactly, and approximations are made only at the boundaries. A comparison between the TEM and FEM methods in terms of speed and accuracy for two-dimensional elements has not yet been attempted.

Another important advantage of the TEM approach is its ability to incorporate general linear viscoelastic damping models in a straightforward manner. Using the correspondance principle, as described by Hughes (1989), the physical parameter of interest is simply replaced with a frequency-dependent counterpart. For example, the Voigt damping mechanism is easily expressed by

$$E(s) = \left[1 + \breve{\sigma}_v \frac{s}{\omega_v}\right] E_0 \tag{2.1}$$

where E is the modulus of elasticity of the material, E_0 is its static value, s is the (generally complex) frequency, ω_v is a characteristic frequency, and $\breve{\sigma}_v$ is an empirically determined nondimensional parameter. A more general damping model, suggested by Hughes, is

$$E(s) = \left[1 + \sum_{i=1}^{N_\sigma} \sigma_i \frac{s^2+2\zeta_i\omega_i s}{s^2+2\zeta_i\omega_i s+\omega_i^2}\right] E_0 \tag{2.2}$$

where, for each value of i, σ_i is a characteristic scaling factor, ω_i is a characteristic frequency, and ζ_i is a characteristic damping ratio, all of which are empirically determined. However, the advantage of the TEM approach lies in its ability to model damping mechanisms of infinite order, such as the fractional derivative models discussed by Bagley (1983). Such models require the use of fractional calculus techniques when employed in the time domian, but are easily cast in the frequency-domain as fractional powers of the complex frequency. For example, the square root damping model is written as

$$E(s) = \left[1 + \bar{\sigma}_s \sqrt{\frac{s}{\omega_s}}\right] E_0 \tag{2.3}$$

where ω_s is a characteristic frequency and $\bar{\sigma}_s$ is empirically determined. Thus, since all linear viscoelastic damping models have frequency-domain representations, any model can be used in the TEM formulation.

Yet another advantage of the TEM approach is the ability to take derivatives of time-domain functions. All that is required is multiplication of the function by the complex frequency variable. Similarly, additional multiplications by s yield higher order derivatives. Thus, given a set of frequency-domain data representing a time-domain response, it is a simple matter of multiplying the data by the complex frequency before invoking the inverse Laplace transform to obtain the derivative of the response.

2.2 Inverse Laplace transform algorithm

In any frequency-domain modelling approach, it is of paramount importance to have the ability to convert data back into the time-domain in a computationally efficient manner. This is the basis for many inverse Laplace transform algorithms, such as the method of expansion by Laguerre functions as described by Weeks (1966) and Wing (1967). However, the most straightforward, stable and accurate method for general functions appears to be the numerical approach of Wilcox (1978). It is this method that has been used exclusively in this research, and it

therefore deserves mention here. A detailed comparison of several other approaches may be found in Davies (1979).

The Laplace transform pair is expressed as

$$\bar{g}(s) = \int_0^\infty g(t)\, e^{st}\, dt$$
$$g(t) = \frac{1}{2\pi j} \int_C \bar{g}(s)\, e^{st}\, ds \qquad (2.4a,b)$$

where C is a closed contour which encloses all the singularities of $\bar{g}(s)$. If we assume that $\bar{g}(s)$ has no poles with real parts greater than α, where α is a small positive number, then the integration contour can be taken as the Bromwich contour, which is shown in Fig. 2-1. Furthermore, assuming that the semicircle part of the contour does not contribute to the integral, the inverse transform reduces to

$$g(t) = \frac{e^{\alpha t}}{2\pi} \int_{-\infty}^{\infty} \bar{g}(s)\, e^{j\omega t}\, d\omega\,, \quad s = \alpha + j\omega \qquad (2.5)$$

Since the path of integration is displaced to the right of the imaginary axis, marginally stable and slightly unstable functions can be inverted. Because g(t) is assumed to be real-valued, it follows from Equation (2.4a) that $\bar{g}(s^*) = \bar{g}(s)^*$. As a result, Equation (2.5) reduces to

$$g(t) = e^{\alpha t}\, \mathrm{Re} \left\{ \frac{1}{\pi} \int_0^\infty \bar{g}(s)\, e^{j\omega t}\, d\omega \right\} \qquad (2.6)$$

The numerical computation of g(t) involves calculating $\bar{g}(s)$ at N evenly-spaced complex frequencies along the Bromwich contour, as shown in Fig. 2-2. These values are given by

$$\omega_k = (2k+1)\Delta\omega\,, \quad k = 0, \ldots, N-1 \qquad (2.7)$$

The algorithm yields 2N values of g(t) at evenly-spaced time intervals, given by

$$t_m = \frac{2m+1}{4N} T\,, \quad m = 0, \ldots, 2N-1 \qquad (2.8)$$

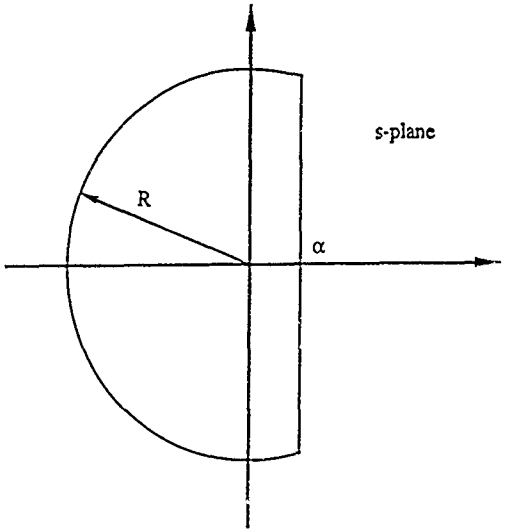

Fig. 2-1: The Bromwich contour used in calculating the inverse Laplace transform.

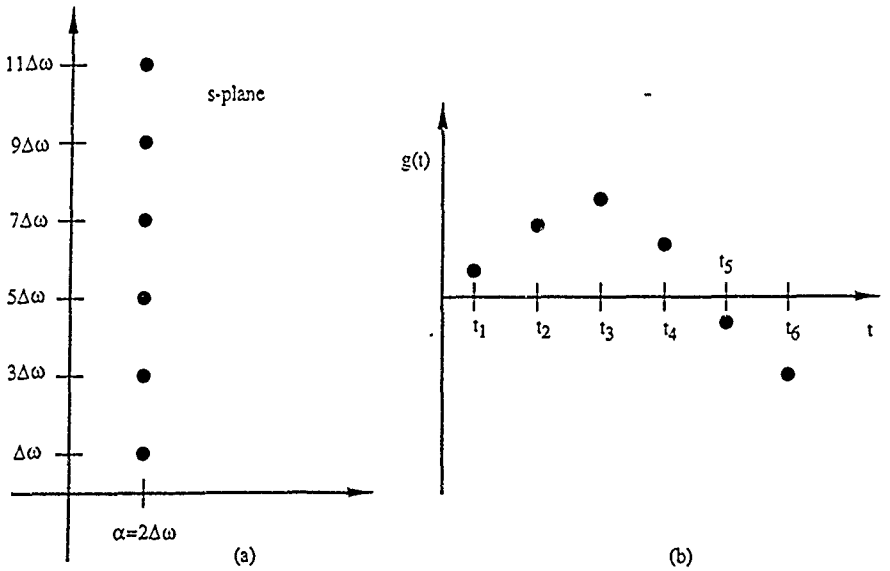

Fig. 2-2: (a) Frequency domain sampling used in the inverse Laplace transform algorithm, (b) Resulting time-domain samples.

where the time interval extends from t=0 to t=T. Wilcox (1978) shows that, for reciprocity, the following relationship must hold:

$$\Delta\omega = \frac{\pi}{T} \tag{2.9}$$

Hence, Equation (2.6) can be approximated by the midpoint rule as follows:

$$g(t_m) \cong e^{\alpha t_m} \mathrm{Re}\left\{ \frac{2}{T} \sum_{k=0}^{N-1} \bar{g}(s_k)\, e^{j\pi(k+1/2)(m+1/2)/N} \right\} \tag{2.10}$$

Factoring out constant terms from within the summation and simplifying yields

$$g(t_m) \cong e^{\alpha t_m} \mathrm{Re}\left\{ \frac{2}{T} Z^{m/2} \sum_{k=0}^{N-1} \left[\bar{g}(s_k)\, Z^{(2k+1)/4} \right] Z^{km} \right\} \tag{2.11}$$

where

$$Z = e^{j\pi/N} \tag{2.12}$$

If we now define $\bar{g}_k$ and g_m by

$$\bar{g}_k = \bar{g}(s_k)\, Z^{(2k+1)/4}, \qquad g(t_m) = e^{\alpha t_m} \mathrm{Re}\left\{ \frac{2}{T} Z^{m/2}\, \bar{g}_m \right\} \tag{2.13a,b}$$

Then Eq. (2.11) becomes

$$g_m = \sum_{k=0}^{N-1} \bar{g}_k\, Z^{km} \tag{2.14}$$

For computational efficiency, it is useful to write Eq. (2.14) in a form amenable to fast Fourier transform techniques. This is accomplished by separating the time-domain samples into even and odd sets. Thus,

$$\left.\begin{aligned} \tilde{g}_n &= g_{2n} \\ \tilde{\bar{g}}_n &= g_{2n+1} \end{aligned}\right\} \qquad n=0, \ldots, N-1 \tag{2.15}$$

and the inverse transform is applied twice, yielding

$$\tilde{g}_n = \sum_{k=0}^{N-1} \tilde{g}_k W^{kn}, \qquad \tilde{\tilde{g}}_n = \sum_{k=0}^{N-1} \tilde{g}'_k W^{kn} \tag{2.16a,b}$$

where

$$\tilde{g}'_k = \tilde{g}_k Z^k, \qquad W = Z^2 = e^{2\pi j/N} \tag{2.17a,b}$$

Thus, given a series of samples, $\tilde{g}(s_k)$, in the frequency-domain, the algorithm is as follows: Use Eq. 2.13a to obtain $\tilde{g}_k$ and Eq. 2.17a to obtain $\tilde{g}'_k$. Next, apply the fast Fourier transform, as described by Cooley (1970), to obtain $\tilde{g}_n$ and $\tilde{\tilde{g}}_n$. Upon reordering the data, which yields g_m, use Eq. 2.13b to obtain $g(t_m)$. Wilcox (1978) shows that, as a general rule of thumb, it is best to take $\alpha=2\pi/T$. Using this rule, the author has determined the algorithm to be accurate to 0.1% for the first 75% of the simulation for all test functions, with some deterioration occuring after this time. This can be overcome by increasing the simulation time slightly and discarding the later data.

In cases where the time-domain response contains step discontinuities, it is useful to scale the frequency-domain data by a Gibbs' oscillation suppression factor, given by

$$f_k = \frac{\sin[(2k+1)\pi/2N]}{(2k+1)\pi/2N} \tag{2.18}$$

This has the equivalent effect in the time-domain of passing the signal through a finite-time integrator with time constant equal to the time between samples, as explained by Lanczos (1957). Consequently, this scaling does not affect the response where it is continuous in time, while it reduces Gibbs' oscillations considerably at discontinuities (at the expense of slightly increased rise time). Fig. 2-3 shows some time-domain responses generated by the inverse Laplace transform algorithm, both with and without the Gibbs suppression factor. The favorable effect of the scaling is obvious. Thus, a numerically robust inversion algorithm has been presented. This algorithm has been used extensively in this reasearch.

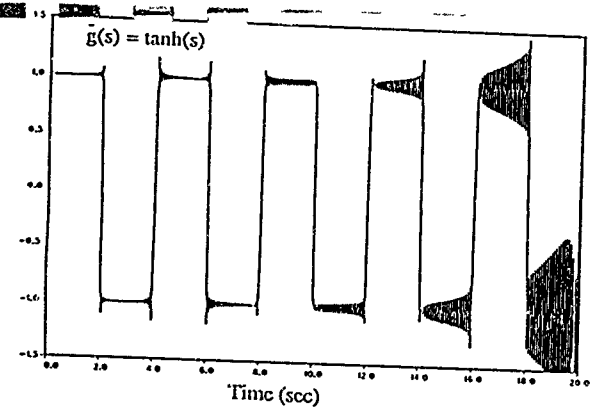

(a)

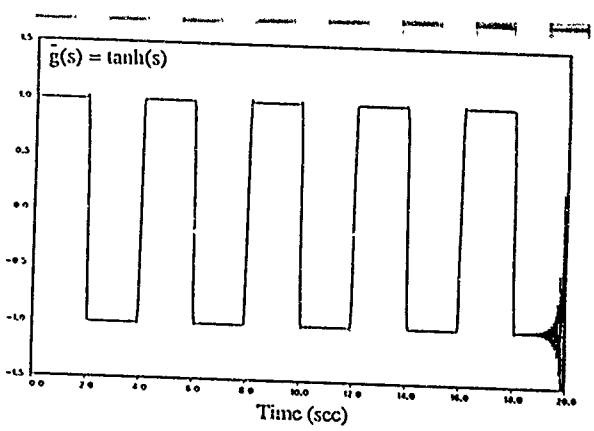

(b)

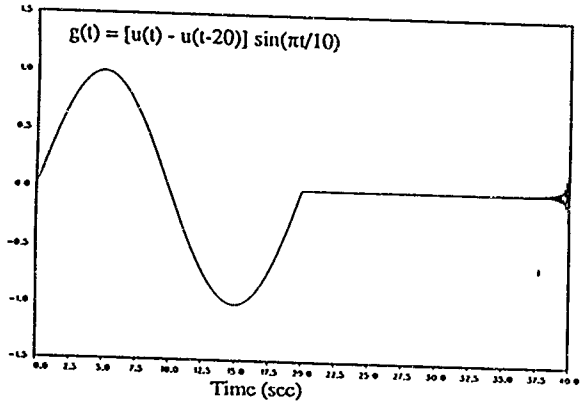

(c)

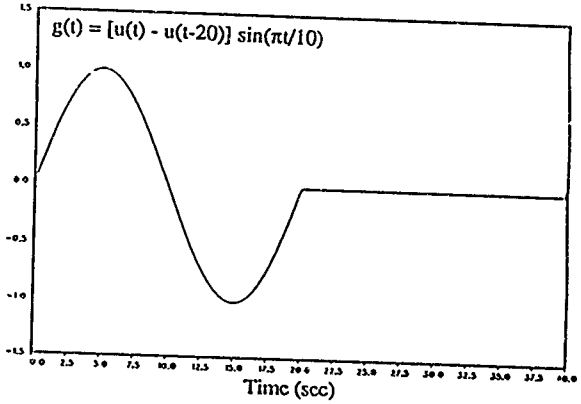

(d)

Fig. 2-3: Time domain responses generated by the inverse transform algorithm: (a) and (c): no Gibbs' suppression factor, (b) and (d): Gibbs' suppression factor used.

2.3 One-dimensional element models

We now proceed to develop the TEM formulation for one-dimensional elements. The general equation of motion for a one-dimensional structural element can be written as

$$k_U L_x[v(x,t)] + k_T \ddot{v}(x,t) = f_d(x,t), \quad x \in [0,L], \quad t \in [0,\infty) \tag{2.19}$$

where $v(x,t)$ is a generalized displacement, $f_d(x,t)$ is a generalized distributed forcing function, L_x is a linear spatial differential operator of order n, and $\dot{(\,)}$ denotes differentiation with respect to time. The constants k_U and k_T are physical parameters related to the internal potential and kinetic energy of deformation of the structural element, respectively. They can be thought of as generalized stiffness and mass parameters. The boundary conditions are as yet unspecified. The equation of motion is such that all relevant internal states (force resultants, moments, etc.) can be obtained via spatial differential operations on $v(x,t)$.

2.3.1 Stiffness matrix formulation

For a one-dimensional element, it is possible to obtain an exact, frequency-dependent stiffness matrix relating generalized boundary forces and displacements. This is possible because the Laplace transform operation converts the partial differential equation into an ordinary differential equation, whose solution can be expressed analytically (usually in the form of transcendental functions of the complex frequency). Taking the Laplace transform of Eq. (2.19) leads to

$$L_x[\bar{v}(x,s)] + \frac{k_T}{k_U} s^2 \bar{v}(x,s) = \frac{1}{k_U}\left[\bar{f}_d(x,s) + k_T \dot{v}_0(x) + k_T\, s\, v_0(x)\right] \tag{2.20}$$

where s is the (generally complex-valued) Laplace variable, $\bar{(\,)}$ denotes the transform of a function, and $v_0(x)$ and $\dot{v}_0(x)$ represent the initial conditions. From this point on, the overbar on transformed functions will be assumed, so as to simplify the notation. Also, the right hand side of Eq. (2.20) will be lumped into a single function, $\bar{f}_d(x,s)$, in the frequency-domain. This leads to

$$L_x[v(x,s)] + \frac{k_T}{k_U} s^2 v(x,s) = \tilde{f}_d(x,s) \tag{2.21}$$

We wish to express the solution to the preceeding equation in terms of generalized displacements and forces at the boundaries of the structural element. This facilitates the assembly of these structural elements into a general structural model, as will be discussed later. Thus, the general solution is expressed as

$$v(x,s) = v_H(x,s)^T a(s) + \int_0^L v_p(x,\xi,s)\, \tilde{f}_d(\xi,s)\, d\xi \tag{2.22}$$

where $v_H(x,s)$ is an n-vector of homogeneous solutions to Eq. (2.21) and a(s) is an n-vector of arbitrary constants. The Green's function, $v_p(x,\xi,s)$, corresponds to the operator $L_x + (k_T/k_U)\, s^2$ and satisfies the essential homogeneous boundary conditions at both boundaries.

We must now express the generalized boundary displacements, w(s), and generalized boundary forces, q(s), in terms of a(s). Since knowledge of v(x,s) implies knowledge of the entire state throughout the element, these boundary conditions are obtained by simply evaluating v(x,s) (and its derivatives) as given in Eq. (2.22) at the boundaries. This leads to linear relationships between the boundary states and the arbitrary constants, which can be expressed as

$$w(s) = \Psi(s)\, a(s) \tag{2.23}$$

and

$$q(s) = \tilde{\Psi}(s)\, a(s) + q_d(s) \tag{2.24}$$

where $\Psi(s)$ and $\tilde{\Psi}(s)$ are n-by-n matrices, and $q_d(s)$ is an n-vector arising from the integral term on the right hand side of Eq. (2.22). Because satisfies $v_p(x,\xi,s)$ satisfies (by construction) the homogeneous essential boundary conditions, there is no term in Eq. (2.23) corresponding to $q_d(s)$. Combining Eqs. (2.23) and (2.24) leads to the desired relationship between the boundary forces and displacements, given by

$$q(s) = K(s)\,w(s) + q_d(s) \tag{2.25}$$

where K(s) is referred to as the dynamic stiffness matrix, and is given by

$$K(s) = \tilde{\Psi}(s)\left[\Psi(s)\right]^{-1} \tag{2.26}$$

It should be noted that, at any complex frequency, Eq. (2.25) is mathematically exact. This is in contrast to traditional finite element stiffness matrices, which are usually derived from an approximate solution to the equation of motion describing the dynamics of the structural element.

2.3.2 *Interpolation*

The exact representation of the structural element is not restricted to the boundary forces and displacements. In addition, the internal states of the element at an arbitrary location can be computed exactly. This is accomplished by first expressing the n-dimensional internal state vector, u(x,s), in terms of v(x,s):

$$^{I}u(x,s) = \tilde{L}_x[v(x,s)] \tag{2.27}$$

Here, $\tilde{L}_x$ is an n-dimensional spatial differential operator vector, and the superscript (^{I}) indicates that the elements of u(x,s) are expressed with respect to an inertial frame. Making use of Eq. (2.22), we obtain

$$^{I}u(x,s) = \Phi(x,s)\,a(s) + u_p(x,s) \tag{2.28}$$

where the following definitions have been employed:

$$\Phi(x,s) = \tilde{L}_x\left[v_H(x,s)^T\right], \quad u_p(x,s) = \int_0^L \tilde{L}_x\left[v_p(x,\xi,s)\right]\,\tilde{f}_d(\xi,s)\,d\xi \tag{2.29}$$

Using Eq. (2.23) to eliminate a(s) yields

$$^{I}u(x,s) = \Phi(x,s)\left[\Psi(s)\right]^{-1} w(s) + u_p(x,s) \tag{2.30}$$

Thus, the internal states are easily expressed in terms of the boundary displacements.

It is usually more desirable to express the internal states in a frame fixed to one of the boundaries of the structural element. This is useful, for example, if the structure is undergoing a rigid motion. Expressing the internal states with respect to a frame fixed to an element boundary would then indicate the amount of internal structural deformation only. This change of reference affects the internal generalized displacements only, since the internal generalized forces are automatically zero for rigid motion. The general linearized relationship between the state vector expressed in the two frames is given by

$$u(x,s) = {}^{I}u(x,s) - \Theta(x)\, w(s) \tag{2.31}$$

where $u(x,s)$ is the state vector expressed in the moving frame and $\Theta(x)$ is an n-by-n matrix which is independant of frequency. Collecting the previous two equations yields

$$u(x,s) = \Gamma(x,s)\, w(s) + u_p(x,s) \tag{2.32}$$

where

$$\Gamma(x,s) = \begin{bmatrix} \gamma_1(x,s)^T \\ \vdots \\ \gamma_n(x,s)^T \end{bmatrix} = \Phi(x,s)\left[\Psi(s)\right]^{-1} - \Theta(x) \tag{2.33}$$

A particular element of the internal state vector is then given by

$$u_i(x,s) = \gamma_i(x,s)^T\, w(s) + u_{p_i}(x,s) \tag{2.34}$$

Thus, once the generalized displacements at the boundaries are known, it is a simple matter to obtain the internal states. Once again, the formulation is exact, and no modal truncation or finite element approximations have been made.

2.3.3 Internal energy formulation

A useful scalar measure of the state of deformation of a flexible element is the total energy due to deformation. It is particularly useful in control applications, as it is a quadratic function of deformation amplitude and is therefore well suited for linear quadratic regulator problems. The internal energy within a particular structural element is obtained by integrating the sum of the potential and kinetic energy densities over the length of the element. This leads to an expression of the form

$$E(t) = \frac{1}{2}\int_0^L \left[k_U u_U^2(x,t) + k_T \dot{u}_T^2(x,t) \right] dx \qquad (2.35)$$

where E(t) is the internal energy at time t, and $u_U(x,t)$ and $u_T(x,t)$ are components of the internal state vector related to the potential and kinetic energies, respectively. Note that these components are now expressed in the time-domain. In order that the internal energy be independant of rigid motion, it is imperative that $u_T(x,t)$ be expressed with respect to one of the boundaries of the element, as described in the previous section.

The terms $u_U(x,t)$ and $u_T(x,t)$ are now expressed as the inverse Laplace transforms of the corresponding frequency-domain functions. This is accomplished via Eq. (2.5) and leads to

$$E(t) = \frac{k(t)}{2}\int_0^L \left\{ k_U \left(\int_{-\infty}^{\infty} \tilde{u}_U(x,s) e^{j\omega t} d\omega \right)^2 + k_T \left(\int_{-\infty}^{\infty} s\, \tilde{u}_T(x,s) e^{j\omega t} d\omega \right)^2 \right\} dx \qquad (2.36)$$

where

$$k(t) = \frac{e^{2\alpha t}}{4\pi^2} \qquad (2.37)$$

We seek an exact expression for the total energy of deformation. It is therefore necessary to replace the squared integrals with double integrals, so that the order of integration with respect to space and frequency may be reversed. This makes it possible to perform the spatial integration

analytically. Thus, by writing each inverse transform integral next to itself, using different dummy variables of integration, and grouping the integrals together, we obtain

$$E(t) = \frac{k(t)}{2}\int_0^L \Big\{ k_U \int_{-\infty}^{\infty}\int_{-\infty}^{\infty} u_U(x,s_1)\, u_U(x,s_2)\, e^{j(\omega_1+\omega_2)t}\, d\omega_1\, d\omega_2$$

$$+ k_T \int_{-\infty}^{\infty}\int_{-\infty}^{\infty} s_1\, s_2\, u_T(x,s_1)\, u_T(x,s_2)\, e^{j(\omega_1+\omega_2)t}\, d\omega_1\, d\omega_2 \Big\}\, dx \qquad (2.38)$$

where

$$s_i = \alpha + j\omega_i \qquad (2.39)$$

For simplicity, we have assumed that the initial conditions are zero and that no distributed forcing occurs in the interior of the element. Interchanging the order of the spatial and frequency integrations in Eq. (2.38) yields

$$E(t) = \frac{k(t)}{2} \int_{-\infty}^{\infty}\int_{-\infty}^{\infty} \Big\{ k_U \int_0^L u_U(x,s_1)\, u_U(x,s_2)\, dx$$

$$+ k_T s_1 s_2 \int_0^L u_T(x,s_1)\, u_T(x,s_2)\, dx \Big\}\, e^{j(\omega_1-\omega_2)t}\, d\omega_1\, d\omega_2 \qquad (2.40)$$

We are now able to express the spatial integrals in terms of the boundary displacements. Making use of Eq. (2.34) leads to

$$\int_0^L u_i(x,s_1)\, u_i(x,s_2)\, dx = w(s_1)^T \Xi_i(s_1,s_2)\, w(s_2) \qquad (2.41)$$

where

$$\Xi_i(s_1,s_2) = \int_0^L \gamma_i(x,s_1)\,\gamma_i(x,s_2)^T\,dx \tag{2.42}$$

Since $\gamma_U(x,s_1)$ and $\gamma_T(x,s_1)$ are expressed analytically, the matrices $\Xi_U(s_1,s_2)$ and $\Xi_T(s_1,s_2)$ can also be computed exactly at each frequency. Finally, substituting Eq. (2.41) into Eq. (2.40) yields

$$E(t) = \frac{k(t)}{2} \int_{-\infty}^{\infty}\int_{-\infty}^{\infty} w(s_1)^T\,\Xi(s_1,s_2)\,w(s_2)\,e^{j(\omega_1+\omega_2)t}\,d\omega_1\,d\omega_2 \tag{2.43}$$

where

$$\Xi(s_1,s_2) = k_U\Xi_U(s_1,s_2) + k_T s_1 s_2 \Xi_T(s_1,s_2) \tag{2.44}$$

Thus, given the boundary displacements in the frequency-domain, the energy of deformation is computable via a double integral. For general motions, an analytical solution does not exist, and E(t) must be computed numerically. The computation time is reduced by a factor of two by exploiting the following symmetry properties of Ξ:

$$\left.\begin{aligned} \Xi(s_2,s_1) &= \Xi(s_1,s_2)^T \\ \Xi(s_1^*,s_2) &= \Xi(s_1,s_2^*)^* \end{aligned}\right\} \tag{2.45b,c}$$

Using these properties makes it possible to reduce the integral to

$$E(t) = k(t) \int_0^{\infty}\int_0^{\infty} \left[w(s_1)^T\,\Xi(s_1,s_2)\,w(s_2)\,e^{j(\omega_1+\omega_2)t} + w(s_1)^T\,\Xi(s_1,s_2^*)\,w(s_2)^*\,e^{j(\omega_1-\omega_2)t} \right] d\omega_1\,d\omega_2 \tag{2.46}$$

In the actual implementation of this formula, the integrals are replaced with summations, the upper limits are replaced with finite frequencies, and a simple midpoint rule algorithm is invoked.

2.3.4 Axial rod example

We first consider a uniform rod constrained to deform axially, as shown in Fig. 2-4. For this element, the simplest model that describes its dynamic behavior is the wave equation, given by

$$-EA\frac{\partial^2}{\partial x^2}v(x,t) + \rho A\ddot{v}(x,t) = f_d(x,t) \tag{2.47}$$

where v represents the axial deflection of the cross section, A is the cross sectional are, and p and E are the material density and modulus of elasticity, respectively. Implicit in this model is the assumption that the deformation of the element is uniform across the cross section. Also, Poisson's ratio effects are ignored. The internal state at any location, x, is therefore completely characterized by two components:

$$u(x,s) = \begin{bmatrix} v(x,s) \\ F(x,s) \end{bmatrix} = \begin{bmatrix} 1 \\ EA\frac{\partial}{\partial x} \end{bmatrix} v(x,s) \tag{2.48}$$

Here, F represents the net force resultant within the rod. The generalized boundary forces and displacements are just these quantities evaluated at x=0 and x=L:

$$w(s) = \begin{bmatrix} v(0,s) \\ v(L,s) \end{bmatrix}, \quad q(s) = \begin{bmatrix} -F(0,s) \\ F(L,s) \end{bmatrix} = \begin{bmatrix} -EA\frac{\partial}{\partial x}v(0,s) \\ EA\frac{\partial}{\partial x}v(L,s) \end{bmatrix} \tag{2.49a,b}$$

The homogeneous solution vector is simply

$$v_H(x,s)^T = \begin{bmatrix} e^{\beta x} & e^{-\beta x} \end{bmatrix}, \quad \beta = \sqrt{\frac{\rho}{E}}\, s \tag{2.50}$$

and the Green's function kernel is

$$v_p(x,\xi,s) = \begin{cases} \frac{\sinh \beta(L-\xi)}{\beta \sinh \beta L} \sinh \beta x & x \le \xi \\ \frac{\sinh \beta \xi}{\beta \sinh \beta L} \sinh \beta(L-x) & x > \xi \end{cases} \tag{2.51}$$

Equations (2.49a,b) and (2.50) can be combined to determine the dynamics stiffness matrix, which is given by

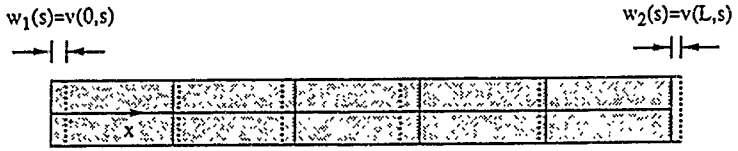

Fig. 2-4: Axial rod model. Deformation is uniform over cross-section.

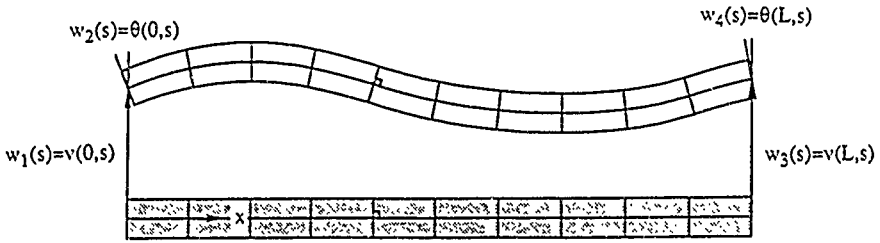

Fig. 2-5: Bernoulli-Euler beam model. Planar cross sections remain planar and perpendicular to deformed beam axis.

$$K(s) = \frac{EA\beta}{\sinh \beta L}\begin{bmatrix} \cosh \beta L & -1 \\ -1 & \cosh \beta L \end{bmatrix} \tag{2.52}$$

As expected, the elements of K are transcendental functions of the complex frequency. Also, this stiffness matrix reduces to the finite element static stiffness matrix for the axial rod in the limit as s approaches zero. The effects of initial conditions and distributed forcing are computed via

$$q_d(s) = -\frac{EA}{\sinh \beta L}\int_0^L \begin{bmatrix} \sinh \beta(L-x) \\ \sinh \beta x \end{bmatrix} \tilde{f}_d(x,s)\, dx \tag{2.53}$$

where the interpolation matrix is given by

$$\Gamma(s) = \frac{1}{\sinh \beta L}\begin{bmatrix} \sinh \beta(L-x) & \sinh \beta x \\ -\beta \cosh \beta(L-x) & \beta \cosh \beta x \end{bmatrix} - \begin{bmatrix} 1 & 0 \\ 0 & 0 \end{bmatrix} \tag{2.54}$$

The internal energy matrices are quite complex, but they are nonetheless expressible in an analytical form. The kinetic energy kernel can be expressed as the sum of the following four matrices:

$$\Xi_T(s_1,s_2) = \frac{1}{\Delta_1\Delta_2}\Lambda(\beta_1)^T\begin{bmatrix} \frac{1}{\beta_1-\beta_2}[e^{(\beta_1+\beta_2)L}-1] & \frac{-1}{\beta_1-\beta_2}[e^{(\beta_1-\beta_2)L}-1] \\ \frac{-1}{\beta_1-\beta_2}[e^{-(\beta_1-\beta_2)L}-1] & \frac{-1}{\beta_1+\beta_2}[e^{-(\beta_1+\beta_2)L}-1] \end{bmatrix}\Lambda(\beta_2) + \begin{bmatrix} L & 0 \\ 0 & 0 \end{bmatrix}$$
$$- \frac{1}{\Delta_1}\Lambda(\beta_1)^T\begin{bmatrix} \frac{1}{\beta_1}[e^{\beta_1 L}-1] & 0 \\ \frac{-1}{\beta_1}[e^{-\beta_1 L}-1] & 0 \end{bmatrix} - \frac{1}{\Delta_2}\begin{bmatrix} \frac{1}{\beta_2}[e^{\beta_2 L}-1] & \frac{-1}{\beta_2}[e^{-\beta_2 L}-1] \\ 0 & 0 \end{bmatrix}\Lambda(\beta_2) \tag{2.55}$$

while the potential energy kernel is given by

$$\Xi_U(s_1,s_2) = \frac{\beta_1\beta_2}{\Delta_1\Delta_2}\Lambda(\beta_1)^T\begin{bmatrix} \frac{1}{\beta_1-\beta_2}[e^{(\beta_1+\beta_2)L}-1] & \frac{-1}{\beta_1-\beta_2}[e^{(\beta_1-\beta_2)L}-1] \\ \frac{1}{\beta_1-\beta_2}[e^{-(\beta_1-\beta_2)L}-1] & \frac{-1}{\beta_1+\beta_2}[e^{-(\beta_1+\beta_2)L}-1] \end{bmatrix}\Lambda(\beta_2) \tag{2.56}$$

where the following definitions have been made:

$$\Lambda(\beta) = \begin{bmatrix} -e^{-\beta L} & 1 \\ e^{\beta L} & -1 \end{bmatrix} \tag{2.57a}$$

$$\Delta_i = 2 \sinh \beta_i L \tag{2.57b}$$

$$\beta_i = \sqrt{\frac{\rho}{E}}\, s_i \tag{2.57c}$$

It is clear that, for even the simplest of structural element models, the internal energy expressions become quite complex. However, this is to be expected, as the energy is a quadratic function of deflection amplitude, and represents an integrated effect over the entire domain of the element.

The preceeding expressions for the stiffness and interpolation matrices are well suited for numerical computation, provided that the complex frequency at which they are evaluated is neither too large nor too small in magnitude. For these extreme situations, numerical accuracy and overflow errors become issues. These problems are readily handled by using asymptotic approximations to the stiffness and interpolation matrices. The approximations are obtained by replacing the trigonometric and hyperbolic functions with appropriate series expansions, and truncating higher order terms.

2.3.5 Bernoulli-Euler beam example

For bending elements, the simplest model is the Bernoulli-Euler beam, shown schematically in Fig. 2-5. The basic assumptions of the model are that planar cross sections of the beam remain planar and normal to the center-line after deformation, and that differential cross sections have negligible rotary inertia. Under these assumptions, the equation of motion becomes

$$EI\frac{\partial^4}{\partial x^4} v(x,t) + \rho A \ddot{v}(x,t) = f_d(x,t) \tag{2.58}$$

where v is the transverse deflection, E and ρ are the modulus of elasticity and density of the material, respectively, and A and I are the cross sectional area and moment of inertia, respectively. Taking the Laplace transform, we obtain

$$\frac{\partial^4}{\partial x^4} v(x,s) - \alpha^4 v(x,s) = \tilde{f}_d(x,s), \quad \alpha^4 = -\frac{\rho A s^2}{EI} \tag{2.59a,b}$$

For this element, the structural state vector has four elements, given by

$$^{I}u(x,s) = \begin{bmatrix} v(x,s) \\ \theta(x,s) \\ M(x,s) \\ S(x,s) \end{bmatrix} = \begin{bmatrix} 1 \\ \frac{\partial}{\partial x} \\ EI \frac{\partial^2}{\partial x^2} \\ -EI \frac{\partial^3}{\partial x^3} \end{bmatrix} v(x,s) \tag{2.60}$$

where θ is the rotation of the cross section, and M and S are the internal moment and shear resultants, respectively. The generalized boundary displacements and forces are then

$$w(s) = \begin{bmatrix} v(0,s) \\ \theta(0,s) \\ v(L,s) \\ \theta(L,s) \end{bmatrix} = \begin{bmatrix} v(0,s) \\ \frac{\partial}{\partial x} v(0,s) \\ v(L,s) \\ \frac{\partial}{\partial x} v(L,s) \end{bmatrix}, \quad q(s) = \begin{bmatrix} -S(0,s) \\ -M(0,s) \\ S(L,s) \\ M(L,s) \end{bmatrix} = \begin{bmatrix} EI \frac{\partial^3}{\partial x^3} v(0,s) \\ -EI \frac{\partial^2}{\partial x^2} v(0,s) \\ -EI \frac{\partial^3}{\partial x^3} v(L,s) \\ EI \frac{\partial^2}{\partial x^2} v(L,s) \end{bmatrix} \tag{2.61a,b}$$

The homogeneous solution vector contains four elements as well, and is given by

$$v_H(x,s)^T = \begin{bmatrix} e^{\alpha x} & e^{-\alpha x} & e^{j\alpha x} & e^{-j\alpha x} \end{bmatrix} \tag{2.62}$$

and the Green's function kernel follows as:

$$v_p(x,\xi,s) = \begin{cases} \dfrac{g_1(\xi,s)\, S^*(\alpha x) + g_2(\xi,s)\, C^*(\alpha x)}{4\alpha^3 (1 - ch\, ct)} & x \le \xi \\ \dfrac{g_3(\xi,s)\, S^*(\alpha(L-x)) + g_4(\xi,s)\, C^*(\alpha(L-x))}{4\alpha^3 (1 - ch\, ct)} & x > \xi \end{cases} \tag{2.63}$$

where

$$g_1(\xi,s) = -C^+(\alpha\xi) + ch\cos(\alpha(L-\xi)) - sh\sin(\alpha(L-\xi)) + ct\cosh(\alpha(L-\xi)) + st\sinh(\alpha(L-\xi)) \tag{2.64a}$$

$$g_2(\xi,s) = S^+(\alpha\xi) + ch\sin(\alpha(L-\xi)) - sh\cos(\alpha(L-\xi)) + ct\sinh(\alpha(L-\xi)) - st\cosh(\alpha(L-\xi)) \tag{2.64b}$$

$$g_3(\xi,s) = -C^+(\alpha(L-\xi)) + ch\cos(\alpha\xi) - sh\sin(\alpha\xi) + ct\cosh(\alpha\xi) + st\sinh(\alpha\xi) \tag{2.64c}$$

$$g_4(\xi,s) = S^+(\alpha(L-\xi)) + ch\sin(\alpha\xi) - sh\cos(\alpha\xi) + ct\sinh(\alpha\xi) - st\cosh(\alpha\xi) \tag{2.64d}$$

and the following trigonometric definitions have been made:

$$
\begin{aligned}
&C^{+}(\alpha\xi) = \cosh(\alpha\xi) + \cos(\alpha\xi) \qquad C^{-}(\alpha\xi) = \cosh(\alpha\xi) - \cos(\alpha\xi)\\
&S^{+}(\alpha\xi) = \sinh(\alpha\xi) + \sin(\alpha\xi) \qquad S^{-}(\alpha\xi) = \sinh(\alpha\xi) - \sin(\alpha\xi)\\
&ch = \cosh(\alpha L) \qquad\qquad\qquad ct = \cos(\alpha L)\\
&sh = \sinh(\alpha L) \qquad\qquad\qquad st = \sin(\alpha L)
\end{aligned}
\tag{2.65a-h}
$$

For the beam element, the stiffness matrix is four-by-four, and is expressed as

$$
K(s) = \frac{EI}{\Delta(s)}\begin{bmatrix} K_6(s) & K_4(s) & -K_5(s) & K_3(s)\\ K_4(s) & K_2(s) & -K_3(s) & K_1(s)\\ -K_5(s) & -K_3(s) & K_6(s) & -K_4(s)\\ K_3(s) & K_1(s) & -K_4(s) & K_2(s)\end{bmatrix} \tag{2.66}
$$

where

$$
\begin{aligned}
K_1(s) &= \frac{1}{\alpha^3}(sh - st)\\
K_2(s) &= \frac{1}{\alpha^3}(ch\ st - sh\ ct)\\
K_3(s) &= \frac{1}{\alpha^2}(ch - ct)\\
K_4(s) &= \frac{1}{\alpha^2}sh\ st\\
K_5(s) &= \frac{1}{\alpha}(sh + st)\\
K_6(s) &= \frac{1}{\alpha}(ch\ st + sh\ ct)\\
\Delta(s) &= \frac{1}{\alpha^4}(1 - ch\ ct)
\end{aligned}
\tag{2.67a-g}
$$

This stiffness matrix also reduces to the static, finite element stiffness matrix as the complex frequency approaches zero. The effects of distributed forcing and initial conditions are determined via

$$
q_d(s) = \frac{EI}{2\alpha(1-ch\,ct)}\int_0^L \begin{bmatrix} \alpha\, g_1(x,s)\\ -\, g_2(x,s)\\ \alpha\, g_3(x,s)\\ g_4(x,s)\end{bmatrix} \tilde{f}_d(x,s)\,dx \tag{2.68}
$$

and the interpolation matrix is most easily expressed by

$$
\Gamma(x,s) = \Phi(x,s)\left[\Psi(s)\right]^{-1} - \begin{bmatrix} 1 & x & 0 & 0\\ 0 & 1 & 0 & 0\\ 0 & 0 & 0 & 0\\ 0 & 0 & 0 & 0\end{bmatrix} \tag{2.69}
$$

where

$$\Phi(x,s) = \begin{bmatrix} e^{\alpha x} & e^{-\alpha x} & e^{j\alpha x} & e^{-j\alpha x} \\ \alpha e^{\alpha x} & -\alpha e^{-\alpha x} & j\alpha e^{j\alpha x} & -j\alpha e^{-j\alpha x} \\ EI\alpha^2 e^{\alpha x} & EI\alpha^2 e^{-\alpha x} & -EI\alpha^2 e^{j\alpha x} & -EI\alpha^2 e^{-j\alpha x} \\ -EI\alpha^3 e^{\alpha x} & EI\alpha^3 e^{-\alpha x} & jEI\alpha^3 e^{j\alpha x} & -jEI\alpha^3 e^{-j\alpha x} \end{bmatrix} \tag{2.70}$$

and

$$\left[\Psi(s)\right]^{-1} = \frac{1}{4\alpha(1 - ch\,ct)} \begin{bmatrix} \alpha p_1 & p_2 & \alpha p_4 & p_3 \\ \alpha e^{\alpha L} p_4 & -e^{\alpha L} p_3 & \alpha e^{\alpha L} p_1 & -e^{\alpha L} p_2 \\ \alpha p_5 & -jp_6 & \alpha p_8 & -jp_7 \\ \alpha e^{j\alpha L} p_8 & j e^{j\alpha L} p_7 & \alpha e^{j\alpha L} p_5 & j e^{j\alpha L} p_6 \end{bmatrix} \tag{2.71}$$

In this last equation, the following definitions have been used:

$$\begin{aligned} p_1 &= 1 - e^{-\alpha L}(ct - st) & p_5 &= 1 - e^{-j\alpha L}(ch - jsh) \\ p_2 &= 1 - e^{-\alpha L}(ct + st) & p_6 &= 1 - e^{-j\alpha L}(ch + jsh) \\ p_3 &= e^{-\alpha L} - (ct - st) & p_7 &= e^{-j\alpha L} - (ch - jsh) \\ p_4 &= e^{-\alpha L} - (ct + st) & p_8 &= e^{-j\alpha L} - (ch - jsh) \end{aligned} \tag{2.72}$$

As was the case with the axial rod, the expressions for the internal energy of deformation are complex, but nonetheless expressible analytically. The potential energy matrix is

$$\Xi_U(s_1,s_2) = \alpha_1^2\alpha_2^2\,\Psi(s_1)^{-T} \begin{bmatrix} F(\beta_1) & F(\beta_2) & -F(\beta_3) & -F(\beta_4) \\ F(-\beta_2) & F(-\beta_1) & -F(-\beta_4) & -F(-\beta_3) \\ -F(j\beta_4) & -F(j\beta_3) & F(j\beta_1) & F(j\beta_2) \\ -F(-j\beta_3) & -F(-j\beta_4) & F(-j\beta_2) & F(-j\beta_1) \end{bmatrix} \Psi(s_2)^{-1} \tag{2.73}$$

while the kinetic energy matrix is

$$\begin{aligned} \Xi_T(s_1,s_2) = {} & \Psi(s_1)^{-T} \begin{bmatrix} F(\beta_1) & F(\beta_2) & F(\beta_3) & F(\beta_4) \\ F(-\beta_2) & F(-\beta_1) & F(-\beta_4) & F(-\beta_3) \\ F(j\beta_4) & F(j\beta_3) & F(j\beta_1) & F(j\beta_2) \\ F(-j\beta_3) & F(-j\beta_4) & F(-j\beta_2) & F(-j\beta_1) \end{bmatrix} \Psi(s_2)^{-1} + \begin{bmatrix} L & \frac{1}{2}L^2 & 0 & 0 \\ \frac{1}{2}L^2 & \frac{1}{6}L^3 & 0 & 0 \\ 0 & 0 & 0 & 0 \\ 0 & 0 & 0 & 0 \end{bmatrix} \\ & - \Psi(s_1)^{-T} \begin{bmatrix} F(\alpha_1) & G(\alpha_1) & 0 & 0 \\ F(-\alpha_1) & G(-\alpha_1) & 0 & 0 \\ F(j\alpha_1) & G(j\alpha_1) & 0 & 0 \\ F(-j\alpha_1) & G(-j\alpha_1) & 0 & 0 \end{bmatrix} - \begin{bmatrix} F(\alpha_2) & F(-\alpha_2) & F(j\alpha_2) & F(-j\alpha_2) \\ G(\alpha_2) & G(-\alpha_2) & G(j\alpha_2) & G(-j\alpha_2) \\ 0 & 0 & 0 & 0 \\ 0 & 0 & 0 & 0 \end{bmatrix} \Psi(s_2)^{-1} \end{aligned} \tag{2.74}$$

where

$$F(\beta) = \frac{1}{\beta}\left[e^{\beta L} - 1\right]$$
$$G(\beta) = \frac{L}{\beta}e^{\beta L} + \frac{1}{\beta^2}\left[1 - e^{\beta L}\right] \qquad (2.75)$$

and

$$\begin{aligned}\beta_1 &= \alpha_1 + \alpha_2\\ \beta_2 &= \alpha_1 - \alpha_2\\ \beta_3 &= \alpha_1 + j\alpha_2\\ \beta_4 &= \alpha_1 - j\alpha_2\\ \alpha_i^4 &= -\frac{\rho A}{EI}s_i^2\end{aligned} \qquad (2.76)$$

As was the case for the axial rod, high and low frequency asymptotic approximations are required for the beam element as well. These approximations allow efficient numerical computation of the required quantities without sacrificing numerical accuracy.

2.3.6 High-frequency elements

In many cases, the simple axial rod and Bernoulli-Euler beam models are insufficient to capture the high frequency behavior of the structural system. This is particularly noticable when analyzing the wave-like propagation of energy associated with impulsive disturbance sources. For these situations, more accurate structural models are required.

The simple axial rod model presented in Section 2.3.4 predicts dispersion-free propagation of elastic waves at all frequencies. For rods of circular cross section, a better model is available if a radial degree of freedom is introduced, as shown in Fig. 2-6. This is the basis for the Mindlin-Herrmann axial rod theory, which can be expressed mathematically by the following system:

$$-a^2(\lambda+2G)\frac{\partial^2}{\partial x^2}v_1(x,s) + \rho a^2 s^2 v_1(x,s) = 2a\lambda\frac{\partial}{\partial x}v_2(x,s) \qquad (2.77a)$$

$$a^2\kappa^2 G\frac{\partial^2}{\partial x^2}v_2(x,s) - \left[8\kappa_1^2(\lambda+G) + \rho a^2 s^2\right]v_2(x,s) = 4a\kappa_1^2\lambda\frac{\partial}{\partial x}v_1(x,s) \qquad (2.77b)$$

In these equations, v_1 and v_2 are the axial and radial displacements, respectively, a represents the radius of the rod, λ and G are the Lame constants of the material, and κ and κ_1 are empirically

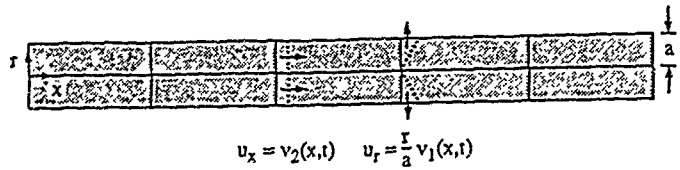

Fig. 2-6: Mindlin-Herrmann rod model. Two deformational degrees of freedom are allowed. Poisson's ratio couples axial and radial deformation modes.

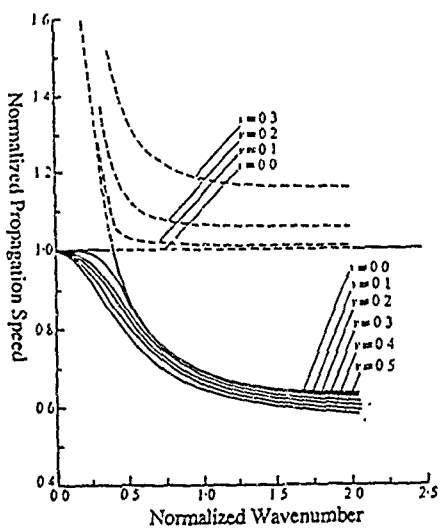

Fig. 2-7: Dispersion curves associated with the Mindlin-Herrmann model.

determined parameters. This model yields the dispersion curves shown in Fig. 2-7, and reproduces the dispersion characteristics of the rod more accurately than the simple rod model. The modified stiffness matrix for the Mindlin-Herrmann model is given in Appendix A.

A more accurate beam model is the Timoshenko beam, shown in Fig. 2-8. This model allows for shearing of the cross sections with respect to the center-line of the beam, and accounts for rotary inertia. The equation of motion is given by

$$EI\frac{\partial^4}{\partial x^4}v(x,t) + \rho A\ddot{v}(x,t) - \rho I\left[1+\frac{Ek}{G}\right]\frac{\partial^2}{\partial x^2}\ddot{v}(x,t) + \frac{\rho^2 Ik}{G}\ddot{\ddot{v}}(x,t) = f_d(x,t) \qquad (2.78)$$

where G is the shear modulus of the material and k is an empirically determined correction factor. The Timoshenko model is capable of supporting both a shear and a bending mode of propagation, as shown in the dispersion curves in Fig. 2-9. This model also places a finite upper limit on the flexural propagation speed, which is unrealistically unbounded in the Bernoulli-Euler model. Details on the stiffness matrix for the Timoshenko model are presented in Appendix A.

2.4 Two-dimensional elements

Two dimensional elements are modelled using partial differential equations with three independant variables (two spatial dimensions and time). Therefore, the modelling of two-dimension elements using the TEM methodology cannot produce exact results, as was the case for one-dimensional models. The reason is that the dynamics equation remains a partial differential equation in two spatial variables after the Laplace transform operation. As a result, there exist an infinity of homogeneous solutions for any particular element model. To this infinite set, these corresponds an infinity of points along the boundary (which spans a one-dimensional domain) on which boundary conditions must be satisfied. Nevertheless, by using a sufficiently large number of homogeneous solutions and considering only a sufficiently large, but finite, set of boundary points, an accurate TEM solution is possible. An example of boundary discretization, for the case of in-plane deformation, is shown in Fig. 2-10. It is conjectured that, for a given amount of

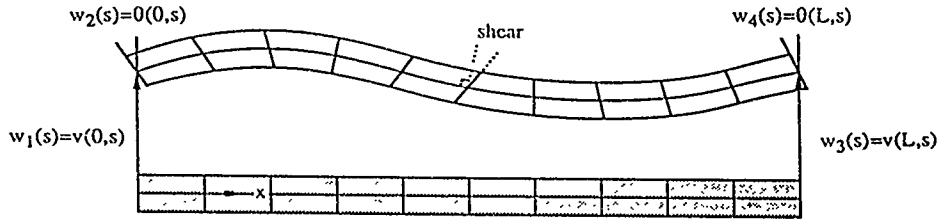

Fig. 2-8: Timoshenko beam model. Shearing of cross-sections is allowed.

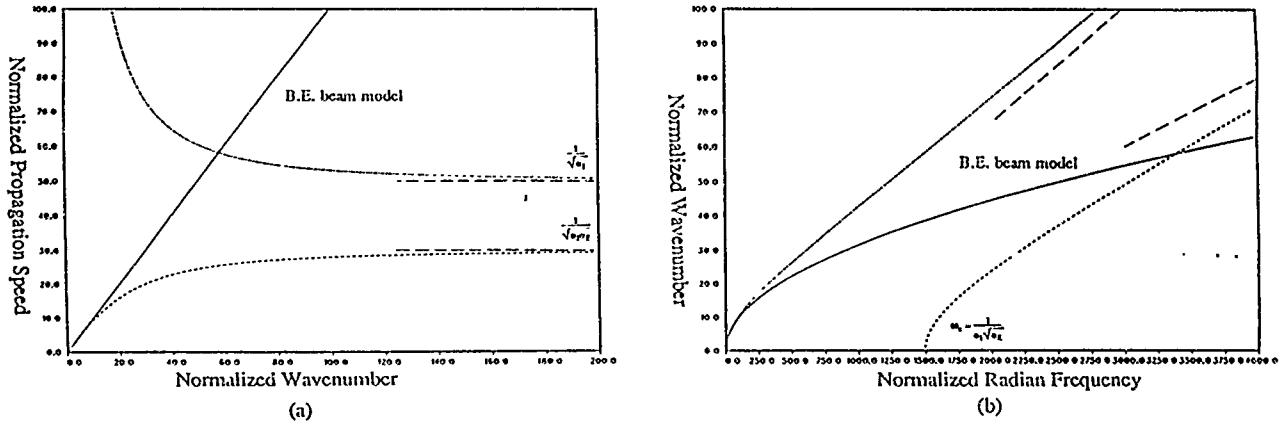

Fig. 2-9: Timoshenko beam dispersion characteristics (α_1=4x10^{-4}, α_L=2.8): (a) Dispersion curves, (b) Frequency spectrum.

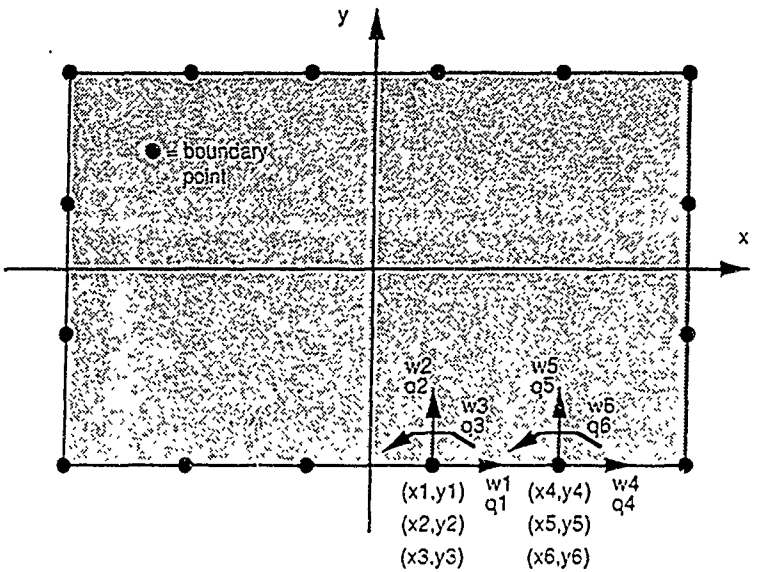

Fig. 2-10: Typical two-dimensional element with three generalized displacements and forces at each boundary point. In-plane deformation is assumed. The numbering scheme shown continues along the entire boundary of the element.

computational capability, this approach yields results superior in accuracy to the traditional FEM methodology. We consider two two-dimensional elements here: a plate bending element and a plane stress element.

2.4.1 Plate bending element

The TEM formulation for plate elements bears some resemblance to previous work by Kulla (1990). The transformed equation of motion for a plate in bending is

$$D\nabla^4 v(x,y,s) + ms^2 v(x,y,s) = 0 \tag{2.79}$$

where v is the deflection normal to the plane of the element, m is the mass per unit area, and ∇^4 is the biharmonic operator. Also, D is the bending rigidity, given by

$$D = \frac{Eh^3}{12(1-\nu^2)} \tag{2.80}$$

where h is the thickness of the plate and ν is the Poisson's ratio of the material. Note that we have assumed no distributed forcing and zero initial conditions. The homogeneous solution vector is of infinite dimension, with each entry having the form

$$v_{H_i}(x,y,s) = e^{\alpha_i x - \beta_i y} \tag{2.81}$$

Substituting this equation into Eq. (2.79) yields the characteristic equation

$$\left[\alpha_i^2 + \beta_i^2\right]^2 + \frac{ms^2}{D} = 0 \tag{2.82}$$

Thus, for each complex-valued α (or β), there exist four independent homogeneous solutions corresponding to the four complex-valued β's (or α's) obtained from the characteristic equation.

To obtain an approximate plate solution, we must select a finite set of values for α (or β). A general method of selecting this set has not been developed in this research. From this set, we obtain a truncated solution vector, and the approximate expression for the deflection field becomes

$$v(x,y,s) = v_H(x,y,s)^T a(s) \tag{2.83}$$

The problem has now been reduced to determining the coefficient vector, a(s), in terms of the boundary conditions. A finite set of boundary points on the element is therefore selected. The total number of boundary conditions specified at these points, n, must equal the dimension of the homogeneous solution vector, so that the problem is not underspecified. (Typically, three boundary conditions are imposed at each point.) The boundary condition constraints can be written in the form

$$w_i(s) = L_{xy}^{(i)}\left[v(x_i,y_i,s)\right] = L_{xy}^{(i)}\left[v_H(x_i,y_i,s)\right]^T a(s), \quad i=1,\ldots,n \tag{2.84a}$$

$$q_i(s) = D_{xy}^{(i)}\left[v(x_i,y_i,s)\right] = D_{xy}^{(i)}\left[v_H(x_i,y_i,s)\right]^T a(s), \quad i=1,\ldots,n \tag{2.84b}$$

where $L_{xy}^{(i)}$ is a linear spatial differential operator (independent of s) relating the approximate solution, v, to the i'th generalized displacement on the boundary, w_i. Similarly, $D_{xy}^{(i)}$ relates v to the corresponding dual generalized force, q_i. Grouping Eqs. (2.84a) and (2.84b) into matrix form yields

$$w(s) = \Psi(s)\,a(s), \quad q(s) = \tilde{\Psi}(s)\,a(s) \tag{2.85a,b}$$

where

$$\Psi(s) \triangleq \begin{bmatrix} L_{xy}^{(1)}\left[v_H(x_1,y_1,s)\right]^T \\ \vdots \\ L_{xy}^{(n)}\left[v_H(x_n,y_n,s)\right]^T \end{bmatrix}, \quad \tilde{\Psi}(s) \triangleq \begin{bmatrix} D_{xy}^{(1)}\left[v_H(x_1,y_1,s)\right]^T \\ \vdots \\ D_{xy}^{(n)}\left[v_H(x_n,y_n,s)\right]^T \end{bmatrix} \tag{2.86a,b}$$

Finally, the dynamic stiffness matrix follows from eliminating a from Eqs. (2.85a) and (2.85b):

$$K(s) = \tilde{\Psi}(s)\left[\Psi(s)\right]^{-1} \tag{2.87}$$

Obviously, the choice of boundary points affects the accuracy of the solution, and should depend on the geometry of the element. Unfortunately, a quantitative relationship between the boundary point locations and the solution accuracy has not yet been developed. However, a

general rule of thumb is to space the boundary points more closely together near corners of the element, where internal stress gradients are large.

2.4.2 Plane stress element

For plane stress problems, the difficulty lies in expressing the state of deformation in terms of a single scalar function, as there are two in-plane deformational degrees of freedom. To remedy this situation, it becomes neces ~y to derive a frequency-dependant stress function, from which all internal stresses and both displacements can be determined. This is accomplished by working directly with the basic plane stress relations, expressed in the frequency-domain. For linear, isotropic, plane stress problems, the stress-strain relations are

$$\varepsilon_x = \frac{1}{E}\left(\sigma_x - \nu\,\sigma_y\right) \tag{2.88a}$$

$$\varepsilon_y = \frac{1}{E}\left(\sigma_y - \nu\,\sigma_x\right) \tag{2.88b}$$

$$\varepsilon_{xy} = \frac{1}{2G}\tau_{xy} = \frac{1+\nu}{E}\tau_{xy} \tag{2.88c}$$

where E,G, and ν are the extensional modulus, shear modulus and Poisson's ratio of the material, respectively. The equations of force equilibrium, expressed in the frequency-domain, are

$$\frac{\partial\sigma_x}{\partial x} + \frac{\partial\tau_{xy}}{\partial y} = \rho s^2 u_x, \qquad \frac{\partial\tau_{xy}}{\partial x} + \frac{\partial\sigma_y}{\partial y} = \rho s^2 u_y \tag{2.89a,b}$$

where ρ is the density of the material and s is the (generally complex) Laplace variable. To these, we must add the geometric relations

$$\varepsilon_x = \frac{\partial u_x}{\partial x}, \qquad \varepsilon_y = \frac{\partial u_y}{\partial y}, \qquad \varepsilon_{xy} = \frac{1}{2}\left(\frac{\partial u_x}{\partial y} + \frac{\partial u_y}{\partial x}\right) \tag{2.90a,b,c}$$

and the compatibility constraint

$$\frac{\partial^2\varepsilon_x}{\partial y^2} + \frac{\partial^2\varepsilon_y}{\partial x^2} = 2\frac{\partial^2\varepsilon_{xy}}{\partial x\partial y} \tag{2.91}$$

Substituting Eqs. (2.88a) and (2.88b) into equation (2.91) yields

$$\frac{\partial^2\sigma_x}{\partial y^2}+\frac{\partial^2\sigma_y}{\partial x^2}-\nu\left(\frac{\partial^2\sigma_x}{\partial x^2}+\frac{\partial^2\sigma_y}{\partial y^2}\right)=2(1+\nu)\frac{\partial^2\tau_{xy}}{\partial x\partial y} \tag{2.92}$$

while adding the derivative of Eq. (2.89a) with respect to x to the derivative of equation (2.89b) with respect to y produces

$$2\frac{\partial^2\tau_{xy}}{\partial x\partial y}+\left(\frac{\partial^2\sigma_x}{\partial x^2}+\frac{\partial^2\sigma_y}{\partial y^2}\right)=\rho s^2\left(\frac{\partial u_x}{\partial x}+\frac{\partial u_y}{\partial y}\right) \tag{2.93}$$

Eliminating τ_{xy} between the previous two relations results in

$$\frac{\partial^2\sigma_x}{\partial y^2}+\frac{\partial^2\sigma_y}{\partial x^2}+\frac{\partial^2\sigma_x}{\partial x^2}+\frac{\partial^2\sigma_y}{\partial y^2}=(1+\nu)\rho s^2\left(\frac{\partial u_x}{\partial x}+\frac{\partial u_y}{\partial y}\right) \tag{2.94}$$

Substituting Eqs. (2.88a), (2.88b), (2.90a) and (2.90b) into equation (2.94) yields

$$\frac{\partial^2\sigma_x}{\partial y^2}+\frac{\partial^2\sigma_y}{\partial x^2}+\frac{\partial^2\sigma_x}{\partial x^2}+\frac{\partial^2\sigma_y}{\partial y^2}=(1+\nu)(1-\nu)\frac{\rho s^2}{E}\left(\sigma_x+\sigma_y\right) \tag{2.95}$$

which reduces to

$$\left[\nabla^2-(1-\nu^2)\frac{\rho s^2}{E}\right]\left(\sigma_x+\sigma_y\right)=0 \tag{2.96}$$

where ∇^2 is the two dimensional spatial Laplacian operator. Because σ_x and σ_y are independent variables, we still need one additional equation, so as to uniquely identify σ_x and σ_y. The second equation is obtained by subtracting the derivative of Eq. (2.89b) with respect to y from the derivative of Eq. (2.89a) with respect to x, yielding

$$(1+\nu)\frac{\rho s^2}{E}\left(\sigma_x-\sigma_y\right)=\frac{\partial^2\sigma_x}{\partial x^2}-\frac{\partial^2\sigma_y}{\partial y^2} \tag{2.97}$$

This relation is equivalent to

$$2(1+\nu)\frac{\rho s^2}{E}\left(\sigma_x-\sigma_y\right)=\nabla^2\left(\sigma_x-\sigma_y\right)+\frac{\partial^2\sigma_x}{\partial x^2}-\frac{\partial^2\sigma_x}{\partial y^2}+\frac{\partial^2\sigma_y}{\partial x^2}-\frac{\partial^2\sigma_y}{\partial y^2} \tag{2.98}$$

from which we obtain

$$\left[\nabla^2-2(1+\nu)\frac{\rho s^2}{E}\right]\left(\sigma_x-\sigma_y\right)=\left[-\frac{\partial^2}{\partial x^2}+\frac{\partial^2}{\partial y^2}\right]\left(\sigma_x+\sigma_y\right) \tag{2.99}$$

Equations (2.96) and (2.99) represent two linear partial differential equations in two variables (the sum and difference of the normal stresses). This system can be reduced to a single equation by defining a frequency dependent stress function, Φ, so that the following relations hold:

$$(\sigma_x + \sigma_y) = \left[\nabla^2 - 2(1+\nu)\frac{\rho s^2}{E}\right]\Phi \tag{2.100a}$$

$$(\sigma_x - \sigma_y) = \left[-\frac{\partial^2}{\partial x^2} + \frac{\partial^2}{\partial y^2}\right]\Phi \tag{2.100b}$$

Then, in terms of Φ, Eq. (2.99) is identically satisfied, while Eq. (2.96) becomes

$$\left[\nabla^2 - \frac{s^2}{c_c^2}\right]\left[\nabla^2 - \frac{s^2}{c_s^2}\right]\Phi = 0 \tag{2.101}$$

where

$$c_c = \sqrt{\frac{E}{\rho(1-\nu^2)}}, \quad c_s = \sqrt{\frac{G}{\rho}}, \quad c_0 = \sqrt{\frac{E}{\rho}} \tag{2.102a,b,c}$$

The constants c_c, c_s and c_0 are readily identified as the propagation velocities of compression and shear waves in a plane and compression waves in a three dimensional medium, respectively. It is interesting to note that, under static conditions (s=0), equation (2.101) reduces to the familiar biharmonic equation associated with the Airy stress function.

It remains to determine the physical entities of interest in terms of Φ. In the traditional stress function formulation, the stresses are expressed as derivative operators on Φ. In order to obtain similar differential operator expressions in this development, it is necessary to define a related function, v, such that the following relationship holds:

$$\Phi = \frac{\partial^2 v}{\partial x \partial y} \tag{2.103}$$

The final form of Eq. (2.101) then becomes

$$\frac{\partial^2}{\partial x \partial y}\left[\nabla^2 - \frac{s^2}{c_c^2}\right]\left[\nabla^2 - \frac{s^2}{c_s^2}\right] v = 0 \tag{2.104}$$

Equations (2.100) and (2.103) can then be used to determine the normal stresses in terms of v.

$$\sigma_x = \frac{\partial^2}{\partial x \partial y}\left[\frac{\partial^2}{\partial y^2} - \frac{s^2}{2c_s^2}\right]v, \quad \sigma_y = \frac{\partial^2}{\partial x \partial y}\left[\frac{\partial^2}{\partial x^2} - \frac{s^2}{2c_s^2}\right]v \qquad (2.105a,b)$$

Now, combining Eqs. (2.88a), (2.90a) and the derivative of Eq. (2.89a) with respect to x leads to

$$\frac{\partial^2 \tau_{xy}}{\partial x \partial y} = \frac{\rho s^2}{E}\left(\sigma_x - \nu\,\sigma_y\right) - \frac{\partial^2 \sigma_x}{\partial x^2} \qquad (2.106)$$

Substituting Eqs. (2.105a) and (2.105b) into equation (2.106) and integrating with respect to both x and y yields

$$\tau_{xy} = \left[-\frac{\partial^4}{\partial x^2 \partial y^2} + \frac{s^2}{c_0^2}\nabla^2 - \frac{s^4}{c_0^2 c_e^2}\right]v \qquad (2.107)$$

Thus, Eqs. (2.105) and (2.107) are the desired relations between the stresses and v. Furthermore, making use of Eqs. (2.88) and (2.90) leads to

$$u_x = \frac{1}{E}\frac{\partial}{\partial y}\left[\frac{\partial^2}{\partial y^2} - \nu\frac{\partial^2}{\partial x^2} - \frac{s^2}{c_e^2}\right]v \qquad (2.108a)$$

$$u_y = \frac{1}{E}\frac{\partial}{\partial x}\left[\frac{\partial^2}{\partial x^2} - \nu\frac{\partial^2}{\partial y^2} - \frac{s^2}{c_e^2}\right]v \qquad (2.108b)$$

Thus, unlike the traditional stress function formulation, this development also expresses the displacements in terms of the frequency dependent function, v.

We are now in a position to apply the same methodology as was used for the plate bending element. Once again, the assumed form of the homogeneous solution is

$$v_{H_i}(x,y,s) = e^{\alpha_i x + \beta_i y}, \quad i=1,\ldots,n \qquad (2.109)$$

where α and β are functions of s, leads to the characteristic equation:

$$\alpha_i\beta_i\left[(\alpha_i^2+\beta_i^2) - \frac{s^2}{c_e^2}\right]\left[(\alpha_i^2+\beta_i^2) - \frac{s^2}{c_s^2}\right] = 0, \quad i=1,\ldots,n \qquad (2.110)$$

Of the four solutions to this equation, two (α=0 and β=0) are spurious. The other two determine the relationship that must hold between α and β for each basis solution. The rigid body modes are

accounted for by setting s equal to zero. As is the case for the plate bending element, the actual choices for α_i and β_i vary depending on the geometry of the element and are not discussed here.

2.5 Assembly Procedure

The assembly of individual elements to form a global structural model is performed in a manner similar to traditional FEM techniques. The element equations are first collected into a large, unreduced matrix equation, given by

$$\begin{bmatrix} q^1(s) \\ \cdot \\ q^N(s) \end{bmatrix} = \begin{bmatrix} K^1(s) & & 0 \\ & K^2(s) & \\ 0 & & K^N(s) \end{bmatrix} \begin{bmatrix} w^1(s) \\ \cdot \\ w^N(s) \end{bmatrix} + \begin{bmatrix} q_d^1(s) \\ \cdot \\ q_d^N(s) \end{bmatrix} \tag{2.111}$$

where the superscripts identify the individual elements. The geometry of the interconnections between elements is specified by a connectivity matrix, C, which relates the local boundary displacements of the elements to a set of global displacements, $w_0^G(s)$, that define the global model.

$$\begin{bmatrix} w^1(s) \\ \cdot \\ w^N(s) \end{bmatrix} = C\, w_0^G(s) \tag{2.112}$$

Figure 2-11 presents a simple structural system and the associated connectivity matrix. Piche (1986a) shows that, for small, linear displacements, the following dual relationship holds:

$$q_0^G(s) = C^T \begin{bmatrix} q^1(s) \\ \cdot \\ q^N(s) \end{bmatrix} \tag{2.113}$$

Using these connectivity relations in Eq. (2.111) yields the unreduced system model

$$q_0^G(s) = K_0^G(s)\, w_0^G(s) + q_{d0}^G(s) \tag{2.114}$$

where

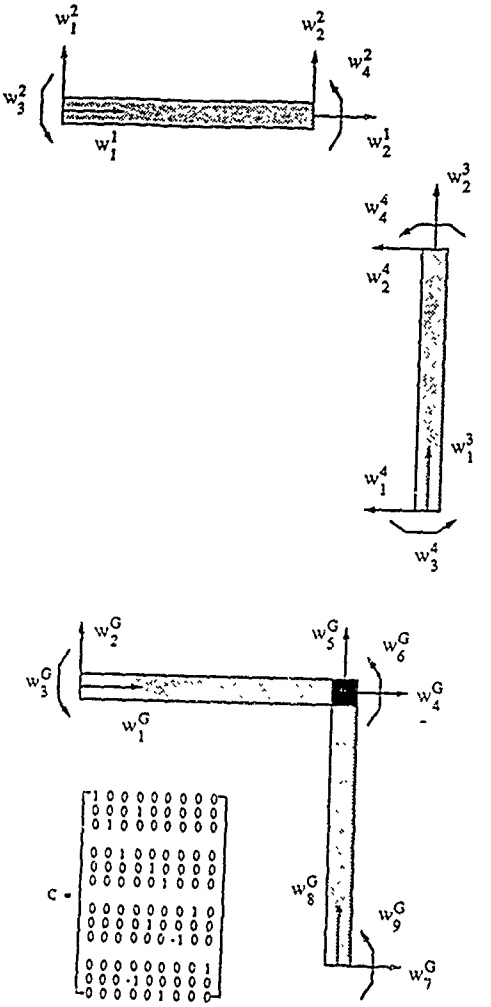

Fig. 2-11: Assembly of simple, four element structure. Elements 1 and 3 are axial models, and elements 2 and 4 are beam models. The joint is assumed to be massless.

$$K_0^G(s) = C^T \begin{bmatrix} K^1(s) & & 0 \\ & K^2(s) & \\ 0 & & K^N(s) \end{bmatrix} C, \quad q_{d0}^G(s) = C^T \begin{bmatrix} q_d^1(s) \\ \cdot \\ q_d^N(s) \end{bmatrix} \tag{2.115a,b}$$

At this point, if there are any global displacements that are constrained, they are removed from the unreduced model. This produces the desired global model, given by

$$q^G(s) = K^G(s)\, w^G(s) + q_d^G(s) \tag{2.116}$$

Equation (2.116) represents the global dynamic stiffness matrix for the structural model. It is mathematically exact, and must be calculated at each frequency of interest. To compute the response of the model to various excitations, we must solve for the global displacements. Thus,

$$w^G(s) = G(s)\left[q^G(s) - q_d^G(s)\right], \quad G(s) = \left[K^G(s)\right]^{-1} \tag{2.117a,b}$$

Here, G(s) represents the global transfer function matrix for the model. If, in addition, the local boundary displacements for a particular element are desired, a partition of the connectivity matrix must be used:

$$w^i(s) = C_w^i\, G(s)\left[q^G(s) - q_d^G(s)\right] \tag{2.118}$$

Finally, the internal states of a particular element are available via

$$u^i(x,s) = \Gamma(x,s)\, C_w^i\, G(s)\left[q^G(s) - q_d^G(s)\right] + u_p^i(x,s) \tag{2.119}$$

In practice, the matrix multiplications are never performed literally. The connectivity and unreduced stiffness matrices are highly structured, making it possible to write specialized algorithms for each equation given above. This dramatically increases the overall computation speed of the assembly process.

2.6 Applications

This section discusses some of the applications of the TEM modelling approach. All applications require global model assembly, and, consequently, a general TEM structural modelling code has been developed.

2.6.1 Modal frequencies

In many cases, all that is required from a structural model is a set of modal frequencies. While the TEM methodology provides significantly more information, it is nonetheless possible to obtain modal frequencies using an algorithm developed by Wittrick (1971). This robust algorithm uses information about the stiffness matrix, evaluated at a trial frequency, to determine the number of modes whose frequencies are below the trial frequency. Also required by the algorithm are the modal frequencies of the individual elements with all boundary displacements constrained to zero. The algorithm is designed for undamped structures only, and additional root searching techniques are required in the analysis of damped structures. Even in damped cases, however, the algorithm provides a reasonable initial estimate of the location of the damped modal frequencies. This algorithm was not implemented in this research, as adequately accurate modal information was available from plots of appropriate transfer functions, as described below.

2.6.2 Frequency response and transfer functions

The primary advantage of the TEM approach is its ability to provide the exact transfer function matrix at any frequency of interest. This is obtained by numerically inverting the dynamic stiffness matrix. The stiffness matrix, K(s), represents a matrix of complex impedances relating generalized boundary forces to boundary displacements. Consequently, G(s) is a matrix of complex admittances, and is often called the dynamic flexibility matrix.

The transfer functions of cantileveled axial rods and Bernoulli-Euler beams with various damping models are shown in Fig. 2-12. For the rod, the input is an applied force on the free end and the output is the axial deflection at that end. Similarly, for the beam, the input is an applied

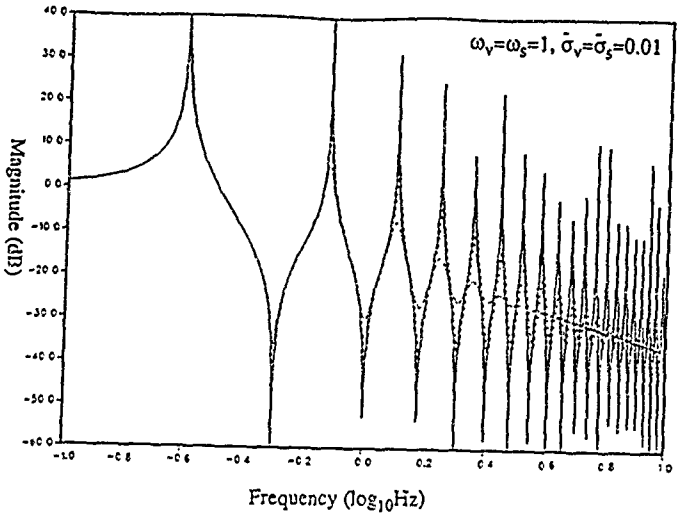

(a)

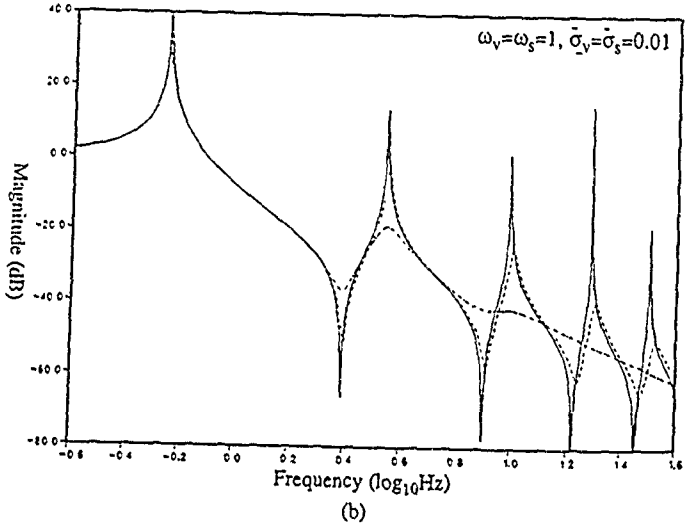

(b)

Fig. 2-12: Transfer functions of simple cantilevered element without damping (——), with Voigt damping (- · -), and with square root damping (- - -): (a) Axial tip force to axial tip displacement, (b) Transverse tip force to transverse tip displacement.

transverse force on the free end and the output is the transverse deflection at that end. It should be noted that the accuracy of these transfer functions extends arbitrarily high in frequency, insofar as the mathematical models represent the actual physical system.

In order to demonstrate the capabilities and advantages of the TEM methodology, a reasonably complex structure was analyzed. The Spacecraft COntrol Laboratory Experiment (SCOLE) model is a three dimensional asymmmetric structure proposed by NASA as a design challenge by Taylor (1986). It consists of a rigid shuttle and hexagonal truss antenna connected by a flexible mast, as shown in Fig. 2-13. Previous authors have treated the antenna as being rigid. In this effort, however, the flexibility of the antenna is considered. The TEM model thus contains thirteen beam elements (the mast and twelve antenna elements) and a six degree of freedom rigid mass representing the shuttle. In addition to the six rigid degrees of freedom, a total of 52 partial differential equations, incorporating axial, bending and torsional modes, are modeled. For comparison, the SCOLE model was also analysed using ASTROS, which incorporates a finite element algorithm similar to that found in NASTRAN. For the finite element model, the mast was divided into 32 equal elements, and each of the antenna beams was divided into four lumped elements, leading to 480 degrees of freedom.

Figure 2-14 compares the transfer functions from a torque applied to the shuttle about the axis of the mast to various points along the mast and antenna. The TEM and FEM models agree rather well at low frequencies. However, it is clear that the finite element model becomes inaccurate beyond the first few modes. What is considerably more striking is the relative computation time requred to generate the transfer functions shown. On a micro-VAX machine, the TEM analysis required approximately one hour of CPU time, in contrast with several *days* of CPU time for the FEM approach. This remarkable acceleration is due primarily to the reduction of the total degrees of freedom in the model, which is associated with the lack of spatial discretization of the beam elements. Since the computation time associated with matrix inversion is roughly

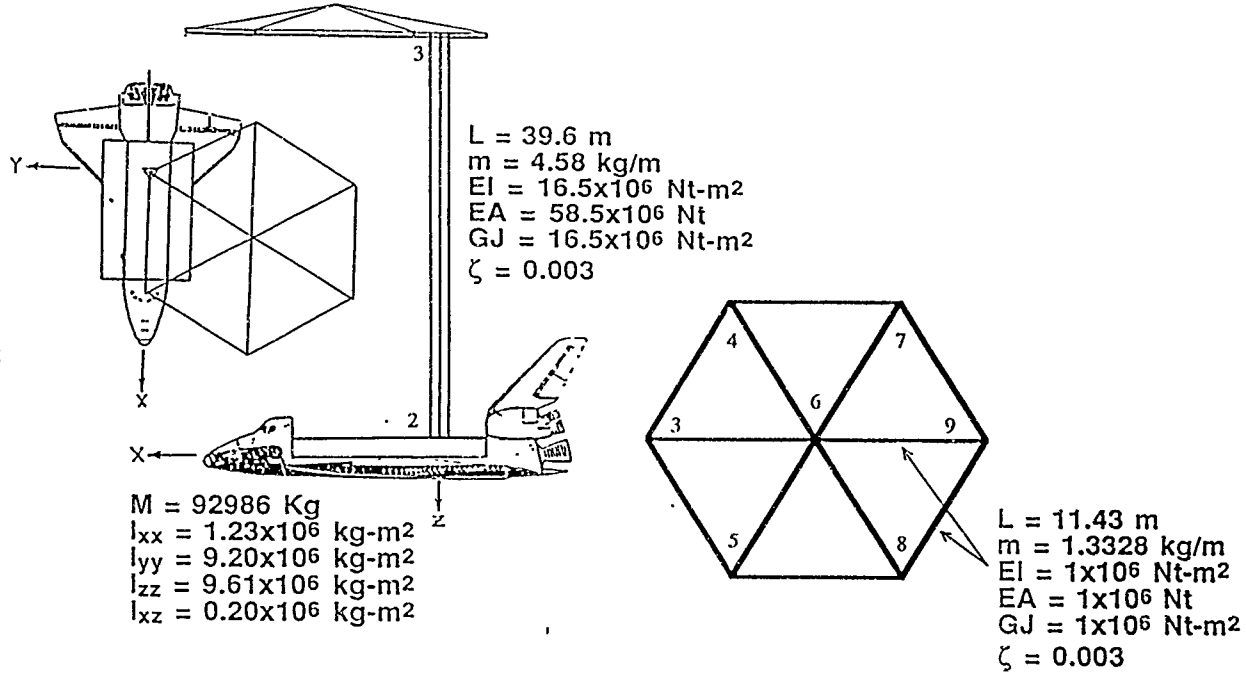

Fig. 2-13: Schematic of the SCOLE structural system with flexible antenna model. Node numbers are indicated.

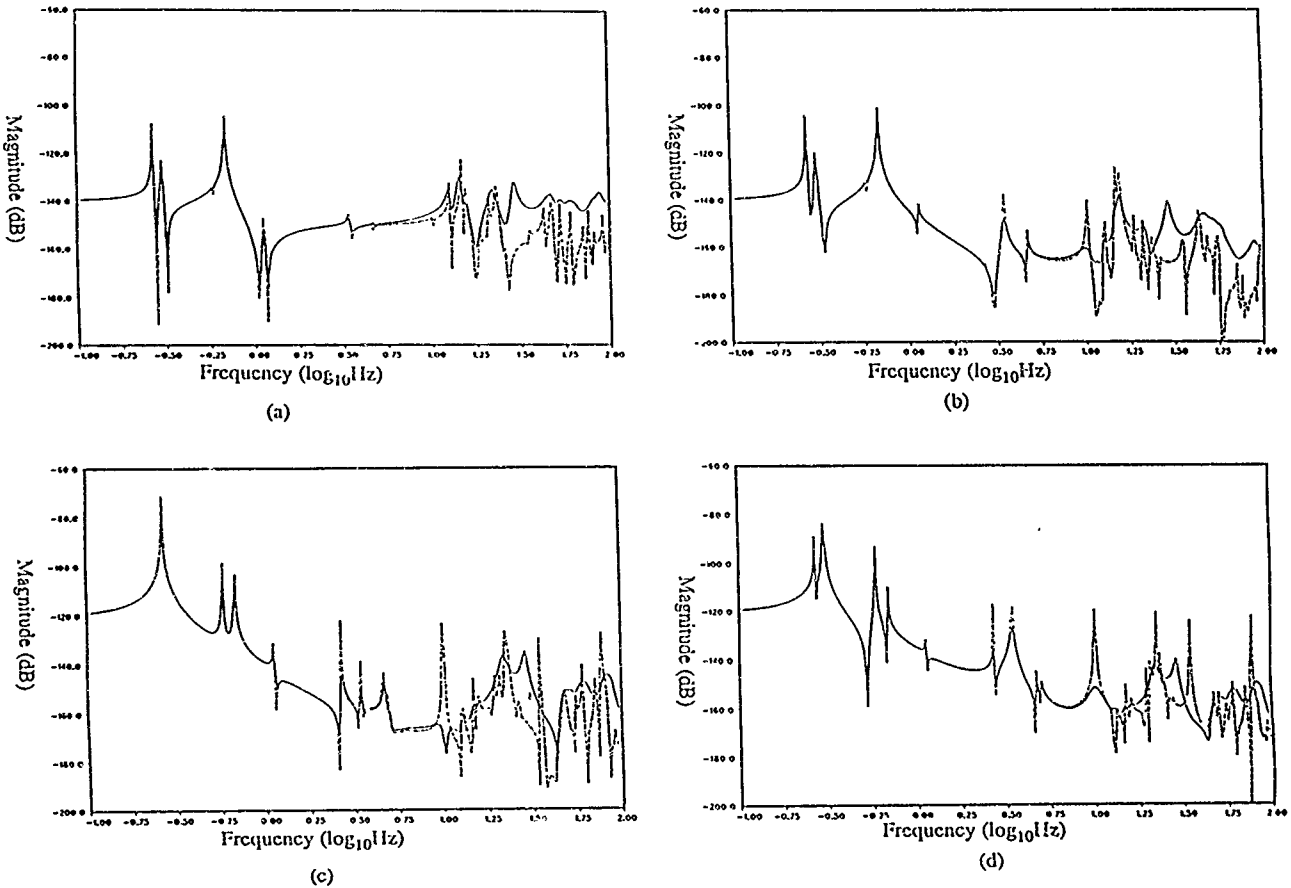

Fig. 2-14: Transfer functions from yaw torque on shuttle to various points on SCOLE model as determined by TEM model (——) and finite element model (- · -): (a) rotation of node 3 about z-axis, (b) rotation of node 6 about z-axis, (c) translation of node 6 in x-direction, (d) translation of node 6 in y-direction.

proportional to the cube of the dimension of the matrix, the reduction in total degrees of freedom has a profound effect on computaion time.

2.6.3 Time-domain simulation

A final application of the TEM approach for structural analysis is in the time-domain simulation of structural responses. This is accomplished via the inverse Laplace transform algorithm presented in Sec. 2.2. The flexibility matrix is evaluated at a finite set of N frequencies, and is multiplied by the global force vector, which contains the Laplace transforms of the forcing functions evaluated at those same frequencies. The resulting displacement vectors are then collected, and the algorithm generates the time-domain responses evaluated at a set of 2N points in time.

Fig. 2-15 compares the time-domain simulations of a simple axial rod and a Mindlin-Herrmann rod. The dispersive effects of the higher order model are apparent. Likewise, Fig. 2-16 compares the Bernoulli-Euler and Timoshenko beam models. Here, the effect of finite disturbance propagation velocity is the primary distinction between the models.

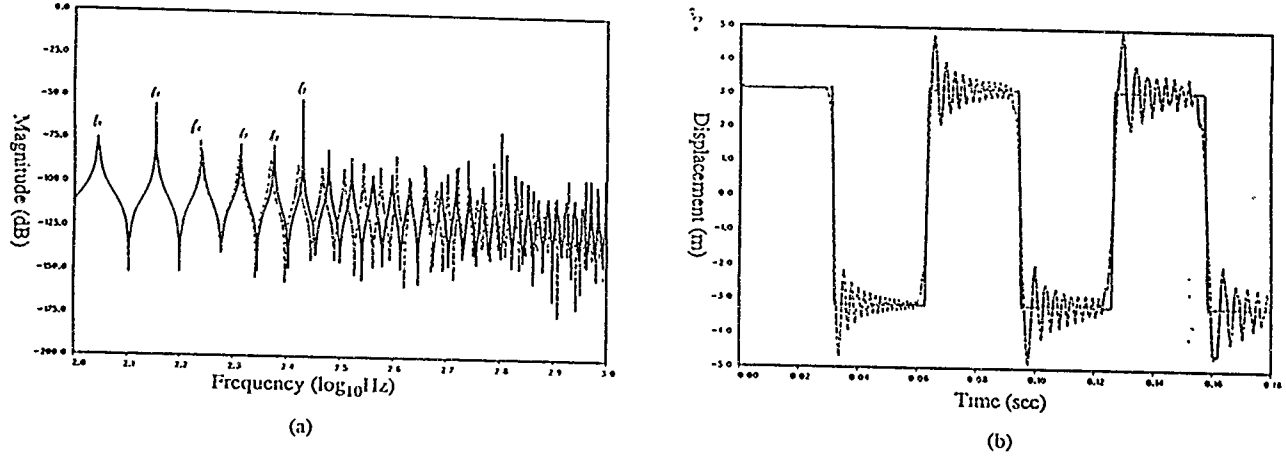

Fig. 2-15: Comparison between simple axial rod model (——) and Mindlin-Herrmann rod model (- · -): (a) Frequency response of cantilevered rod from tip force to tip displacement, (b) Time-domain response of rod impacted with unit tip impulse.

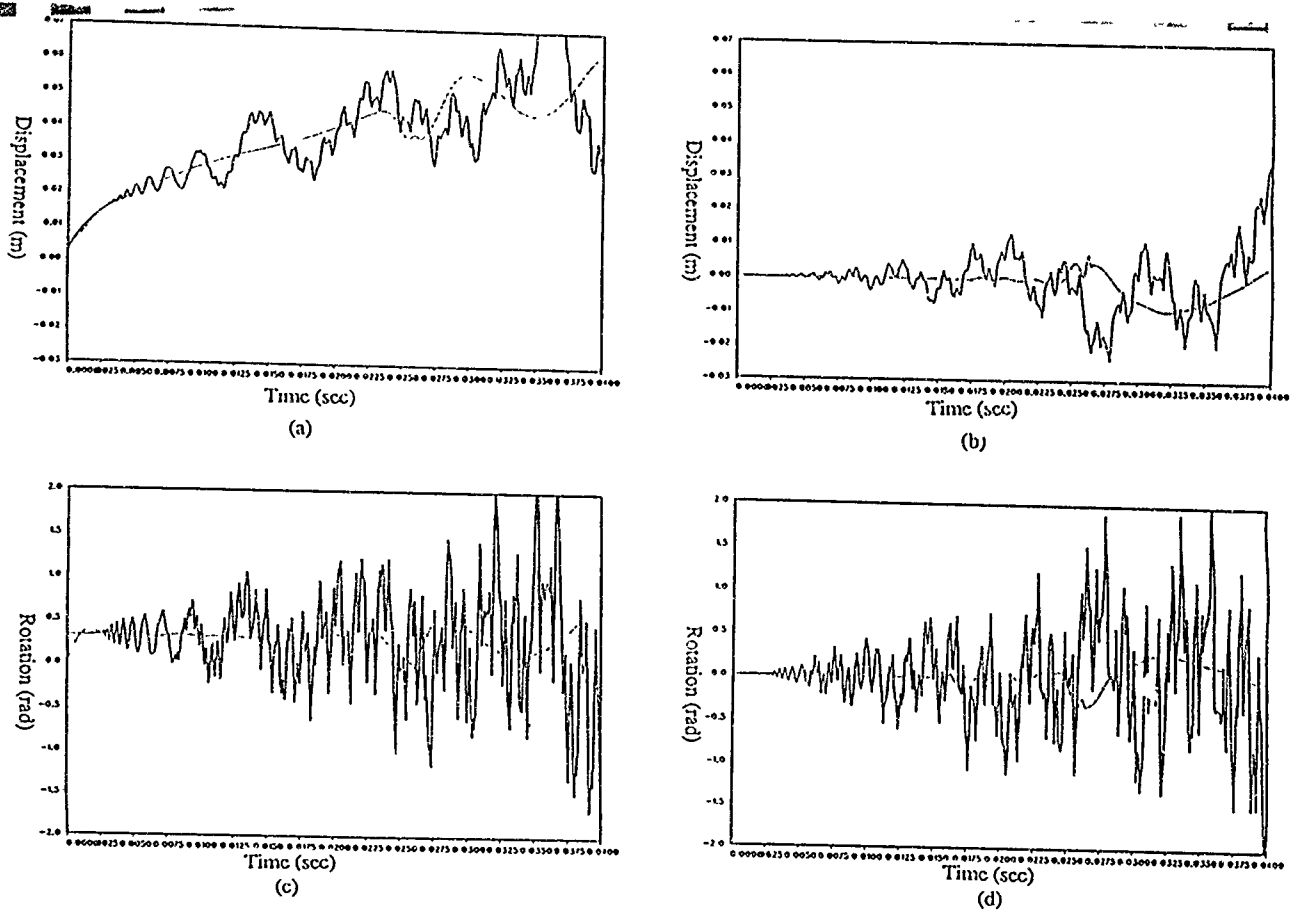

Fig. 2-16: Time-domain responses of free-free beam element impacted with unit transverse impulse on left end using Bernoulli-Euler (——) and Timoshenko (- · -) models: (a) Transverse deflection of left end, (b) transverse deflection of right end, (c) rotation of left end, (d) rotation of right end.

3 MULTIBODY TEM FORMULATION

The TEM formulation described in Chapter 2 provides an exact PDE model of complex structures with small motions. Because the nodal displacements are all referenced to the inertial frame, the small deformation assumption for the elastic deformation also implies small rigid body motion of the total structure. To allow larger ranges of motion at articulated joints, one can embed the element reference frames at the undeformed element location, which may have both rigid body rotational and translational motion. This type of approach has been used in multibody tools such as DISCOS, TREETOPS, DADS and ADAMS. As shown in the following sections, the coupling of the rigid and elastic degrees of freedom results in a set of integro-partial differential equations. The formulation will be derived using a planar example. The extension to three dimensions should be straightforward.

3.1 Mathematical Model

3.1.1 Equations of Motion

Consider a single uniform beam, cantilevered to a rigid mass, as shown in Fig. 3-1. The beam's coordinate frame is fixed to the rigid mass, which can undergo rigid body motion. For simplicity, the motion of the system is assumed to be planar. Torques and forces can be applied to either end of the beam/mass system. The equations of motion will be derived using Hamilton's principle.

The vector from the inertial origin to an arbitrary point on the beam is given by

$$p = \begin{bmatrix} X \\ Y \end{bmatrix} + \begin{bmatrix} x+v_x \\ v_y \end{bmatrix} \tag{3.1}$$

where all the vectors are expressed in body coordinates. The velocity of the point is given by

$$\dot{p} = \begin{bmatrix} V_x \\ V_y \end{bmatrix} + \begin{bmatrix} \dot{v}_x - \omega v_y \\ \dot{v}_y + \omega(x+v_x) \end{bmatrix} \tag{3.2}$$

where

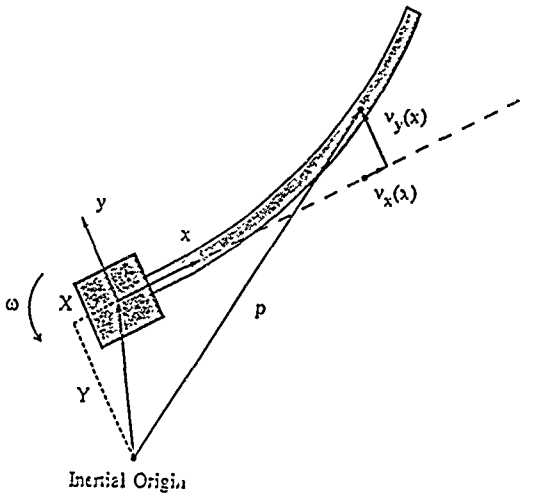

(a)

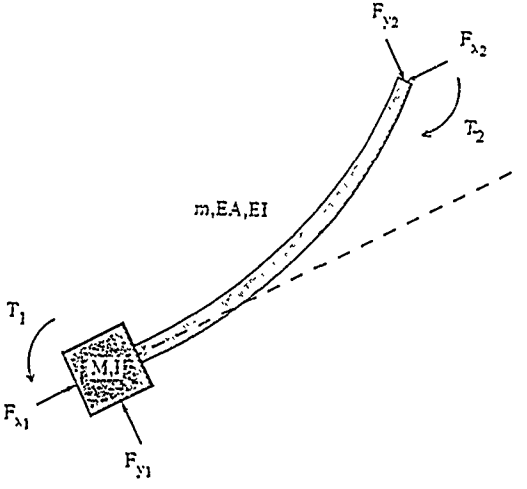

(b)

Fig. 3-1: Beam cantilevered to rigid mass: (a) Deformation geometry, (b) Physical properties and applied forces and torques.

$$\begin{bmatrix} V_x \\ V_y \end{bmatrix} = \begin{bmatrix} \dot{X} - \omega Y \\ \dot{Y} + \omega X \end{bmatrix} \tag{3.3}$$

The kinetic energy for both the rigid mass and the beam can then be written

$$T = \tfrac{1}{2}M\left[V_x^2+V_y^2\right] + \tfrac{1}{2}m\int_0^L \left[V_x^2 + \dot{v}_x^2 + \omega^2\dot{v}_y^2 + 2\dot{v}_x V_x - 2\omega v_y V_x - 2\dot{v}_x\omega v_y \right.$$
$$\left. + V_y^2 + \dot{v}_y^2 + \omega^2(x+v_x)^2 + 2\dot{v}_y V_y + 2\omega(x+v_x)V_y + 2\dot{v}_y\omega(x+v_x)\right] dx \tag{3.4}$$

where M and I are the mass and inertia, respectively, of the lumped mass, and m is the mass per unit length of the beam. The potential energy due to bending and axial extension is given by

$$U = \tfrac{1}{2}EI\int_0^L \left[\frac{\partial^2}{\partial x^2}v_y(x)\right]^2 dx + \tfrac{1}{2}EA\int_0^L \left[\frac{\partial}{\partial x}v_x(x)\right]^2 dx \tag{3.5}$$

Virtual work due to the external loads is given by

$$\delta W = (F_{x_1}-F_{x_2})\delta X + (F_{y_1}-F_{y_2})\delta Y + \left[T_1 - T_2 + XF_{y_1} - Y(F_{x_1}-F_{x_2}) - (X+L)F_{y_2}\right]\delta\theta$$
$$+ \left[YF_{x_2} - (X+L)F_{y_2} - T_2\right]\delta v_y'(L) - F_{y_2}\delta v_y(L) \tag{3.6}$$

One can then invoke Hamilton's priciple:

$$\int_{t_1}^{t_2}\left[\delta(T-U)+\delta W\right]dt = 0, \qquad \left.\begin{matrix} \delta v_y = 0 \quad 0\le x\le L \\ \delta X = \delta Y = \delta\theta = 0 \end{matrix}\right\} \quad t=t_1,t_2 \tag{3.7}$$

Substituting the kinetic and potential energies into Eq. (3.7), performing the appropriate variational differentiation, and collecting the coefficients of δX, δY, $\delta\theta$, δv_x, and δv_y, one can obtain the following set of integro-partial differential equations:

$$(I+\tfrac{1}{3}mL^3)\dot{\omega} + \tfrac{1}{2}mL^2\dot{V}_y + m\int_0^L x\,\ddot{v}_y(x)\,dx = T_1 - T_2 - LF_{y_2} \tag{3.8}$$

$$(M+mL)\dot{V}_x + m\int_0^L \ddot{v}_x(x)\,dx = F_{x_1}-F_{x_2} \tag{3.9}$$

$$\frac{1}{2}mL^2\dot{\omega} + (M+mL)\dot{V}_y + m\int_0^L \ddot{v}_y(x)\,dx = F_{y_1}-F_{y_2} \tag{3.10}$$

$$m\dot{V}_x + m\ddot{v}_x(x) = EA\frac{\partial^2}{\partial x^2}v_x(x) \tag{3.11}$$

$$mx\dot{\omega} + m\dot{V}_y + m\ddot{v}_y(x) = -EI\frac{\partial^4}{\partial x^4}v_y(x) \tag{3.12}$$

The nonlinear terms have been ignored in the above equations, assuming small rigid body velocities and small elastic deformations.

3.1.2 Solution for the Integral-Partial Differential Equations

Equations (3.8) through (3.10) are integral-differential equations, and Eqs. (3.11) and (3.12) are partial differential equations. The set of equations can be reduced by transforming to the Laplace frequency-domain, solving Eqs. (3.11) and (3.12) for v_x and v_y in terms of ω, V_x, and V_y, and then substituting the result into Eqs. (3.8) through (3.10).

For axial extension, let us define the axial state vector in Laplace transform space by

$$u_a(\lambda) = \left[v_\lambda(x) \;\; EA\frac{\partial}{\partial x}v_\lambda(x)\right]^T \tag{3.13}$$

Equation (3.11) can then be replaced by the axial state equation

$$\frac{\partial}{\partial x}u_a(x) = C_a\,u_a(x) + m\,s\,V_x\,p_2 \tag{3.14}$$

which has the following matrix exponential solution:

$$u_a(x,s) = e^{C_a x}u_a(0,s) + m\,s\,V_x\int_0^x e^{C_a(x-\xi)}\,d\xi\;p_2 \tag{3.15}$$

where

$$C_a(s) = \begin{bmatrix} 0 & \frac{1}{EA} \\ ms^2 & 0 \end{bmatrix}, \quad p_1 = \begin{bmatrix} 1 \\ 0 \end{bmatrix}, \quad p_2 = \begin{bmatrix} 0 \\ 1 \end{bmatrix} \tag{3.16a,b,c}$$

The integral of v_x, which is needed in the transformed version of Eq. (3.9), is then found to be

$$\int_0^L v_x(x,s)\,dx = p_1^T \int_0^x e^{C_a x}\,dx\; u_a(0,s) + p_1^T m s V_x \int_0^L \int_0^x e^{C_a \xi}\,d\xi\,dx\; p_2 \tag{3.17}$$

Similarly, for transverse bending, let us define the bending state vector in transform space by

$$u_b(x) = \left[v_y(x) \;\; \frac{\partial}{\partial x} v_y(x) \;\; EI\frac{\partial^2}{\partial x^2} v_y(x) \;\; EI\frac{\partial^3}{\partial x^3} v_y(x) \right]^T \tag{3.18}$$

The bending equation is then given by

$$\frac{\partial}{\partial x} u_b(x) = C_b\, u_b(x) - [m x s \omega + m s V_y]\, p_4 \tag{3.19}$$

with the exponential matrix solution

$$u_b(x,s) = e^{C_b x} u_b(0,s) - m s \omega \int_0^x \xi e^{C_b(x-\xi)}\,d\xi\; p_4 - m s V_y \int_0^x e^{C_b(x-\xi)}\,d\xi\; p_4 \tag{3.20}$$

where

$$C_b = \begin{bmatrix} 0 & 1 & 0 & 0 \\ 0 & 0 & \frac{1}{EI} & 0 \\ 0 & 0 & 0 & 1 \\ -ms^2 & 0 & 0 & 0 \end{bmatrix}, \quad p_1 = \begin{bmatrix} 1 \\ 0 \\ 0 \\ 0 \end{bmatrix}, \quad p_4 = \begin{bmatrix} 0 \\ 0 \\ 0 \\ 1 \end{bmatrix} \tag{3.21a,b,c}$$

The two integrals of v_y in the Laplace transform of Eqs. (3.8) and (3.10) can then be written as

$$\int_0^L v_y(x,s)\,dx = p_1^T \int_0^x e^{C_b x}\,dx\; u_b(0,s) - p_1^T m s \omega \int_0^{Lx}\int_0^{Lx} \xi e^{C_b(x-\xi)}\,d\xi\,dx\; p_4$$

$$- p_1^T m s V_y \int_0^{Lx}\int_0^{Lx} e^{C_b(x-\xi)}\,d\xi\,dx\; p_4 \qquad (3.22)$$

and

$$\int_0^L x v_y(x,s)\,dx = p_1^T \int_0^x x e^{C_b x}\,dx\; u_b(0,s) - p_1^T m s \omega \int_0^L x \int_0^x \xi e^{C_b(x-\xi)}\,d\xi\,dx\; p_4$$

$$- p_1^T m s V_y \int_0^L x \int_0^x e^{C_b(x-\xi)}\,d\xi\,dx\; p_4 \qquad (3.23)$$

The integral expressions are substituted into Eqs. (3.8) through (3.10), and the coefficients of $s\omega$, sV_x, sV_y, s^2v_x, and s^2v_y are collected into a matrix. Equations (3.15) and (3.20) are evaluated at $x=L$, the left and right sides interchanged, and the coefficients are again collected into a matrix, Φ. This yields an equation of motion of the form

$$\Phi \begin{bmatrix} s\,\gamma(s) \\ s^2 u_a(0,s) \\ s^2 u_b(0,s) \end{bmatrix} = f(s) \qquad (3.24)$$

where

$$\gamma(s) = \left[\omega(s)\;\; V_x(s)\;\; V_y(s)\right]^T \qquad (3.25)$$

$$f(s) = \left[T_1 - T_2 - LF_{y2}\quad F_{x1} - F_{x2}\quad F_{y1} - F_{y2}\quad u_a(L,s)^T\quad u_b(L,s)^T\right]^T \qquad (3.26)$$

Let us now replace the axial states, $u_a(0,s)$, and the bending states, $u_b(0,s)$, on the left of Eq. (3.24) by the nodal displacements at the two ends of the beam/mass model. The

transformation is done by partitioned matrix solution of Eqs. (3.15) and (3.20) for $EAv_x'(0)$ and $[EIv_y''(0)\ EIv_y'''(0)]$, respectively. As a result, the axial and bending partitions of the force vector are replaced by nodal forces. These nodal forces are equated to the external forces and torques by the equations

$$EA\begin{bmatrix} v_x'(0) \\ v_x'(L) \end{bmatrix} = \begin{bmatrix} msV_x - F_{x_1} \\ -F_{x_2} \end{bmatrix} \tag{3.27}$$

$$EI\begin{bmatrix} v_y''(0) \\ v_y'''(0) \\ v_y''(L) \\ v_y'''(L) \end{bmatrix} = \begin{bmatrix} Is\omega - T_1 \\ -msV_y + F_{x_1} \\ -T_2 \\ F_{y_2} \end{bmatrix} \tag{3.28}$$

Terms in Eqs. (3.27) and (3.28) involving $s\omega$, sV_x and sV_y are moved to the right hand side. Finally, the equation of motion becomes

$$\tilde{\Phi}\, sw = \tilde{f} \tag{3.29}$$

where

$$w = \left[\gamma^T \quad s\left[v_x(0)\ v_x(L)\right] \quad s\left[v_y(0)\ v_y'(0)\ v_y(L)\ v_y'(L)\right]\right]^T \tag{3.30}$$

$$\tilde{f} = H_I\begin{bmatrix} T_1 \\ F_{x_1} \\ F_{y_1} \end{bmatrix} + H_O\begin{bmatrix} T_2 \\ F_{x_2} \\ F_{y_2} \end{bmatrix} \tag{3.31}$$

$$H_I = \begin{bmatrix} 1 & 0 & 0 & 0 & 0 & -s^2 & 0 & 0 & 0 \\ 0 & 1 & 0 & -s^2 & 0 & 0 & 0 & 0 & 0 \\ 0 & 0 & 1 & 0 & 0 & 0 & s^2 & 0 & 0 \end{bmatrix} \tag{3.32}$$

$$H_O = \begin{bmatrix} -1 & 0 & 0 & 0 & 0 & 0 & 0 & -s^2 & 0 \\ 0 & -1 & 0 & 0 & -s^2 & 0 & 0 & 0 & 0 \\ -L & 0 & -1 & 0 & 0 & 0 & 0 & 0 & s^2 \end{bmatrix} \tag{3.33}$$

3.1.3 Connection to Adjacent Elements

Let us now consider the beam/mass model as one element of a larger truss/frame structure, as shown in Fig. 3-2. The external forces and torques at the two ends of the beam can be expressed as the sum of applied forces/torques and constraint forces/torques:

$$\begin{bmatrix} T_1 \\ F_{x1} \\ F_{y1} \end{bmatrix} = g_{Ij} + B_{Ij}^T \tilde{\Phi}_{Ij} \lambda_{Ij} \tag{3.34}$$

$$\begin{bmatrix} T_2 \\ F_{x2} \\ F_{y2} \end{bmatrix} = g_{Oj} + \tilde{\Phi}_{Oj} \lambda_{Oj} \tag{3.35}$$

where

$$B_{Ij} = \begin{bmatrix} 1 & 0 & 0 \\ 0 & \cos\theta_{Ij} & -\sin\theta_{Ij} \\ 0 & \sin\theta_{Ij} & \cos\theta_{Ij} \end{bmatrix} \tag{3.36}$$

The vector g contains applied forces/torques, the subscripts $(_{Ij})$ and $(_{Oj})$ indicate inboard and outboard joints, respectively, of the j'th body, the λ vectors are the constraint forces/torques at the joints, B_{Ij} is a matrix of kinematic coefficients which transforms the constraint forces/torques from the coordinates of the inboard body to the coordinates of the current body, θ_{Ij} is the angle at the joint, and $\tilde{\Phi}$ is a selection matrix which picks out which degrees of freedom are to be constrained at the joint. Without loss of generality, Eq. (3.36) has arbitrarily assumed that the constraint forces at the inboard joint are in the inboard body's coordinate system. Substitution of Eqs. (3.34) and (3.35) into Eq. (3.29) give, for the j-th body,

$$\tilde{\Phi}_j \, sw_j = \tilde{g}_j + H_{Ij} B_{Ij}^T \tilde{\Phi}_{Ij} \lambda_{Ij} + \sum_O H_{Oj} \tilde{\Phi}_{Oj} \lambda_{Oj} \tag{3.37}$$

where

$$\tilde{g}_j = H_{Ij} g_{Ij} + H_{Oj} g_{Oj} \tag{3.38}$$

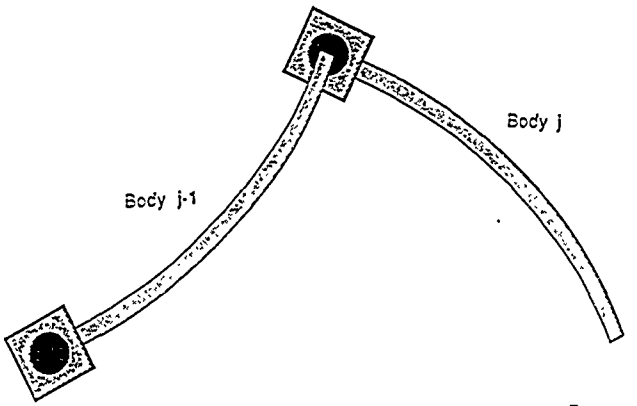

Fig. 3-2: Example joint connection.

The summation in Eq. (3.37) is carried out over all of the outboard joints for tree topologies. Note that, for an end body, there is only an inboard hinge and no outboard hinge, so that the last term in Eq. (3.37) disappears.

The hinge kinematics relate the absolute velocities of adjacent bodies to the relative velocities at the adjoining hinge. For the inboard hinge of the j-th body, we have

$$\Phi_{Ij}\dot{\beta}^{f}_{Ij} + \bar{\Phi}_{Ij}\dot{\alpha}_{Ij} = [B_{Oj}\ 0]\,w_j + B_{O,j-1}[I\ P]\,w_{j-1} \tag{3.39}$$

where

$$B_{Oj} = \begin{bmatrix} -1 & 0 & 0 \\ 0 & -1 & 0 \\ -L & 0 & -1 \end{bmatrix}_j \tag{3.40}$$

$$\dot{P} = \begin{bmatrix} 0 & 0 & 0 & 0 & 0 & 1 \\ 0 & 1 & 0 & 0 & 0 & 0 \\ 0 & 0 & 0 & 0 & 1 & 0 \end{bmatrix} \tag{3.41}$$

The matrix Φ is a selection matrix for the unconstrained degrees of freedom, $\dot{\alpha}$ is a vector of rheonomic constraints, $\dot{\beta}^{f}$ is a vector of unconstrained relative hinge velocities, and B_{Oj} is a matrix of kinematic coefficients that relate body velocities to the outboard joint. For the base body (j=1), the last term in Eq. (3.39) disappears, because the base body's inboard body is the inertial origin, which, by definition, has zero velocity.

3.1.4 Recursion Solution for the Total Structure

We now combine the dynamics, represented by Eq. (3.37), and the kinematics, represented by Eq. (3.39). Let us consider an end body (j=e) and solve the kinematics equation for γ:

$$\gamma_e = B_{Ie}^{-1}\left[\Phi_{Ie}\dot{\beta}^{f}_{Ie} + \bar{\Phi}_{Ie}\dot{\alpha}_{Ie} - B_{O,e-1}[I\ P]\,w_{e-1}\right] \tag{3.42}$$

Equation (3.42) is augmented by the nodal velocities and re-written as

$$w_e = \Psi_e\beta_e + \begin{bmatrix} I \\ 0 \\ 0 \end{bmatrix} B_{Ie}^{-1}\left[\bar{\Phi}_{Ie}\dot{\alpha}_{Ie} - B_{O,e-1}[I\ P]\,w_{e-1}\right] \tag{3.43}$$

where

$$\Psi_e = \begin{bmatrix} B_{Ie}^{-1}\Phi_{Ie} & 0 & 0 \\ 0 & I & 0 \\ 0 & 0 & I \end{bmatrix} \tag{3.44a}$$

$$\beta_e = \left[\dot{\beta}_{Ie}^{fT} \quad s[v_x(0)\ v_x(L)] \quad s[v_y(0)\ v_y'(0)\ v_y(L)\ v_y'(L)]\right]^T \tag{3.44b}$$

Equation (3.43) expresses the body j velocities in terms of the velocities of its inboard joint and inboard body.

Substitution of Eq. (3.43) into the dynamics equation, pre-multiplying by Ψ_e^T and solving for β_e gives an expression in terms of inboard body velocities and inboard hinge constraint forces/torques:

$$\beta_e = [\Psi_e^T \tilde{\Phi}_e \Psi_e]^{-1} \Psi_e^T \left\{ \left[\tilde{g}_e + H_{Ie} B_{Ie}^T \tilde{\Phi}_{Ie} \lambda_{Ie}\right] \frac{1}{s} - \tilde{\Phi}_e \begin{bmatrix} I \\ 0 \\ 0 \end{bmatrix} B_{Ie}^{-1} \left[\dot{\Phi}_{Ie} \dot{\alpha}_{Ie} - B_{O,e-1} [I\ P] w_{e-1}\right] \right\} \tag{3.45}$$

The unknown constraint torques can be solved for by pre-multiplying Eq. (3.39) by $\tilde{\Phi}_{Ie}^T$ and substituting Eq. (3.37):

$$\lambda_{Ie} = \tilde{J}_e \tilde{\Phi}_{Ie}^T \left[\dot{\Phi}_{Ie} \dot{\alpha}_{Ie} - \frac{1}{s} [B_{Ie}\ 0] \tilde{\Phi}_e^{-1} \tilde{g}_e - B_{O,e-1} [I\ P] w_{e-1}\right] \tag{3.46}$$

where

$$\tilde{J}_e = \left[\frac{1}{s} \dot{\Phi}_{Ie}^T [B_{Ie}\ 0] \tilde{\Phi}_e^{-1} H_{Ie} B_{Ie}^T \tilde{\Phi}_{Ie}\right]^{-1} \tag{3.47}$$

The unconstrained relative joint velocity term has disappeared because $\tilde{\Phi}_{Ie}$ and Φ_{Ie} are orthogonal to each other.

Equations (3.43), (3.45) and (3.46) are the recursion relations for the end body. Given the velocities of body e-1, one can compute the constraint forces/torques via Eq. (3.46), substitute into Eq. (3.45) to get the relative velocities, and substitute into Eq. (3.43) to get the body velocities.

To obtain the recursion for intermediate bodies in the middle of the chain or tree topology, let us consider the e-1 body as the current body and relate its velocities to its inboard hinge. The interconnection constraint forces/torques have been defined so that $\lambda_{I,j+1} = \lambda_{Oj}$. We can therefore substitute Eq. (3.46) into Eq. (3.37) with j equal to e-1, and rearrange to yield

$$\Phi^*_{e-1}\, sw_{e-1} = g^*_{e-1} + H_{I,e-1}\, B_{I,e-1}{}^T \bar{\Phi}_{I,e-1}\, \lambda_{I,e-1} \tag{3.48}$$

where

$$\Phi^*_{e-1} = \tilde{\Phi}_{e-1} + \sum_{O} \frac{1}{s} H_{Oe-1}\, \bar{\Phi}_{Ie}\, \tilde{J}_e\, \bar{\Phi}^T_{Ie} B_{Oe-1}\, [I\ P] \tag{3.49}$$

$$g^*_{e-1} = \tilde{g}_{e-1} + \sum_{O} H_{Oe-1}\, \bar{\Phi}_{Ie}\, \tilde{J}_e\, \bar{\Phi}^T_{Ie} \left\{ \bar{\Phi}_{Ie}\, \dot{\alpha}_{Ie} - \frac{1}{s} [B_{Ie}\ 0]\, \tilde{\Phi}^{-1}_e\, \tilde{g}_e \right\} \tag{3.50}$$

Equation (3.50) is now in the same form as for an end body, and the same derivation can be followed to produce a recursion for the e-1, as well as all intermediate bodies. Recall that at the base body (j=1) the vector w_{j-1}, which corresponds to the inertial frame, disappears because the inertial origin has zero velocity. This gives the initial value for the forward recursion to begin from the base body to the end bodies. The multibody algorithm thus involves a backward recursion to compute the equivalent matrices and vectors, Φ^* and g^*, and a forward recursion to compute the w_j vectors.

3.2 Discussion

The mathematical formulation has been presented for a linearized model. The linearization has been necessary for the Laplace transformation to be applied in solving the PDE models. It is felt that, even though the equations have been linearized, the range of angular motion that can be simulated has been enlarged when compared to the cartesian-based TEM models. The derivation was shown for a planar model for ease of presentation. The extension to three dimensional motion should be straightforward.

The current formulation is applicable to chain and tree topologies. In order for this formulation to be applied to trusses and frames, it must be extended to handle closed topological loops. This type of formulation has been performed for modally based dynamic models by Chun (1991) and can be easily adapted to PDE models.

Arbitrarily large angular motion of the total structure, as well as articulated joints, requires a nonlinear model for the correct description of both the dynamics of the motion and the kinematics at the joints. Future efforts should explore the use of perturbation techniques that allow the Laplace transform to be used while still including the effects of the nonlinear terms.

4 CONTROL DESIGN BASED ON TEM MODELS

The exactness of the TEM formulation makes it possible to achieve remarkable performance in open-loop slewing maneuvers of flexible structures. This is the subject of Section 4.1 of this chapter. Unfortunately, because the TEM methodology does not immediately yield a state-space representation of the structual system, traditional state-space control methods are not directly applicable in the closed-loop case. (In actuality, no finite representation can exist, as the structural model is of infinite order.) Methods for achieving closed-loop control solutions without state-space models are discussed in Section 4.2.

4.1 Open-Loop Control

In this section, we develop an open-loop control algorithm that takes advantage of the quality of the structural model available via the TEM methodology. We restrict attention to finite-time, linear maneuvers with a quadratic cost functional. We also assume that the structure is initially at rest. The desired terminal state is expressed by

$$y(t_f) = y_d \tag{4.1}$$

where t_f is the maneuver time, $y(t)$ is a vector of variables of interest, and y_d contains the desired terminal values of these variables. The elements of y could include, for example, the displacement and rotation of a rigid mass on the structure, or the relative transverse deflection of a point on a flexible member. The available control forces are also collected into a single vector, $q_c(t)$, of dimension N_c. These control forces are then a subset of the global generalized forces defined by the system model. In order that these forces be continuous in time, we must impose the additional constraint

$$q_c(0) = q_c(t_f) = 0 \tag{4.2}$$

Also, the quadratic cost functional is given by

$$J = \frac{1}{2}\left[y(t_f) - y_d\right]^T R_{yy}\left[y(t_f) - y_d\right] + \frac{1}{2}\int_0^{t_f}\left[q_c(t)^T R_{qq} q_c(t) + \dot{q}_c(t)^T \tilde{R}_{qq}\dot{q}_c(t)\right] dt \qquad (4.3)$$

where R_{yy}, R_{qq}, and $\tilde{R}_{qq}$ are symmetric, positive definite weighting matrices.

We must now express the output vector in terms of the control vector via the system dynamics. This is accomplished using the convolution integral

$$y(t) = \int_0^t G_y(t-\tau)\, q_c(\tau)\, d\tau \qquad (4.4)$$

where $G_y(t)$ represents the impulse response matrix relating $y(t)$ to $q_c(t)$. This convolution integral is calculated efficiently using the inverse Laplace transform algorithm of Sec. 2.2:

$$y(t) = L^{-1}\left[G_y(s)\, q_c(s)\right] \qquad (4.5)$$

4.1.1 Band-limited control approximation

By substituting Eq. (4.4) in Eq. (4.3), we observe that the cost functional depends on $q_c(t)$ only. Setting the first variation in cost to zero therefore yields

$$\delta J = \left[\int_0^{t_f} G_y(t_f-t)\, q_c(t)\, dt - y_d\right]^T R_{yy}\left[\int_0^{t_f} G_y(t_f-t)\, \delta q_c(t)\, dt\right]$$
$$+ \int_0^{t_f}\left[q_c(t)^T R_{qq}\delta q_c(t) + \dot{q}_c(t)^T \tilde{R}_{qq}\delta\dot{q}_c(t)\right] dt = 0 \qquad (4.6)$$

The problem then lies in solving this equation for $q_c(t)$. Unfortunately, this is not a simple matter, as both the control vector and its variation appear within the integrals. However, if the control inputs are band-limited (as is often the case), a numerical solution is easily obtained. Each control input is first approximated by

$$q_{c_i}(t) = f_q(t)^T c_i\,, \quad i = 1,\ldots,N_c \qquad (4.7)$$

where $f_q(t)$ is a vector of known basis functions of time (usually sine and cosine functions), and c_i is a vector of undetermined coefficients corresponding to the i'th control input. The entire control vector can then be conveniently expressed as

$$q_c(t) = F_q(t)\, c \tag{4.8}$$

where the following definitions have been used:

$$F_q(t) = \begin{bmatrix} f_q(t)^T & & 0 \\ & f_q(t)^T & \\ 0 & & f_q(t)^T \end{bmatrix}, \quad c = \begin{bmatrix} c_1 \\ \vdots \\ c_{Nc} \end{bmatrix} \tag{4.9a,b}$$

Using this band-limited approximation, the optimal control problem is reduced to determining the coefficient vector, c. The variations in the control vector are then

$$\delta q_c(t) = F_q(t)\, \delta c, \quad \delta \dot{q}_c(t) = \dot{F}_q(t)\, \delta c \tag{4.10a,b}$$

and the constraints given by Eq. (4.2) reduce to

$$F_q(0)\, c = F_q(t_f)\, c = 0 \tag{4.11}$$

Furthermore, the vector of desired outputs is expressed by

$$y(t_f) = Y(t_f)\, c \tag{4.12}$$

where Y(t) is the basis function response matrix, and is given by

$$Y(t) = \int_0^t G_y(t-\tau)\, F_q(\tau)\, d\tau = L^{-1}\left[G_y(s)\, F_q(s)\right] \tag{4.13}$$

4.1.2 Solution without minimization

Grouping Eqs. (4.11) and (4.12) yields the matrix equation

$$\begin{bmatrix} Y(t_f) \\ F_q(0) \\ F_q(t_f) \end{bmatrix} c = \begin{bmatrix} y_d \\ 0 \\ 0 \end{bmatrix} \tag{4.14}$$

If the number of desired outputs and the number of unknown coefficients are such that the matrix in this equation is square, then c is uniquely determined. Typically, however, there are many elements in c, so that Eq. (4.14) is underdetermined. Consequently, many choices for c will meet the terminal constraints. We therefore have some freedom in choosing which particular c to use. For a given problem, the particular choice minimizes some predefined cost functional, which provides a measure of nominal performance. The next two subsections describe two such cost functionals.

4.1.3 Minimization with point constraints

We first use the cost functional given by Eq. (4.3) and adjoin the constraints given by Eq. (4.11) via two Lagrange multipliers, λ_0 and λ_f. Taking variations in c yields

$$\begin{aligned}\delta J = {} & \left[Y(t_f)c - y_d\right]^T R_{yy} Y(t_f)\,\delta c \\ & + c^T \left\{ \int_0^{t_f} \left[F_q(t)^T R_{qq} F_q(t) + \dot{F}_q(t)^T \tilde{R}_{qq} \dot{F}_q(t) \right] dt \right\} \delta c \\ & + \lambda_0^T F_q(0)\,\delta c + \lambda_f^T F_q(t_f)\,\delta c + \delta\lambda_0^T F_q(0)\,c + \delta\lambda_f^T F_q(t_f)\,c = 0 \end{aligned} \tag{4.15}$$

leading to the following matrix equation:

$$\begin{bmatrix} W & F_q(0)^T & F_q(t_f)^T \\ F_q(0) & 0 & 0 \\ F_q(t_f) & 0 & 0 \end{bmatrix} \begin{bmatrix} c \\ \lambda_0 \\ \lambda_f \end{bmatrix} = \begin{bmatrix} Y(t_f)^T R_{yy} y_d \\ 0 \\ 0 \end{bmatrix} \tag{4.16}$$

where

$$W = Y(t_f)^T R_{yy} Y(t_f) + \int_0^{t_f} \left[F_q(t)^T R_{qq} F_q(t) + \dot{F}_q(t)^T \tilde{R}_{qq} \dot{F}_q(t) \right] dt \tag{4.17}$$

This is a symmetric system, and can be solved using standard linear algebra routines.

A unique advantage of this approach is that it readily accomodates penalties in higher derivatives of both control effort and structural deformation. In the frequency-domain,

differentiation merely requires multiplication of the data by the Laplace transform variable. The inverse transformation then produces the derivative of the original signal. Higher order derivatives are obtained by multiplying by higher powers of the complex frequency. Incorporating higher derivative penalties in the traditional optimal control formulation is considerably more difficult.

It should be noted that the only approximation in the entire development involves expressing the control inputs in terms of the basis functions. The dynamics of the entire structure are accounted for, since the impulse responses are exact (insofar as the original equations represent physical reality). Also, the structural deformations are assumed to be small, so that linearization does not introduce significant errors. As a result, large angle slew maneuvers are not included in this class of problems. It is possible, however, to express structural deformations with respect to a nominal condition during a large angle slew, and then linearize about that reference, as discussed in the previous Chapter.

In an earlier analytical study by Skaar (1984), the open-loop control of a rigid mass with a flexible appendage, shown in Fig. 4-1, was studied. In his work, structural deformation penalties were not incorporated into the cost function; rather, the terminal conditions were adjoined to the cost functional as constraints. Skaar derived analytical expressions for impulse responses of the simple mass/appendage structure and thus obtained closed form optimal control solutions for the structure. Though successful for this application, his approach does not readily generalize for more complex structures. In contrast, the formulation presented here readily generalizes for realistic complex structures. Skaar's example, however, is used as a first example to validate the optimal control formulation.

The maneuver involves translating the mass a distance of 10 meters along the axis of the flexible appendage, bringing it to rest with minimal residual energy and post-maneuver drift after 20 seconds. The first case places terminal penalties on the final position and velocity of the rigid mass and on a point 4/5 of the length along the flexible appendage. A small penalty is also placed on control rate, and 17 basis functions are used to approximate the control input. The results, shown in Fig. 4-2, indicate that the terminal conditions are matched, and residual energy is

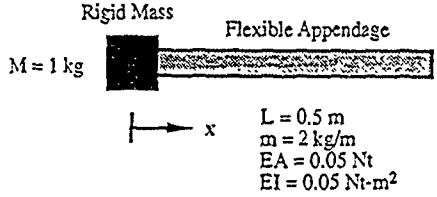

Fig. 4-1: Simple mass/flexible appendage structural model.

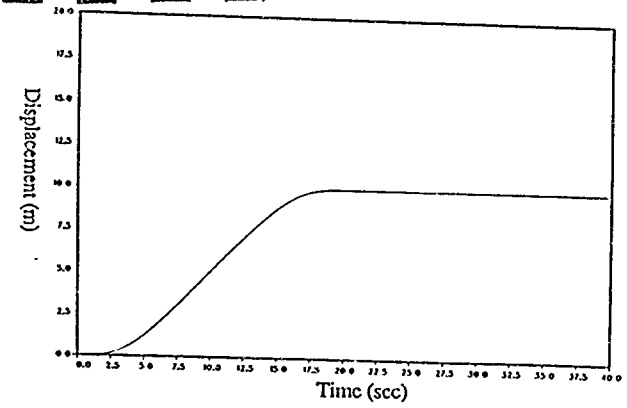

(a)

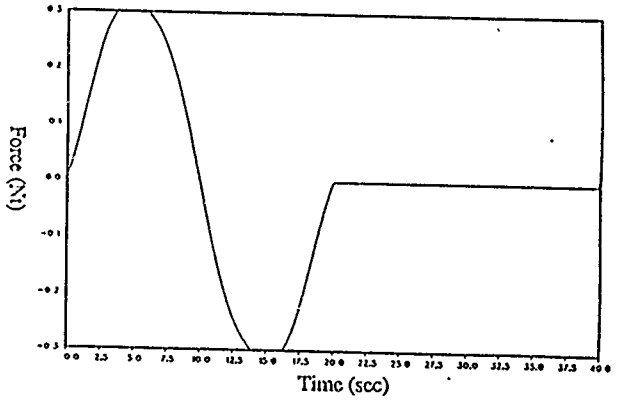

(b)

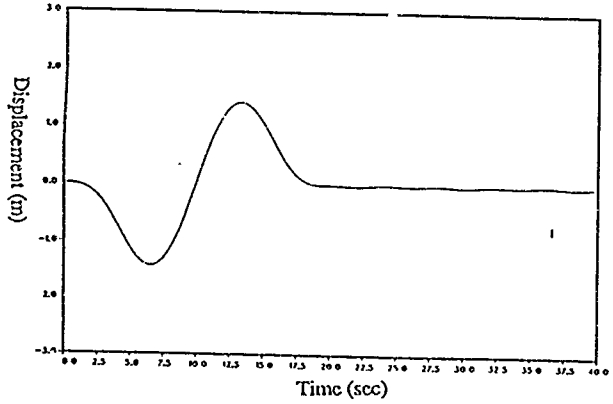

(c)

Fig. 4-2: Results of optimal maneuver of mass/flexible appendage system: (a) position of rigid mass, (b) control force applied to rigid mass, (c) deformation of tip of flexible appendage with respect to position of rigid mass.

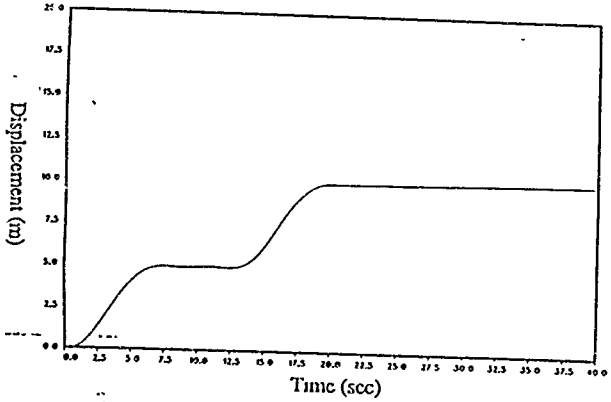

(a)

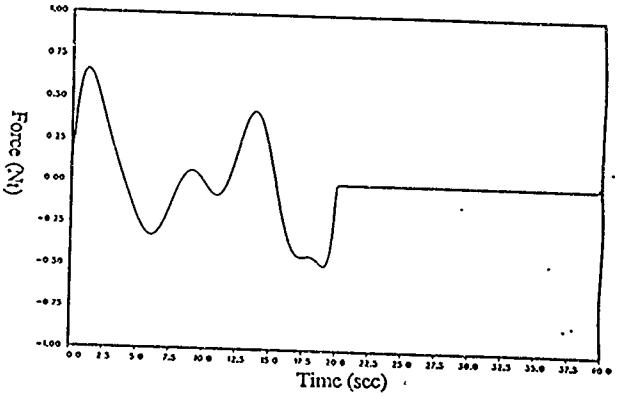

(b)

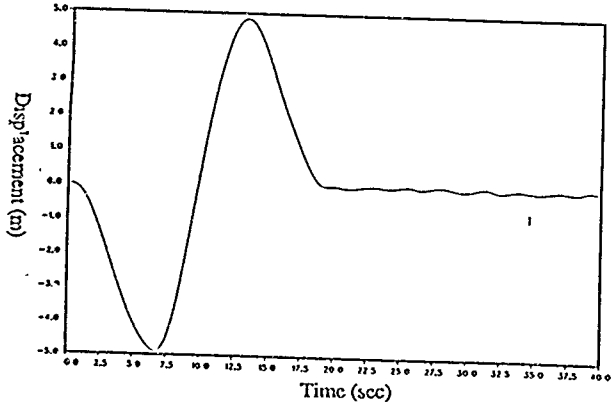

(c)

Fig. 4-3: Results of optimal maneuver of mass/flexible appendage system with reduced axial stiffness: (a) position of rigid mass, (b) control force applied to rigid mass, (c) deformation of tip of flexible appendage with respect to position of rigid mass.

negligible. In the second case, the member stiffness is reduced by a factor of four, so that the primary modal frequency of the structure corresponds approximately with the frequency of the first basis function of the control input. The results of this case, presented in Fig. 4-3, indicate that the control input has been adjusted so that excitation of the primary mode of the structure is suppressed. Again, the terminal conditions are matched, and residual internal energy is negligible.

The second example is the SCOLE structure analysed in Sec. 2.6.2. The maneuver presented here consists of a ten second, 0.1 radian rotation about the z-axis of the shuttle. This maneuver is a purely academic exercise, and is unrelated to the maneuver specified in the original design challenge. For the first case, torque controls directed along the z-axis are placed at either end of the mast. Due to the asymmetry of the structure, gyroscopic coupling is expected. Consequently, roll and pitch torque controls are also located on the shuttle. The cost of control effort is equally weighted among the control inputs. Equal terminal magnitude and rate penalties are applied to the roll, pitch and yaw angles of the shuttle, as well as the torsional deformation of the mast at its midpoint and at the mast/antenna junction.

The results of the first SCOLE slew are shown in Fig. 4-4. It is clear that, although the shuttle has rotated the prescribed amount, there is a small amount of residual torsional energy in the structure. This energy is due primarily to the deformation of the antenna and mast at the terminal time. Also, the set of controls utilized are incapable of suppressing out-of-plane deflection of the antenna, which is caused by the asymmetry of the structure.

In order to suppress this residual energy, additional controls are placed on the antenna. In-plane forces are available at the mast/antenna junction and directly across the antenna. In addition, an out-of-plane thruster is placed at the latter location. Furthermore, additional penalties are placed on antenna deformation. The improvement in the slew response can be seen in Fig. 4-5. For this maneuver, most of the torque is generated by the antenna thrusters across from the mast. In reality, this distribution of control effort would be unwise, as it would lead to excessive stress in the mast/antenna junction. Also, as shown in the figure, this trajectory causes a large amount of torsional deformation of the mast. By adjusting the relative weights on the controls and structural

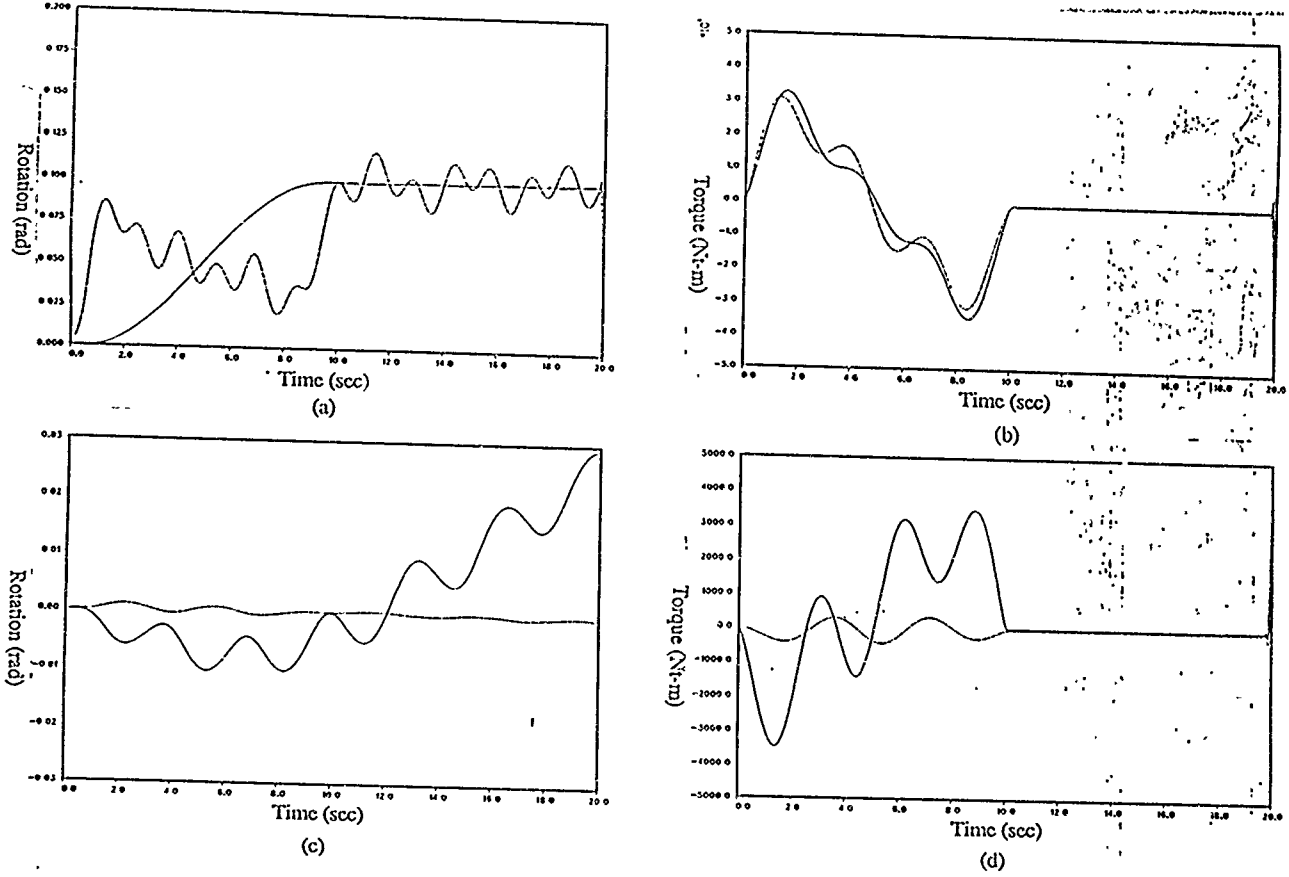

Fig. 4-4: Optimal rotational slew of SCOLE structure with four control inputs (see text): (a) yaw angle of shuttle (——) and rotation of node 3 about z-axis (- · -), (b) yaw torque applied to shuttle (——) and node 3 about z-axis (- · -), (c) roll angle (——) and pitch angle (- · -) of shuttle, (d) roll torque (——) and pitch torque (- · -) applied to shuttle.

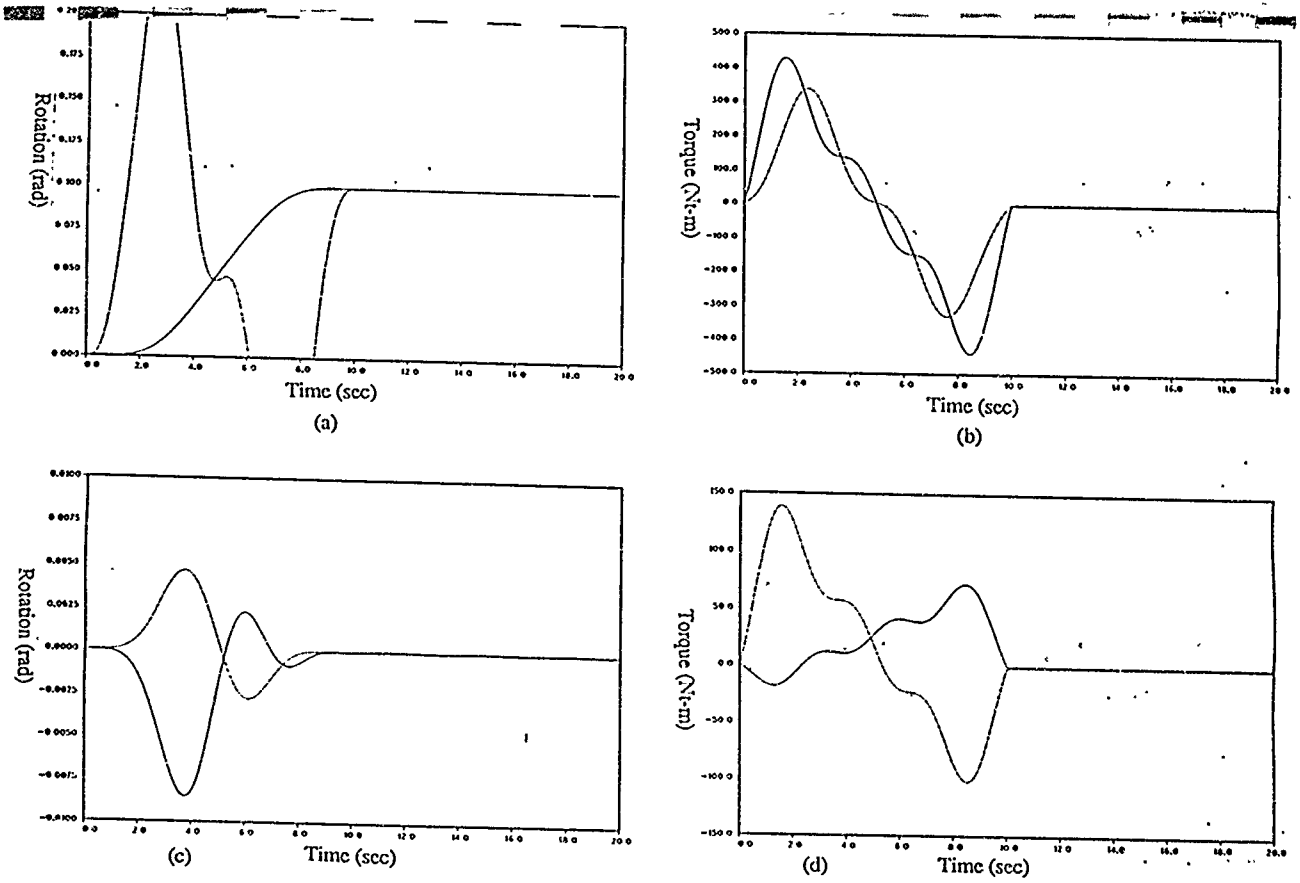

Fig. 4-5: Optimal rotational slew of SCOLE structure with nine control inputs (see text): (a) yaw angle of shuttle (——) and rotation of node 3 about z-axis (- · -), (b) yaw torque applied to shuttle (——) and node 3 about z-axis (- · -), (c) roll angle (——) and pitch angle (- · -) of shuttle, (d) roll torque (——) and pitch torque (- · -) applied to shuttle, (e) deflection of node 3 in x-direction (——) and y-direction (- · -), (f) control force applied to node 3 in x-direction (——) and y-direction (- · -), (g) deflection of node 6 in x-direction (——) and y-direction (- · -), (h) control force applied to node 9 in x-direction (——) and y-direction (- · -).

Force (Nt)
Time (sec)
(f)
Force (Nt)
Time (sec)
(h)
Displacement (m)
Time (sec)
(e)
Displacement (m)
Time (sec)
(g)

deformation outputs, it is possible to converge upon a more realistic trajectory. However, this control solution provides an adequate demonstration of the formulation presented here.

4.1.4 Minimization of flexible energy

Another method of obtaining an optimal solution consists of minimizing the residual flexural energy within the structural elements at the terminal time. This is achieved by expressing the generalized boundary displacements of the i'th element in terms of the undermined coefficients:

$$w^i(s) = C_w^i G_q(s) F_q(s) c = H^i(s) c \tag{4.18}$$

Making use of Eq. (2.43) then yields

$$E^i(t) = \frac{1}{2} c^T E_0^i(t) c \tag{4.19}$$

where

$$E_0^i(t) = k(t) \int_{-\infty}^{\infty} \int_{-\infty}^{\infty} H^i(s_1)^T \Xi^i(s_1,s_2) H^i(s_2) e^{j(\omega_1+\omega_2)t} d\omega_1 d\omega_2 \tag{4.20}$$

Included in the cost functional are the weighted penalties on residual energy for a set of N_f flexible elements and weighted penalties on control effort and control rate. To this we adjoin the desired terminal conditions and the constraints on the controls at the beginning and end of the maneuver. The cost functional is thus

$$J = \sum_{i=1}^{N_f} r_i E^i(t_f) + \frac{1}{2} \int_0^{t_f} \left[q_c(t)^T R_{qq} q_c(t) + \dot{q}_c(t)^T \tilde{R}_{qq} \dot{q}_c(t) \right] dt + \lambda^T \left[y(t_f) - y_d \right] + \lambda_0^T q_c(0) + \lambda_f^T q_c(t_f) \tag{4.21}$$

Setting variations in J due to c to zero yields

$$\begin{bmatrix} W & Y(t_f)^T & F_q(0)^T & F_q(t_f)^T \\ Y(t_f) & 0 & 0 & 0 \\ F_q(0) & 0 & 0 & 0 \\ F_q(t_f) & 0 & 0 & 0 \end{bmatrix} \begin{bmatrix} c \\ \lambda \\ \lambda_0 \\ \lambda_f \end{bmatrix} = \begin{bmatrix} 0 \\ y_d \\ 0 \\ 0 \end{bmatrix} \tag{4.22}$$

where

$$W = \sum_{i=1}^{N_f} r_i E_0^i(t_f) + \int_0^{t_f} \left[F_q(t)^T R_{qq} F_q(t) + \dot{F}_q(t)^T \tilde{R}_{qq} \dot{F}_q(t) \right] dt \tag{4.23}$$

Again, this system is symmetric, and can be solved with standard linear algebra software packages.

The minimum residual energy approach was applied to the simple mass/appendage system studied in the previous section. Two maneuvers were performed, both with a prescribed final displacement of 10 meters after 20 seconds. In the first maneuver, the desired final velocity of the rigid mass was zero, while in the second, the final velocity was 1 meter/second. The results of these maneuvers are shown in Fig.'s 4-6 and 4-7. In each case, the residual energy is seen to be negligible.

The same structure was used to perform rotational maneuvers. In this case, the bending of the flexible appendage was considered. A 0.1 radian slew with both zero and 1 radian/second terminal angular velocity were studied. The results, shown in Fig.'s 4-8 and 4-9, indicate that performance comparable to the axial cases was achieved.

The minimum energy cost functional leads to system trajectories with far less residual energy than those obtained via point constraints. Furthermore, minimization of total deformational energy also avoids the problem of selecting which points to constrain. All that is required is a relative cost weighting for each flexible element of interest. However, because the calculation of internal energy involves a double integral, the minimum energy approach requires more computational effort. The minimum energy cost functional was not applied to the SCOLE maneuver problem.

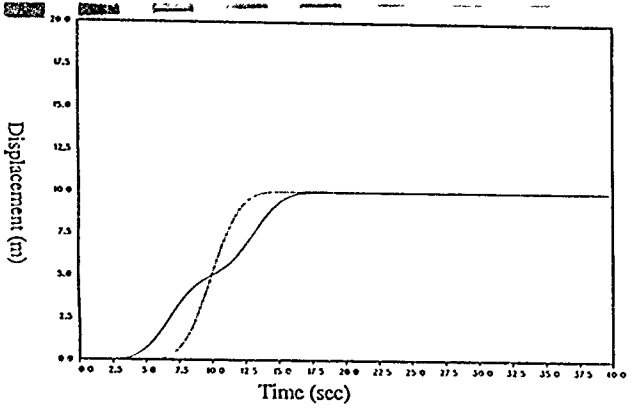

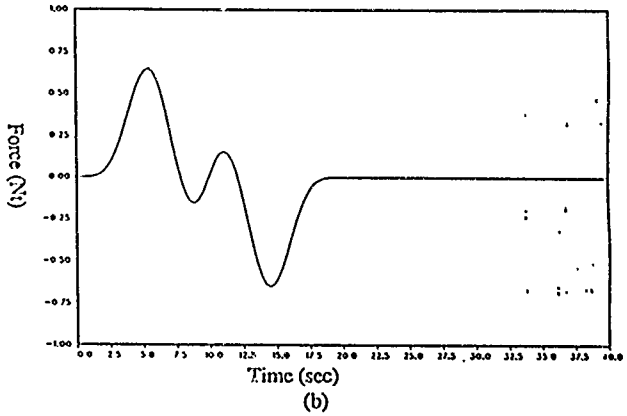

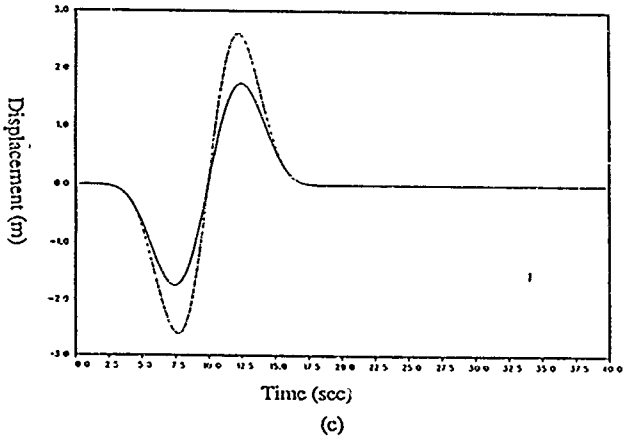

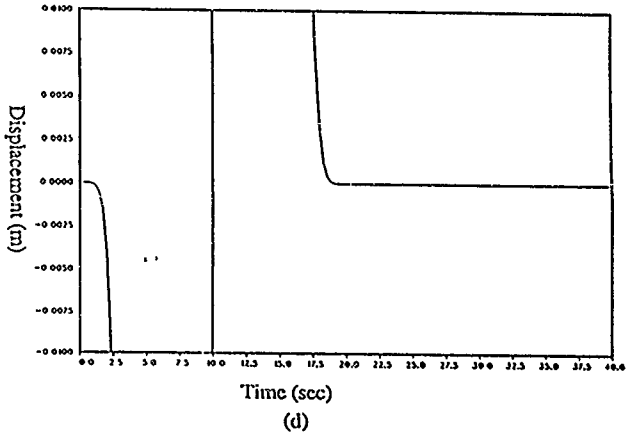

Fig. 4-6: Linear slew maneuver with residual energy cost functional, terminal time of 20 sec, terminal displacement of 10 m and terminal velocity of 0 m/sec. Control force was approximated with 18 basis functions: (a) Position of rigid mass (——) and tip of flexible appendage (- · -), (b) control force applied to rigid mass, (c) axial deformation of flexible appendage at center-span (——) and tip (- · -) with respect to position of rigid mass, (d) same plot as (c) with expanded vertical scale.

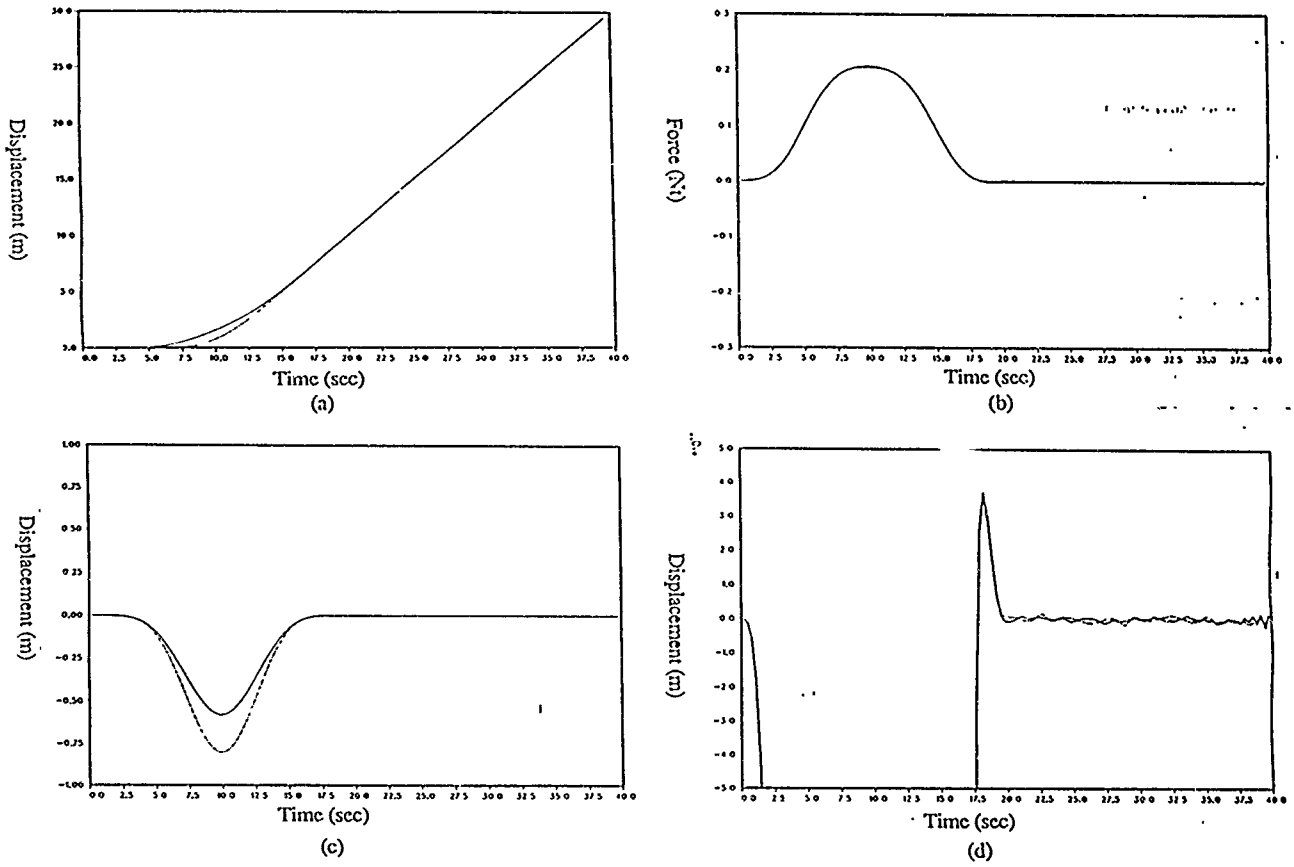

Fig. 4-7: Linear slew maneuver with residual energy cost functional, terminal time of 20 sec, terminal displacement of 10 m and terminal velocity of 1 m/sec. Control force was approximated with 18 basis functions: (a) Position of rigid mass (——) and tip of flexible appendage (- · -), (b) control force applied to rigid mass, (c) axial deformation of flexible appendage at center-span (——) and tip (- · -) with respect to position of rigid mass. (d) same plot as (c) with expanded vertical scale.

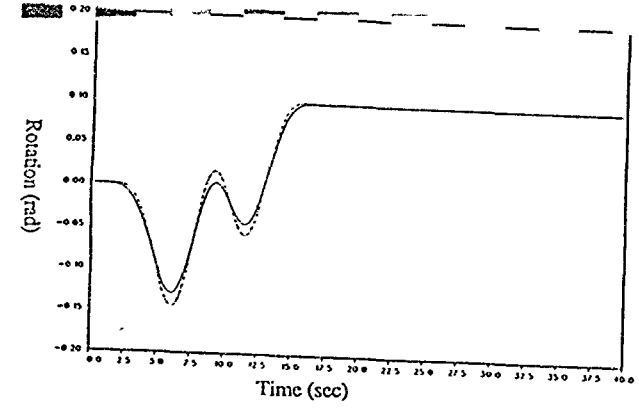

(a)

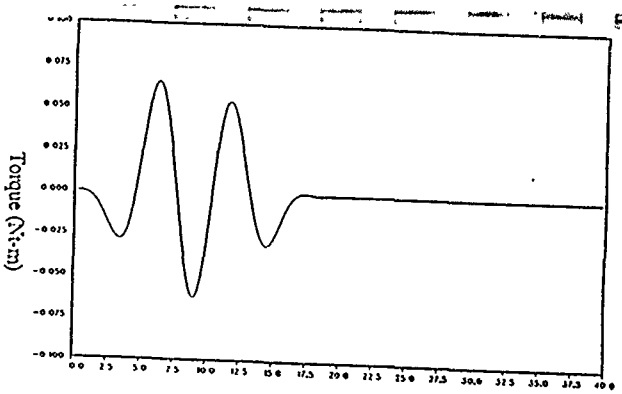

(b)

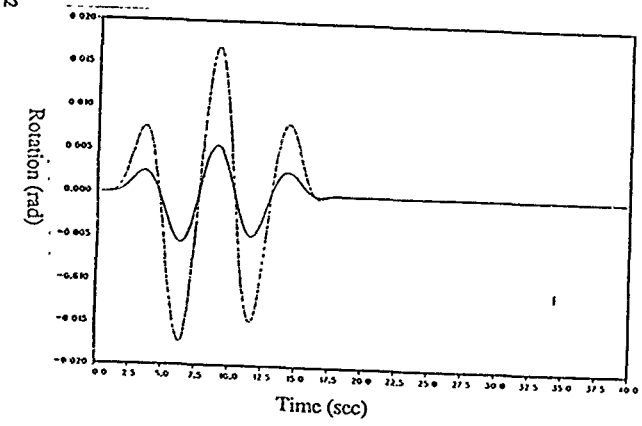

(c)

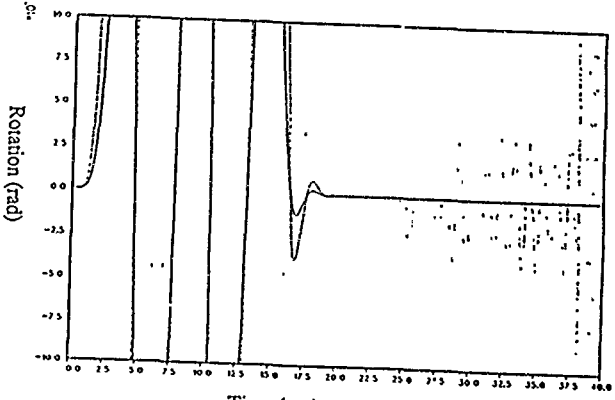

(d)

Fig. 4-8: Rotational slew maneuver with residual energy cost functional, terminal time of 20 sec, terminal rotation of 0.1 rad and terminal angular velocity of 0 rad/sec. Control torque was approximated with 18 basis functions: (a) Rotation of rigid mass (——) and tip of flexible appendage (- - -), (b) control torque applied to rigid mass, (c) transverse deformation of flexible appendage at center-span (——) and tip (- - -) with respect to position of rigid mass, (d) same plot as (c) with expanded scale.

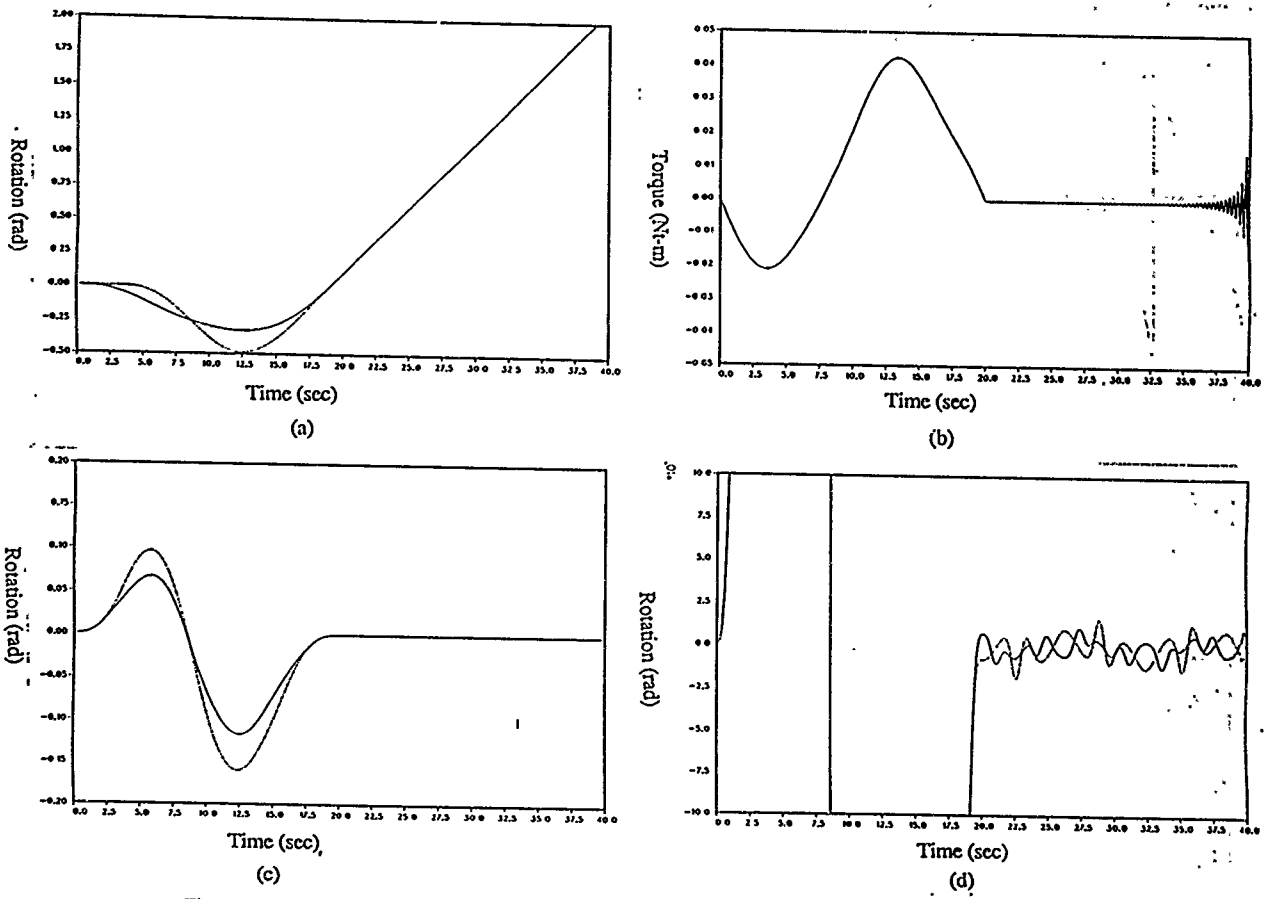

Fig. 4-9: Rotational slew maneuver with residual energy cost functional, terminal time of 20 sec, terminal rotation of 0.1 rad and terminal angular velocity of 0.1 rad/sec. Control torque was approximated with 18 basis functions: (a) Rotation of rigid mass (——) and tip of flexible appendage (- · -), (b) control torque applied to rigid mass, (c) transverse deformation of flexible appendage at center-span (——) and tip (- · -) with respect to position of rigid mass, (d) same plot as (c) with x- and y-scale.

4.2 Closed-loop control

The closed-loop control of infinite order systems expressed in the transformed domain is a considerably more difficult problem. The exact dynamics are available in the frequency-domain only, and no finite dimensional state space realization is possible. As a result, full order techniques, such as LQR and LQG methodologies, are not applicable. However, the control problem can be posed in a form amenable to frequency-domain design techniques. It is assumed that, for a given structural model, a set of disturbance forces act at global element junctions, and performance is measured in terms of some set of global generalized displacements. The control objective is then to minimize, in some sense, the transfer function from the set of disturbances, w(t), to the performance measure, z(t). This is to be accomplished by a finite order controller which has available as inputs a finite set of measured generalized displacements, y(t), and acts on a finite set of actuators, u(t), located on the structure. The situation is depicted in Fig. 4-10. The transfer functions from disturbances and control inputs to the performance metric and measured outputs are easily obtained as partitions of the dynamic flexibility matrix. Note that this control problem is in the "standard form," which has been studied extensively by Francis (1987) and Doyle (1989) for finite dimensional plants.

For this problem, the transfer functions are partitioned as

$$\begin{bmatrix} z(s) \\ y(s) \end{bmatrix} = \begin{bmatrix} G_{zw}(s) & G_{zu}(s) \\ G_{yw}(s) & G_{yu}(s) \end{bmatrix} \begin{bmatrix} w(s) \\ u(s) \end{bmatrix} \tag{4.24}$$

and the controller is expressed as

$$u(s) = G_c(s)y(s) \tag{4.25}$$

The closed-loop transfer function is then given by

$$T_{zw}(s) = G_{zw}(s) + G_{zu}(s)G_c(s)\left[I - G_{yu}(s)G_c(s)\right]^{-1}G_{yw}(s) \tag{4.26}$$

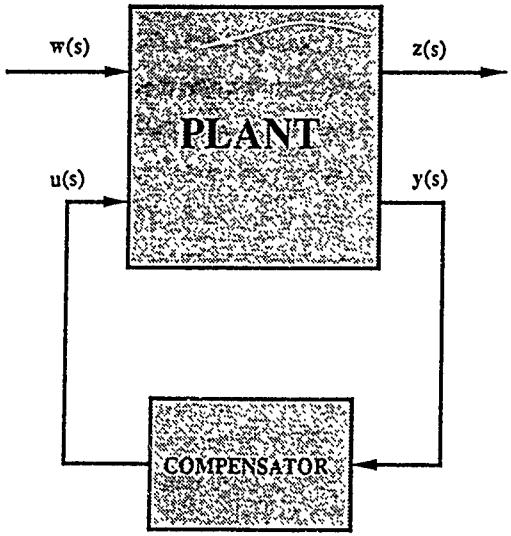

Fig. 4-10: The prototypical control problem posed in the standard form.

The design objective is then to determine $G_c(s)$ such that the closed-loop system is stable and meets the performance specifications. Although general solutions have been obtained for finite dimensional systems, the situation for infinite dimensional systems is much more complicated. As a result, only simple systems have been considered. For example, the coprime factorization technique is applied to a single torsional element in Piche (1986b). The extension of such an approach to complex structures would indeed be a significant achievement.

It is assumed that the controller has finite order, so that it can be physically implementable. The n-th order controller has the state-space form

$$\dot{x}_c(x,t) = A_c x_c(t) + B_c y(t), \quad u(t) = C_c x_c(t) + D_c y(t) \qquad (4.27a,b)$$

which is represented in the frequency domian by

$$G_c(s) = C_c(sI - A_c)^{-1}B_c + D_c \qquad (4.28)$$

The objective, then, is to find the matrices A_c, B_c, C_c, and D_c, that both stabilize the closed-loop system and minimize $T_{zw}(s)$ in some sense. A method of selecting the order of the controller is also required. The only data available are the partitioned transfer function matrices, which are mathematically exact at all frequencies. The optimal solution would then be valid for the exact mathematical model, rather than some truncation of it. As a result, the modelling error is restricted to the deviation of the mathematical model from the actual physical structure. This will result in a less conservative control design approach and, consequently, enhanced performance.

4.3 Limitations of the TEM Control Design Methodology

Although the control designs based on the TEM methodology have demonstrated remarkable performance (at least in the open-loop case), it is important to note some limitations of this approach. First, the control actuation is available only on the boundaries of the structural elements. For a small number of actuators, this may be overcome by dividing each element into smaller sub-elements at the point of control actuation. If many actuators are employed, however,

this approach is clearly not feasible. Another limitation is the requirement that the initial conditions be zero. Only in this way was it possible to obtain a simple expression for the control solution. Nonzero initial conditions introduce an extra term, $q_d(s)$, in the dynamic stiffness equation for each structural element. In addition to making the optimal control expressions more complex, this term must be computed by integrating over the domain of the element, as described in Sec. 2.3.1. Consequently, the treatment of initial conditions (and distributed forcing, for that matter) increases the computation time associated with the TEM approach considerably, as a numerical integration is required for each element at each complex frequency of interest.

Some of these limitations can be overcome by working with the original PDE for the element, expressed in the time-domain. This forms the basis of the direct PDE modelling approach, which leads naturally to a different type of control theory. The direct approach is the subject of the next two chapters.

5 DIRECT PDE MODELLING

All physical systems are distributed in nature. This fact is a consequence of the laws of physics, which always take the form of a set of field equations which must be satisfied over each infinitestimal region in the spatial domain of interest. As a result, any exact model of a physical system must be of infinite order. Lumped parameter models are, in general, low-frequency approximations to these field equations. Examples include lumped electrical component models (such as capacitors, resistors and inductors), rigid body structural idealizations, and finite element models. In this last example, the finite order approximation is achieved by restricting the deformational degrees of freedom of the system rather than employing a low-frequency approximation directly, but the result is essentially the same: The model fails to recover the high-frequency dynamics of the system. In this chapter, we introduce the concept of a distributed, infinite-order model of a system, which retains the dynamics of the physical system at all frequencies. This approach, hereinafter referred to as the direct PDE modelling approach, is superior to the TEM approach when forces of a distributed nature act within the spatial domain of the structural elements. Such forces include aerodynamic and gravitational loads, inertial forces, and distributed control actuators.

Distributed system models can be characterized in either of two forms. The first is an integral form, in which the response of the system at a particular time is determined by integrating (with respect to time and/or space) the product of the distributed forcing inputs and a Green's function kernel. Here, the Green's function relates the response of the system at some arbitrary point and time to an impulse applied at some other point and time. Thus, this characterization is global in nature. Given this approach, it is possible to develop, for example, a distributed control theory. The work of Brogan (1968) proceeds along these lines. However, the Green's function for an arbitrary system is extremely difficult to obtain. Indeed, analytical expressions are only available for the simplest of cases. The other characterization is differential in nature. Here, partial differential equations, describing the local behavior of the system, are used to develop a system model. This characterization is mush easier to obtain, as the physical laws that describe the system

are always local. Consequently, more emphasis has been placed on developing the differential approach for control system design. Breakwell (1981), for example, uses the differential description to obtain solutions to the boundary control of a simple flexible system. The differential description of distributed systems will be used here throughout.

5.1 One-dimensional elements

For a structural system undergoing small deformations, the underlying differential equations are, of course, the equations of elasticity. A completely rigorous and exact linear structural model must therefore account for general three-dimensional deformation. However, for long, slender structural elements, the deformation is primarily a function of position along the element. The variation in deformation with respect to the other two directions can usually be expressed in terms of the deformation along the length of the element. Therefore, only one spatial coordinate is needed to describe the dynamics. This is the basis for the axial rod and Bernoulli-Euler beam models discussed in Chapter 2. While these idealizations fail to hold at extremely high frequencies, their ranges of validity are much greater than those of finite-order representations, such as finite element models.

5.1.1 General Formulation

We will restrict our attention to one-dimensional, linear, time-invariant distributed systems. Such systems can be written in the form

$$\dot{x}(x,t) = L_x(x)x(x,t) + B_x(x)u(x,t) + D_x(x)n(x,t), \quad x\in[0,1], \quad t\in[0,\infty) \qquad (5.1)$$

where x is the state vector, u is the distributed control input, and n is the distributed disturbance input. In contrast with lumped-parameter state space models, these vectors exhibit both spatial and temporal dependance. Also, L_x, B_x and D_x are linear (possibly spatially varying) matrix operators. Note that the spatial domain has been normalized to unity. The boundary conditions are assumed to be homogeneous, and are expressed as

$$x(0,t) = x(1,t) = 0, \quad t \in [0,\infty) \tag{5.2}$$

The entire development presented here applies to modelling of systems with homogeneous boundary conditions only. It is therefore assumed that no control or disturbance forces are applied at the boundaries of the system. Finally, the initial conditions are expressed as

$$x(x,0) = x_0(x), \quad x \in [0,1] \tag{5.3}$$

5.1.2 Bernoulli-Euler Beam Example

One of the simplest examples of a one-dimensional distributed parameter system is a Bernoulli-Euler beam. A diagram of the physical system is shown in Fig. 5-1. The requirement that the boundary conditions for the mathematical model be homogeneous corresponds to pinned-pinned boundary conditions for the beam, as will be shown in the next subsection. In addition to casting the equation of motion of the beam in the form given by Eq. (5.1), the following subsections describe a method for simulating the response of the beam system to various control and disturbance forces.

5.1.2.1 Normalization of Equations of Motion

In dimensional form, the beam dynamics are described by

$$\frac{\partial^2}{\partial x_d^2}\left[EI(x)\frac{\partial^2}{\partial x_d^2}v_d(x_d,t_d)\right] + m(x)\frac{\partial^2}{\partial t_d^4}v_d(x_d,t_d) = f_d(x_d,t_d), \quad x_d \in [0,L] \tag{5.4}$$

where x_d and t_d are the dimensionalized spatial and temporal variables, respectively, v_d is the transverse deflection, f_d is the applied distributed control and/or disturbance force, L is the beam length, EI(x) is the bending stiffness, and m(x) is the beam mass per unit length. To this equation we must add the boundary conditions

$$v_d(0,t_d) = \frac{\partial^2}{\partial x_d^2}v_d(0,t_d) = v_d(1,t_d) = \frac{\partial^2}{\partial x_d^2}v_d(1,t_d) = 0 \tag{5.5}$$

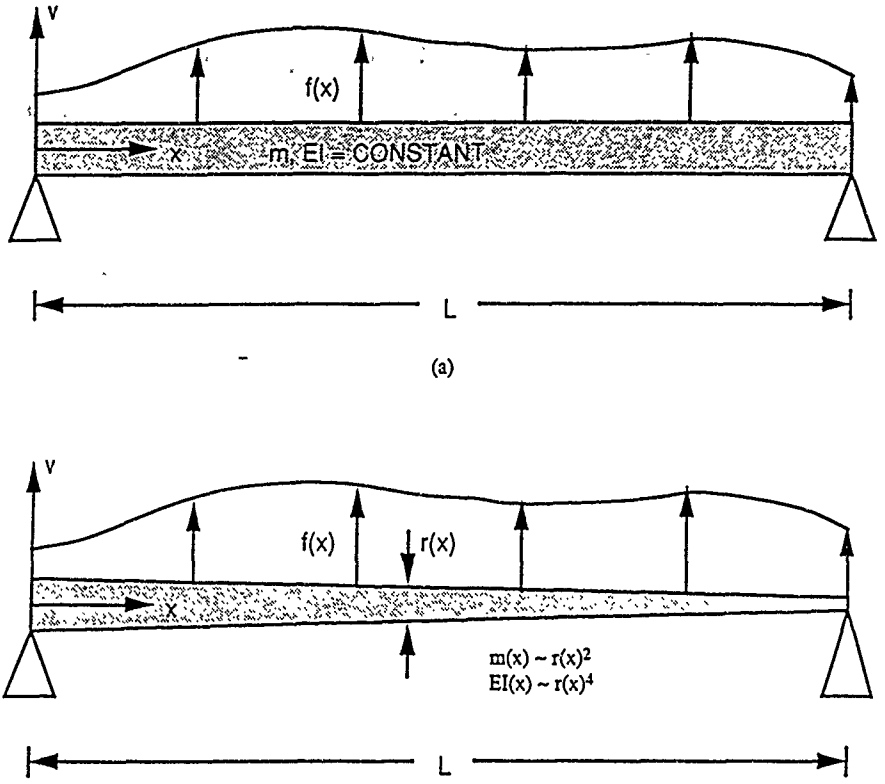

Fig. 5-1: Bernoulli-Euler beam models: (a) Uniform beam, (b) Tapered beam.

and the initial conditions

$$v_d(x_d,0) = v_{0d}(x_d), \quad \frac{\partial}{\partial t_d} v_d(x_d,0) = \dot{v}_{0d}(x_d) \tag{5.6a,b}$$

We now introduce nondimensional independant variables according to

$$x = \frac{x_d}{L}, \quad t = t_d \sqrt{\frac{EI(0)}{m(0)L^4}} \tag{5.7a,b}$$

and the normalized deflection and distributed force as

$$v(x,t) = \frac{1}{L} v_d(x_d,t_d), \quad f(x,t) = \frac{L^3}{EI(0)} f_d(x_d,t_d) \tag{5.8a,b}$$

We can also parametrize the bending stiffness and mass per unit length by

$$\eta(x) = \frac{EI(x)}{EI(0)}, \quad \beta(x) = \frac{m(0)}{m(x)} \tag{5.9a,b}$$

where η and β are nondimensional functions. These normalizations lead to the following nondimensional form of the equation of motion

$$\frac{\partial^2}{\partial x^2}\left[\eta(x) \frac{\partial^2}{\partial x^2} v(x,t)\right] + \frac{1}{\beta(x)} \frac{\partial^2}{\partial t^2} v(x,t) = f(x,t) = f_u(x,t) + f_n(x,t) \tag{5.10}$$

Here, f_u and f_n represent the normalized distributed control and disturbance forces, respectively. To obtain the state space representation of the dynamics, we define the state vector and control and disturbance scalars by

$$x(x,t) = \begin{bmatrix} \eta(x) \frac{\partial^2}{\partial x^2} v(x,t) \\ \frac{\partial}{\partial t} v(x,t) \end{bmatrix}, \quad u(x,t) = f_u(x,t), \quad n(x,t) = f_n(x,t) \tag{5.11a-c}$$

The first and second elements of x correspond to the normalized curvature and velocity of the bending motion, respectively. These choices for the state vector components ensure the well-posedness of the system model, as explained by Richtmyer (1957). Equation (5.5), which is a consequence of the pinned-pinned boundary conditions, ensures that $x(0,t)=x(1,t)=0$ for all values of t. The equation of motion then takes the form of Eq. (5.1), with

$$L_x(x) = \begin{bmatrix} 0 & \eta(x) \\ -\beta(x) & 0 \end{bmatrix} \frac{\partial^2}{\partial x^2}, \quad b_x(x) = d_x(x) = \begin{bmatrix} 0 \\ \beta(x) \end{bmatrix} \tag{5.12a,b}$$

5.1.2.2 The Case of Curvature Actuation

In most active structural control applications, it is difficult to implement lightweight inertial force actuators. This is particularly challenging for space-based structures, where stringent constraints are placed on structural mass. As a result, practical structural control actuators are usually imbedded within the structure itself, and are capable of producing only relative deformation between points on the structure. For example, deLuis (1989) demonstrates how an embedded piezoelectric actuator can be used to induce a local curvature in the beam. Many such actuators, placed along the span of a large, beam-like structure will then approximate distributed curvature actuation.

It is therefore useful to develop the model of a beam with a distributed curvature actuator. Such is the limiting case of a beam with many embedded piezoelectric actuators distributed along its span. For this system, the equation of motion is modified to

$$\frac{\partial^2}{\partial x^2}\left[\eta(x)\frac{\partial^2}{\partial x^2}v(x,t)\right] + \frac{1}{\beta(x)}\frac{\partial^2}{\partial t^2}v(x,t) = \frac{\partial^2}{\partial x^2}m_u(x,t) \tag{5.13}$$

where $m_u(x,t)$ represents the net action of the distributed piezoelectrics. The state vector, x, is unchanged, as is L_x, but u and b_x must be modified to

$$u(x,t) = m_u(x,t), \quad b_x = \begin{bmatrix} 0 \\ \beta(x) \end{bmatrix} \frac{\partial^2}{\partial x^2} \tag{5.14a,b}$$

5.1.2.3 Numerical Simulation Using Laplace Transform

Given the beam dynamics model, there remains the problem of actually simulating the response of the beam to control and disturbance forces. Various methodologies exist to achieve this end. At one extreme, the dynamics equation is discretized in both space and time and then

integrated forward in time. This constitutes a partial differential equation with mixed boundary and initial conditions. Although this method is widely used, it requires rather fine discretizations in both the temporal and spatial dimensions to achieve accurate results, and errors tend to accumulate in time. At the other extreme, one can Laplace-transform the equation into the s-domain and search for analytic solutions. However, due to the distributed nature of the control and/or disturbance forces, this transformation results in an integro-partial differential equation rather than a simple ordinary differential equation (as would be the case for boundary forcing only). Due to the generality of the distributed forces, a general analytical solution is not available.

In order to achieve accurate solutions with relatively coarse discretizations, a third alternative is proposed. The dynamics equation is Laplace-transformed, resulting in the above mentioned integro-partial differential equation. At each desired complex frequency, a finite differencing scheme is used to solve for the displacement field. The data from a set of frequencies is collected, and the numerically robust inverse Laplace transform algorithm described in Section 2.2 is used to convert the data back into the time-domain. Because the transformed equation represents a boundary value problem, it is anticipated that its approximate solution will be more stable and accurate than the corresponding solution to the mixed problem associated with time-domain integration. The stability and accuracy of the inverse transform algorithm has already been demonstrated in Chapters 2 and 3.

The development presented here corresponds to distributed force actuation only, and the case of distributed curvature actuation is addressed in Appendix B. We first transform Eq. (5.10) into the frequency-domain:

$$\frac{\partial^2}{\partial x^2}\left[\eta(x)\frac{\partial^2}{\partial x^2}\tilde{v}(x,s)\right]+\frac{1}{\beta(x)}\left[s^2\tilde{v}(x,s) - s\,v_0(x) - \dot{v}_0(x)\right] = \tilde{f}_u(x,s) + \tilde{f}_n(x,s) \quad (5.15)$$

The normalized frequency, s, is related to the dimensional frequency, s_d, by

$$s = s_d\sqrt{\frac{\rho A l^4}{EI}} \quad (5.16)$$

In this way, we can relate the transform pair $v(x,t_d) \sim \bar{v}(x,s_d)$ with the pair $v(x,t) \sim \bar{v}(x,s)$. We now assume that the feedback control law is distributed and linear, and relates the components of the state vector to the control input by

$$f_u(x,t) = -\int_0^1 k(x,y)^T x(y,t)\, dy$$

$$= -\int_0^1 \left[k_1(x,y)\, \eta(y) \frac{\partial^2}{\partial y^2} v(y,t) + k_2(x,y) \frac{\partial}{\partial t} v(y,t) \right] dy \qquad (5.17)$$

In this last equation, $k_1(x,y)$ and $k_2(x,y)$ represent feedback gain kernels. This type of control law will arise in the next chapter as the optimal solution to the distributed control problem. Substituting the Laplace-transformed version of this control law in Eq. (5.15) leads to

$$\frac{\partial^2}{\partial x^2}\left[\eta(x) \frac{\partial^2}{\partial x^2} \bar{v}(x,s) \right] + \frac{s^2}{\beta(x)} \bar{v}(x,s) + \int_0^1 \left[k_1(x,y)\, \eta(y) \frac{\partial^2}{\partial y^2} \bar{v}(y,s) + s\, k_2(x,y)\, \bar{v}(y,s) \right] dy$$

$$= \bar{f}_n(x,s) + \frac{1}{\beta(x)} \left[\dot{v}_0(x) + s\, v_0(x) \right] + \int_0^1 k_2(x,y)\, v_0(y)\, dy \qquad (5.18)$$

The term involving k_1 in this equation can be integrated by parts twice so that the derivative with respect to y operates on k_1. The boundary term arising from this operation vanishes due to the homogeneous boundary conditions. By making the following associations

$$k(x,y,s) = \frac{\partial^2}{\partial y^2}\left[k_1(x,y)\, \eta(x) \right] + s\, k_2(x,y) \qquad (5.19a)$$

$$\bar{f}(x,s) = \bar{f}_n(x,s) + \bar{f}_i(x,s) + \bar{f}_c(x,s) \qquad (5.19b)$$

$$\bar{f}_i(x,s) = \frac{1}{\beta(x)} \left[\dot{v}_0(x) + s\, v_0(x) \right] \qquad (5.19c)$$

$$\bar{f}_c(x,s) = \int_0^1 k_2(x,y)\, v_0(y)\, dy \qquad (5.19d)$$

the dynamics equation reduces to

$$\frac{\partial^2}{\partial x^2}\left[\eta(x)\frac{\partial^2}{\partial x^2}\tilde{v}(x,s)\right] + \frac{s^2}{\beta(x)}\tilde{v}(x,s) + \int_0^1 k(x,y,s)\,\tilde{v}(y,s)\,dy = \tilde{f}(x,s) \qquad (5.20)$$

A similar result is available for the case of curvature actuation, and can be found in Appendix B.

Equation (5.20) must be solved numerically for each value of s needed to construct the time response. To do so requires a discretization of the spatial domain into N uniform subregions. The boundaries of these subregions are given by

$$x_i = \frac{i}{N}, \quad i = 0, \ldots, N \qquad (5.21)$$

We can now use the values of $\tilde{f}(x,s)$ evaluated at these x_i to determine $\tilde{v}(x,s)$ at these same coordinates. By defining the vectors

$$\tilde{v}(s) \approx \left\{\tilde{v}(x_i,s)\right\}, \quad \tilde{f}(s) \approx \left\{\tilde{f}(x_i,s)\right\} \qquad (5.22a,b)$$

and the matrix

$$K(s) \approx \left[k(x_i,y_j,s)\right] \qquad (5.23)$$

an approximation to Eq. (5.20) is easily obtained. The first term is replaced by the finite difference approximation

$$\frac{\partial^2}{\partial x^2}\left[\eta(x)\frac{\partial^2}{\partial x^2}\tilde{v}(x,s)\right] \approx N^4\,DHD\,\tilde{v}(s) \qquad (5.24)$$

where D is a constant banded matrix of coefficients representing the second derivative operation:

$$D = \begin{bmatrix} 2 & -2 & & & \\ -1 & 2 & -1 & & 0 \\ & -1 & 2 & -1 & \\ & & \ddots & \ddots & \ddots \\ 0 & & & -1 & 2 & -1 \\ & & & & -2 & 2 \end{bmatrix} \qquad (5.25)$$

and H is the discretized representation of $\eta(x)$:

$$H = \text{diag}\left[\eta(x_i)\right] \qquad (5.26)$$

The second term in Eq. (5.20) is trivially approximated by

$$\frac{s^2}{\beta(x)}\bar{v}(x,s) \approx s^2 B \bar{v}(s) \tag{5.27}$$

where

$$B = \text{diag}\left[\frac{1}{\beta(x_i)}\right] \tag{5.28}$$

Finally, the integral term is replaced with a summation:

$$\int_0^1 k(x,y,s)\,\bar{v}(y,s)\,dy \approx \frac{1}{N} K(s)\,\bar{v}(s) \tag{5.29}$$

Collecting terms, the discretized equation becomes

$$\left[N^4 D H D + s^2 B + \frac{1}{N} K(s)\right] \bar{v}(s) = \bar{f}_n(s) + \bar{f}_I(s) + \bar{f}_c(s) \tag{5.30}$$

Thus, a single matrix inversion is required at each complex frequency. If the frequencies required for the inverse Laplace transform are given by

$$s = s_1, \ldots, s_n \tag{5.31}$$

then the solutions of Eq. (5.30) can be grouped according to

$$\bar{V} = \left\{\bar{v}(s_1) \ldots \bar{v}(s_n)\right\} \tag{5.32}$$

The time-domain responses at each x_i are then obtained by applying the inverse transform algorithm to each row of $\bar{V}$.

Figure 5-2 presents the response of a uniform and a linearly tapered beam to a sinusoidal initial displacement and zero initial velocity. (The plots display time and x-coordinate along the beam as independent variables, with transverse deflection along the vertical axis.) For the uniform beam, these initial conditions correspond to the second mode of vibration. Consequently, no other modes are excited, as can be seen in the figure. For the tapered beam, other modes become involved, as the individual mode shapes are more complicated. Figure 5-3 displays the simulation

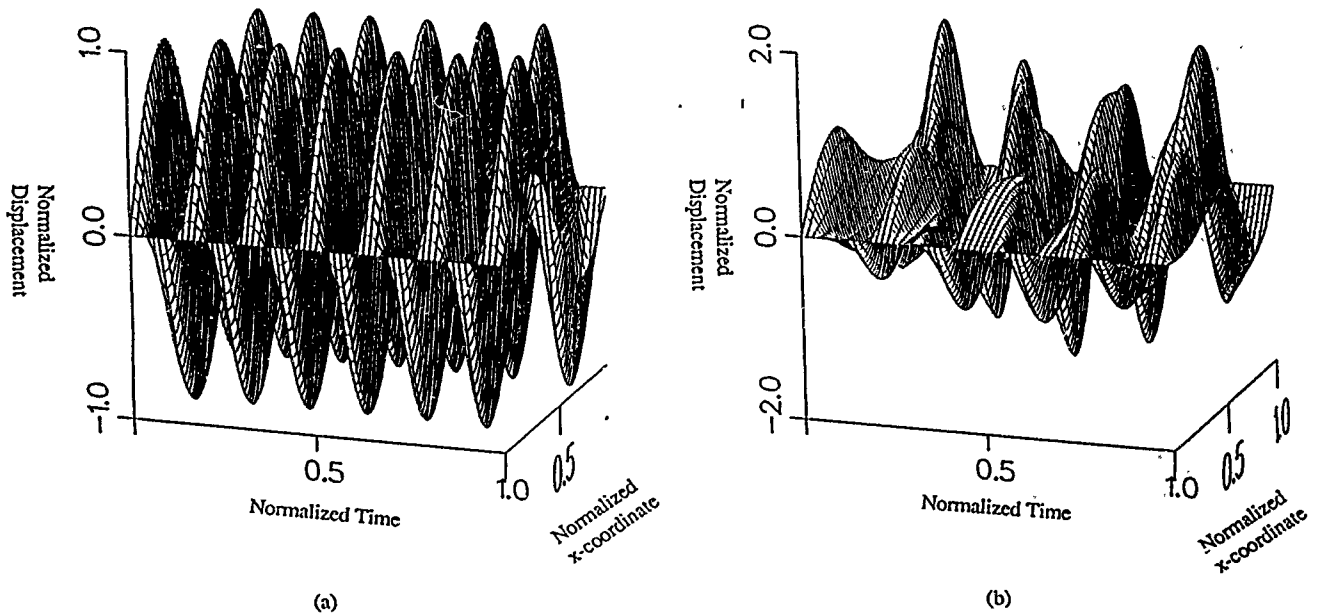

Fig. 5-2: Uncontrolled response of beam with initial displacement $v_0(x)=\sin(2\pi x)$: (a) Uniform beam, (b) Tapered beam (Beam diameter varies linearly from 1.0 at x=0 to 0.4 at x=1).

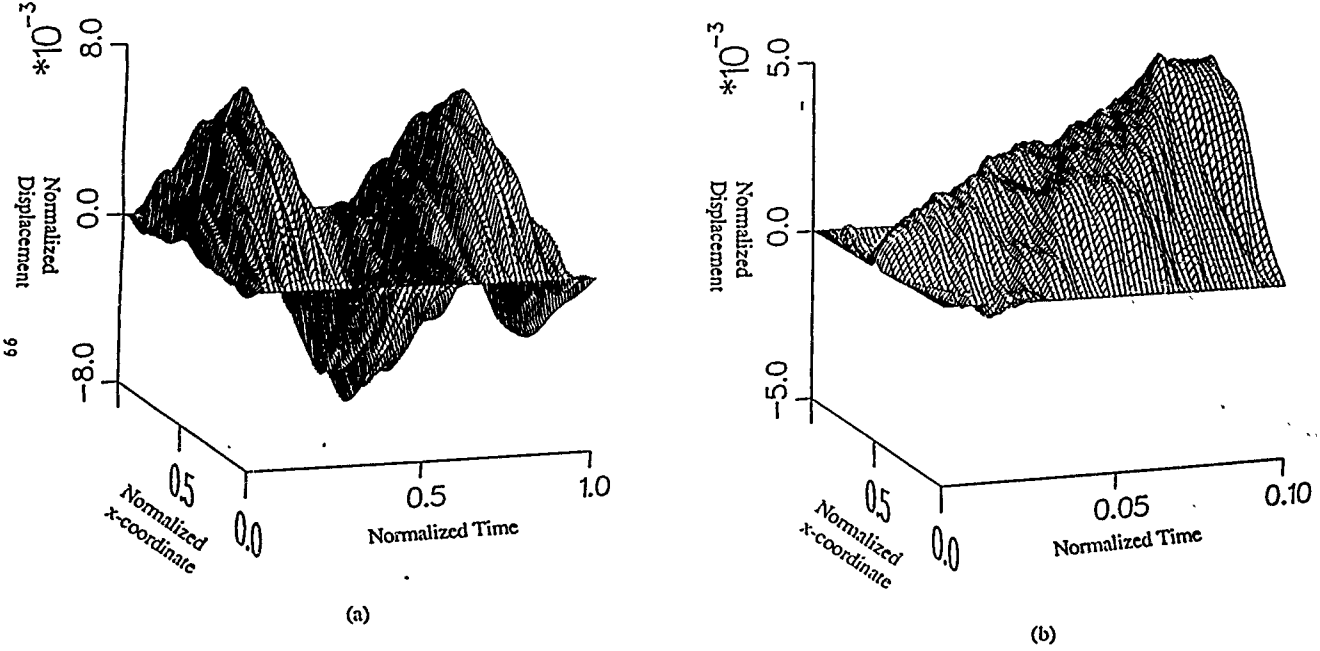

Fig. 5-3: Response of uniform beam to unit impulse applied at center-span: (a) Long time scale, (b) Short time scale.

results for a uniform beam impacted with a unit transverse impulse at its center-span. The plot on the left corresponds to a long time scale, and indicates that the resulting motion is predominantly composed of a first mode vibration with odd harmonics. The plot on the right, which corresponds to a shorter time scale, accentuates the wave-like characteristics of the response. The disturbance, which begins at the center-span, quickly moves towards the boundaries and reflects. These reflections eventually set up the complex modal motion observed in the long time scale plot. Note that, for a short time following the impact, the deflection of the center-span varies as the square-root of time. This behavior agrees with the beam theory presented by Nowacki (1963), where the response of a beam of infinite extent is addressed. Note also that the disturbance reaches the boundaries almost instantly, which is characteristic of the Bernoulli-Euler beam assumption of no cross section rotary inertia. This effect is more apparent in Fig. 5-4, where the responses of a Bernoulli-Euler beam (on the left) and a Timoshenko beam (on the right) are compared. The simulation of the Timoshenko beam is discussed in Appendix C. For these simulations, free-free boundary conditions are assumed, and the impact occurs at a boundary. The effect of rotary inetia is immediately apparent, and manifests itself as a finite disturbance propagation velocity in the beam. Also, the reflection of the shear wave propagating through the Timoshenko beam can be seen in the plot on the right of the figure.

5.2 Two-dimensional elements

Many element models require two independant spatial coordinates to specify the domain of the element. These models include membranes, plates in bending, shells, and plane stress elements. In all cases, the third spatial dimension is of sufficiently small extent in comparison with the other two dimensions so that a two-dimensional idealization is reasonably accurate. These models have the general differential form

$$\dot{x}(x,y,t) = L_x x(x,y,t) + B_x u(x,y,t), \quad x,y \in [0,1], \quad t \in [0,\infty) \tag{5.33}$$

Two examples of two-dimensional elements are given below.

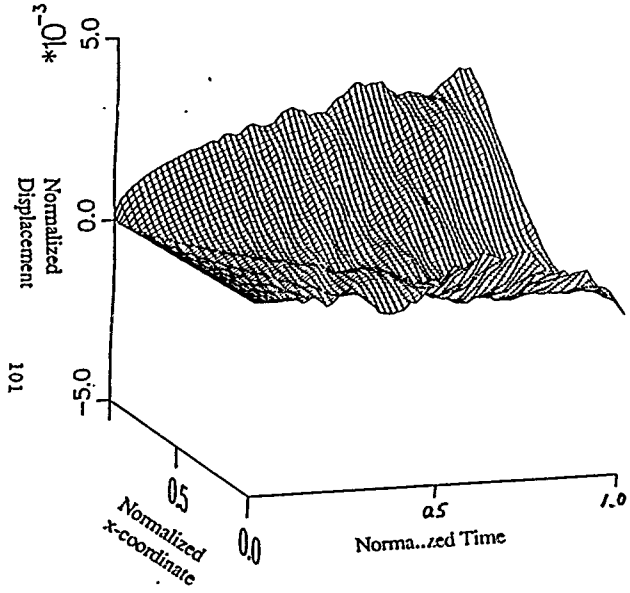

(a)

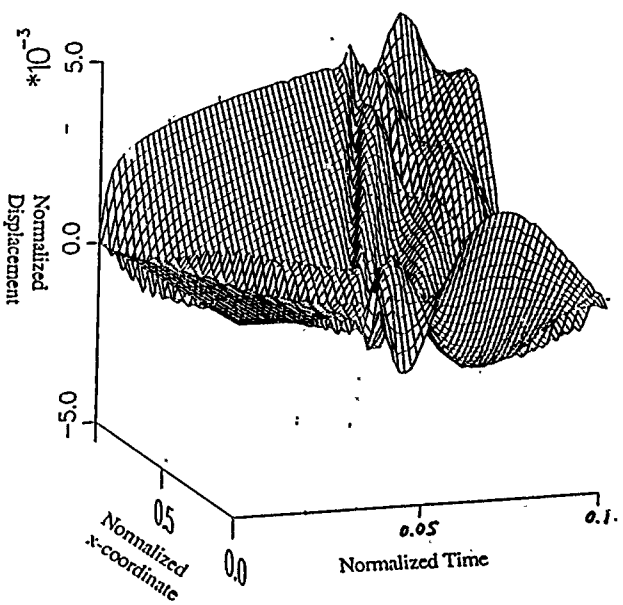

(b)

Fig 5-4: Response of free-free beam to unit impulse applied at x=0: (a) Bernoulli-Euler beam, (b) Timoshenko beam (α_I=4x10^{-4}, α_E=2.8).

5.2.1 Membrane model

The normalized equation of motion of a membrane is given by

$$-\nabla^2 v(x,y,t) + \ddot{v}(x,y,t) = f(x,y,t) \tag{5.34}$$

where v represents the normalized deflection, f represents a normalized force per unit area, and ∇^2 is the Laplacian operator. Taking the deflection and its velocity as the state variables:

$$x(x,y,t) = \begin{bmatrix} v(x,y,t) \\ \dot{v}(x,y,t) \end{bmatrix}, \quad u(x,y,t) = f(x,y,t) \tag{5.35a,b}$$

and defining the operators L_x and b_x by

$$L_x = \begin{bmatrix} 0 & 1 \\ \nabla^2 & 0 \end{bmatrix}, \quad b_x = \begin{bmatrix} 0 \\ 1 \end{bmatrix} \tag{5.36a,b}$$

leads to the relation given by Eq. (5.33).

5.2.2 Plate model

Another two dimensional element is a plate in bending. Here, the equation of motion is

$$\nabla^4 v(x,y,t) + \ddot{v}(x,y,t) = f(x,y,t) \tag{5.37}$$

In this case, the following state vector and forcing input definitions are appropriate:

$$x(x,y,t) = \begin{bmatrix} \nabla^2 v(x,y,t) \\ \dot{v}(x,y,t) \end{bmatrix}, \quad u(x,y,t) = f(x,y,t) \tag{5.38a,b}$$

The equation of motion then takes the form of Eq. (5.33), with

$$L_x = \begin{bmatrix} 0 & \nabla^2 \\ -\nabla^2 & 0 \end{bmatrix}, \quad b_x = \begin{bmatrix} 0 \\ 1 \end{bmatrix} \tag{5.39a,b}$$

5.2.3 Complexity Issues

Unfortunately, the direct simulation of two-dimensional elements is considerably more computationally intensive than the simulation of one-dimension elements. Because the spatial domain is given by two independant variables, discretization in two dimensions in required. As a result, no simulation results are currently available. A complete development of the direct simulation of two dimensional elements is the subject of future research.

5.3 Multiple Element Formulation

Distributed modelling and simulation of multiple member structures, such as space frames and trusses, is a considerably more difficult problem than the single element situation, even for one-dimensional elements. The primary difficulty is in the mathematical treatment of the boundary conditions that arise at element junctions. A rigorous, general assembly procedure for complex structures using direct PDE modelling remains to be developed. One approach currently considered is to define a normalized local coordinate system (x=0 at one end of an element and x=1 at the other end) for each structural member, as shown in Fig. 5-5, and collect the states associated with each element into a large state vector. The dynamics of the entire structure is then still represented by Eq. (5.1), and L_x becomes block diagonal, with each block representing the dynamics of one member. The boundary conditions then relate various elements of the state vector at x=0 and/or x=1. The difficulty in the direct modelling approach then lies in utilizing these awkward boundary conditions for the purposes of simulation and control design. The direct multiple element formulation remains an open area of research.

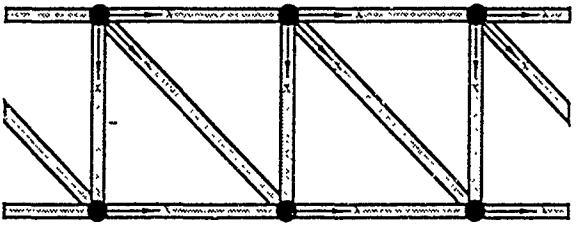

Fig. 5-5: Schematic of multi-element truss structure.

6 CONTROL DESIGN BASED ON DIRECT PDE MODELS

This chapter studies the properties of optimal solutions to the distributed control of systems described by direct PDE models. By distributed control, we imply that control effort is imparted to the structure in a spatially distributed sense. This can be thought of as the limiting process of employing an increasing number of actuators, all of which have a decreasing spatial domain of influence. Particular emphasis is placed on a specific example, that of a Bernoulli-Euler beam. Both finite- and infinite-length beam systems are studied, and comparisons are made between the corresponding optimal solutions. Also, two types of beam actuation are addressed. The first is force actuation, which is commonly used in theoretical studies yet is rarely achievable. The second is curvature actuation, which is more realizable (as mentioned in the previous chapter) but less often addressed in theoretical works.

Distributed control is by no means a new topic. In fact, the essential mathematical groundwork was established in the 1960's by Butkovskii (1960), Wang (1964), and Lions (1971). The results then obtained were analogous to the classical LQR solution (e.g., the Riccati matrix equation was replaced by a Riccati operator equation), and were derived using the principle of optimality and/or advanced functional analysis. A later work by Tzafestas (1970) derived the necessary conditions for optimality from a variational calculus approach. A mathematically rigorous derivation of the Riccati operator equation is performed by Gibson (1979). Also, Balas (1982) addresses several implementation issues, including the use of a finite set of sensors and actuators and a finite order controller. Perturbation methods are utilized to determine criteria for closed-loop stability. Until now, the complexity of the distributed control problem has rendered it a mere mathematical curiousity, rather than a practical tool. With today's computer resources, however, the solutions to simple problems, such as the Bernoulli-Euler beam system described below, are within reach.

6.1 Linear Quadratic Optimal Control Theory in the 1-D Case

The theory presented in this subsection closely resembles the work of Tzafestas (1970). We restrict our attention to one-dimensional, linear, time-invariant distributed systems. Such systems can be written in the form

$$\dot{x}(x,t) = L_x(x)x(x,t) + B_x(x)u(x,t), \quad x\in[0,1], \quad t\in[0,\infty) \tag{6.1}$$

which is identical to Eq. (5.1), except that the disturbance input has been set to zero. As before, the boundary conditions are assumed to be homogeneous, and are expressed as

$$x(0,t) = x(1,t) = 0, \quad t\in[0,\infty) \tag{6.2}$$

while the initial conditions are expressed as

$$x(x,0) = x_0(x), \quad x\in[0,1] \tag{6.3}$$

The simplest optimal distributed compensator is derived under the assumption of full state feedback. That is, perfect measurements of x(x,t) are available in a continuous sense throughout the spatial domain at every instant of time. It is also assumed that control actuation is available in a similar distributed sense. While these assumptions are rather crude, they serve to define an upper limit of achievable performance for the control system to be designed. The optimal distributed control problem can then be stated as follows: Given an arbitrary initial condition, determine the control required to return the system to the zero state while minimizing some cost criterion. We will assume a linear quadratic cost functional of the form

$$J = \frac{1}{2}\int_0^\infty\int_0^1 \left[x(x,t)^T Q(x)x(x,t) + u(x,t)^T R(x)u(x,t)\right] dx\, dt \tag{6.4}$$

where Q and R are symmetric (possibly spatially varying) weighting matrices. This is the distributed analogue of the classical linear-quadratic regulator (LQR) problem. Its solution is obtained by extending the classical variational calculus approach to distributed systems. Note that

the cost functional has infinite time horizon. This corresponds to the steady-state LQR problem. The finite time problem is also of interest, but provides no additional insight.

We first augment the cost functional with the system dynamics via a costate vector, p(x,t):

$$J_a = J + \int_0^{\infty}\int_0^1 p(x,t)^T\left[L_x(x)x(x,t) + B_x(x)u(x,t) - \dot{x}(x,t)\right] dx\, dt \qquad (6.5)$$

The augmented cost functional now depends on the three vectors, x, u, and p. The cost is minimized by setting the variation in cost due to independent perturbations in these three vectors to zero. Thus,

$$\delta J_a(\delta p) = \int_0^{\infty}\int_0^1 \delta p(x,t)^T\left[L_x(x)x(x,t) + B_x(x)u(x,t) - \dot{x}(x,t)\right] dx\, dt = 0\,, \quad \forall\, \delta p(x,t) \qquad (6.6a)$$

$$\delta J_a(\delta u) = \int_0^{\infty}\int_0^1 \left[u(x,t)^T R(x)\delta u(x,t) + p(x,t)^T B_x(x)\delta u(x,t)\right] dx\, dt$$

$$= \int_0^{\infty}\int_0^1 \left[u(x,t)^T R(x) + [B_x^*(x)p(x,t)]^T\right]\delta u(x,t)\, dx\, dt = 0\,, \quad \forall\, \delta u(x,t) \qquad (6.6b)$$

$$\delta J_a(\delta x) = \int_0^{\infty}\int_0^1 \left[x(x,t)^T Q(x)\delta x(x,t) + p(x,t)^T L_x(x)\delta x - p(x,t)^T \delta\dot{x}(x,t)\right] dx\, dt$$

$$= \int_0^{\infty}\int_0^1 \left[x(x,t)^T Q(x) + [L_x^*(x)p(x,t)]^T + \dot{p}(x,t)^T\right]\delta x(x,t)\, dx\, dt = 0\,, \quad \forall\, \delta x(x,t) \qquad (6.6c)$$

Equation (6.6a) recovers the system dynamics, while Eq. (6.6b) determines the control law. The superscript (*) represents the formal adjoint operator, which is defined by

$$\int_0^1 a(x)^T L_x(x) b(x)\, dx = \int_0^1 [L_x^*(x)a(x)]^T b(x)\, dx \tag{6.7}$$

for homogeneous boundary conditions. For a linear spatial differential operator, its adjoint is determined by integrating by parts with respect to the spatial dimension. Solving for u in Eq. (6.6b) yields

$$u(x,t) = - R(x)^{-1} B_x^*(x) p(x,t) \tag{6.8}$$

The integrated terms resulting from the integration by parts in Eq. (6.6c) vanish, due to the homogeneous boundary conditions and the added requirement that

$$p(0,t) = p(1,t) = 0, \quad t \in [0,\infty) \tag{6.9}$$

The third term in the integrand of Eq. (6.6c) is integrated by parts with respect to time. The integrated terms go to zero due to the specification of the initial conditions for the system and the requirement that

$$p(x,\infty) = 0, \quad x \in [0,1] \tag{6.10}$$

Equations (6.1), (6.8), and the integrand in Eq. (6.6c) lead to the following equations:

$$\begin{aligned} \dot{x}(x,t) &= L_x(x)x(x,t) - B_x(x)R(x)^{-1}B_x^*(x)p(x,t) \\ \dot{p}(x,t) &= - Q(x)x(x,t) - L_x^*(x)p(x,t) \end{aligned} \tag{6.11a,b}$$

Equations (6.11a,b) represent the state-costate equations for the distributed control problem. Lions (1971) shows that there exists a relation between the state and the costate of the form

$$p(x,t) = P_x(x)x(x,t) \tag{6.12}$$

where P_x is some linear matrix operator on x. Substituting this form in Eq. (6.11) results in a nonlinear matrix Riccati operator equation in P_x. Such an equation is, in general, difficult to solve. Several approximate solution techniques are described in Juang (1983), Schaechter (1982), and Zambettakis (1989). However, it is possible to express the linear operator in a different form, so that a solution is easily attained by numerical methods. The assumed form of the solution is the same as used by Wang (1964) and Tzafestas (1970):

$$p(x,t) = \int_0^1 S(x,y)\, x(y,t)\, dy \tag{6.13}$$

where S is the distributed-parameter analogue of the Riccati matrix for lumped-parameter systems. Equation (6.9) automatically imposes the constraints

$$S(0,y) = S(1,y) = 0, \quad y \in [0,1] \tag{6.14}$$

For complete generality, S must include generalized functions, such as Dirac delta functions and their derivatives, if necessary. Also, Wang (1964) shows that S is symmetric in its arguments (i.e., S(x,y) = S(y,x)). Using Eqs. (6.8) and (6.13), the feedback control law becomes

$$u(x,t) = -\int_0^1 K(x,y)\, x(y,t)\, dy, \quad K(x,y) = R(x)^{-1} B_x^*(x) S(x,y) \tag{6.15a,b}$$

Thus, the control law is linear and distributed.

It remains to derive a relation that enables the computation of S. Differentiating Eq. (6.13) and introducing Eq. (6.11a) leads to

$$\dot{p}(x,t) = \int_0^1 S(x,y)\left[L_y(y)x(y,t) - B_y(y)R(y)^{-1}B_y^*(y)p(y,t)\right]dy$$

$$= \int_0^1 \left[S(x,y)L_y^*(y)^T x(y,t) - S(x,y)B_y(y)R(y)^{-1}B_y^*(y)\int_0^1 S(y,z)x(z,t)\,dz\right]dy$$

$$= \int_0^1 \left[S(x,y)L_y^*(y)^T - \int_0^1 S(x,z)B_z(z)R(z)^{-1}B_z^*(z)S(z,y)\,dz\right]x(y,t)\,dy \qquad (6.16)$$

Once again, an integration by parts applied to the first term in the integral results in the adjoint operator. The boundary terms again vanish, subject to the restriction

$$S(x,0) = S(x,1) = 0, \quad x\in[0,1] \qquad (6.17)$$

It should be noted that the transposes of adjoint operators operate to the left in this case. Similarly, substituting Eq. (6.13) into the right side of Eq. (6.11b) yields

$$\dot{p}(x,t) = -Q(x)x(x,t) - \int_0^1 \left[L_x^*(x)S(x,y)x(y,t)\right]dy$$

$$= -\int_0^1 \left[Q(x)\delta(x-y) + L_x^*(x)S(x,y)\right]x(y,t)\,dy \qquad (6.18)$$

where $\delta(x)$ is the Dirac delta function. Note that the state vector, x, is isolated from each term under the integral in Eqs. (6.16) and (6.18). Thus, subtracting these two equations and setting the resulting integrand to zero yields the desired relation:

$$L_x^*(x)S(x,y) + S(x,y)L_y^*(y)^T + Q(x)\delta(x-y) - \int_0^1 S(x,z)B_z(z)R(z)^{-1}B_z^*(z)S(z,y)\,dz = 0 \qquad (6.19)$$

This relation is a *functional nonlinear matrix integro-partial differential equation* in x and y, and represents the distributed parameter analogue of the control algebraic Riccati equation. Note that we have assumed S to be time-invariant, which corresponds to the steady-state linear quadratic

regulator. For a finite time problem, the zero on the right hand side of Eq. (6.19) would be replaced by $-\frac{\partial}{\partial t}S(x,y)$.

6.2 Distributed Control of a Finite Beam

In this section, we apply the distributed control theory just presented to a Bernoulli-Euler beam of finite length, as described in Lupi (1991a). Force actuation will be assumed initially, and curvature actuation will be deferred to Section 6.2.5. The feedback gains will be determined by numerical solution of the Riccati equations given by Eq. (6.19). Although these equations are quite complex, their solutions are readily attainable with the proper mix of algebraic manipulation and numerical computation. Pinned-pinned boundary conditions are assumed for the example applications presented in this section.

6.2.1 Cost Functional

The dimensionalized form of the cost functional for this system is expressed by

$$J_d = \frac{1}{2}\int_0^{\infty}\int_0^1 \left\{ q_U(x)EI(x)\left[\frac{\partial^2 v_d}{\partial x_d^2}\right]^2 + q_T(x)m(x)\left[\frac{\partial v_d}{\partial t_d}\right]^2 + r(x)\frac{L^4}{EI(x)}f_d^2 \right\} dx_d\, dt_d \qquad (6.20)$$

Thus, q_U represents a weighting on deformational potential energy, q_T represents a weighting on kinetic energy, and r weighs control effort. The physical parameters EI, m and L are introduced so that all three weights have the same units. The cost functional can then be normalized, yielding

$$J = \frac{1}{2}\int_0^{\infty}\int_0^1 \left\{ q_U(x)\eta(x)\left[\frac{\partial^2 v}{\partial x^2}\right]^2 + \frac{q_T(x)}{\beta(x)}\left[\frac{\partial v}{\partial t}\right]^2 + \frac{r(x)}{\eta(x)}f_u^2 \right\} dx\, dt \qquad (6.21)$$

where the nondimensional cost is defined by

$$J = \frac{1}{\sqrt{EI(0)m(0)L^2}} J_d \tag{6.22}$$

The cost functional then takes the form of Eq. (6.4), with

$$Q(x) = \begin{bmatrix} q_U(x)\eta(x) & 0 \\ 0 & \frac{q_T(x)}{\beta(x)} \end{bmatrix}, \quad R(x) = \frac{r(x)}{\eta(x)} \tag{6.23}$$

6.2.2 Derivation of the Necessary Conditions

We must first determine the adjoint operators corresponding to L_x and b_x. This is accomplished by using the formal definition expressed in Eq. (6.7) and integrating by parts, yielding

$$L_x^*(x) = L_x^T(x) = \begin{bmatrix} 0 & -\beta(x) \\ \eta(x) & 0 \end{bmatrix} \frac{\partial^2}{\partial x^2}, \quad b_x^*(x) = b_x^T(x) = [0\ \beta(x)] \tag{6.24a,b}$$

Using these expressions in (6.19) yields

$$L_x^* S(x,y) + S(x,y) L_y^{*T} + Q(x)\,\delta(x-y) - \int_0^1 \frac{\eta(x)\beta(z)^2}{r(z)} S(x,z) \begin{bmatrix} 0 & 0 \\ 0 & 1 \end{bmatrix} S(z,y)\,dz = 0 \tag{6.25}$$

Also, making use of Eq. (6.15), the feedback law becomes

$$u(x,t) = -\int_0^1 k(x,y)^T x(y,t)\,dy, \quad k(x,y) = \begin{bmatrix} k_1(x,y) \\ k_2(x,y) \end{bmatrix} = \frac{\eta(x)\beta(x)}{r(x)} \begin{bmatrix} S_{12}(x,y) \\ S_{22}(x,y) \end{bmatrix} \tag{6.26a,b}$$

The effect of the curvature feedback term (k_1) is to stiffen the beam, which reduces the settling time of the system, while the effect of the velocity feedback term (k_2) is to increase the damping of the system.

Equation (6.25) represents a system of four coupled, nonlinear, integro-partial differential equations. Due to the symmetry of S, the fourth is redundant. Also, only S_{12} and S_{22} are needed

to compute the feedback gains. The equation for S_{12}, which represents the curvature feedback gain kernel, is uncoupled from the others:

$$\frac{\partial^2}{\partial x^2}\left[\beta(x)\, S_{12}(x,y)\right] + \frac{\partial^2}{\partial y^2}\left[\beta(y)\, S_{12}(x,y)\right]$$

$$= q_U(x)\eta(x)\,\delta(x-y) - \int_0^1 \frac{\eta(x)\beta(z)^2}{r(z)} S_{12}(x,z) S_{12}(z,y)\, dz \qquad (6.27)$$

Similarly, for the velocity feedback gain kernel, the relevant integro-partial differential equation is

$$\frac{\partial^2}{\partial x^2}\left[\eta(x)\, S_{12}(x,y)\right] + \frac{\partial^2}{\partial y^2}\left[\eta(y)\, S_{12}(x,y)\right]$$

$$+ \frac{q_\eta(x)}{\beta(x)}\,\delta(x-y) - \int_0^1 \frac{\eta(x)\beta(z)^2}{r(z)} S_{22}(x,z) S_{22}(z,y)\, dz = 0 \qquad (6.28)$$

Note that this second equation requires knowledge of $S_{12}(x,y)$, which is determined upon solving (6.27). Thus, the two equations must be solved consecutively, using approximate numerical methods.

6.2.3 Numerical Solution of the Riccati Equations

Previous attempts to obtain a numerical solution to the optimal distributed control problem for a particular system have most often dealt with the operator form of the Riccati equation, which is derived by Gibson (1979) using Eq. (6.12) rather than Eq. (6.13). Usually, the solution is expressed as a series expansion of spatial differential operators of increasing order, as in Juang (1983). In some cases, the distributed control law is only solved at points where discrete controls are to be applied, which leads to a slightly suboptimal design. Balas (1982) takes this approach. However, in this formulation, the functional form of the Riccati equations leads naturally to a numerical solution procedure. Because of the fundamental differences in the forms of Eqs. (6.27) and (6.28), a separate algorithm is developed for each equation, as discussed below.

6.2.3.1 Solution of the First Riccati Equation

Equation (6.27) is solved by spatially discretizing the domain of S_{12} and using finite differencing and summation to approximate the derivative and integral operations, respectively. A modified relaxation algorithm is then invoked to converge upon the solution. We begin by discretizing the spatial variables according to

$$x_i = \frac{i}{N}, \quad i = 0,\ldots,N \tag{6.29}$$

and defining the mesh

$$s_{ij} = s_{12}(x_i, y_j) \tag{6.30}$$

A simple approximation to the derivative terms is then

$$\frac{\partial^2}{\partial x^2}\left[\beta(x)\, S_{12}(x,y)\right] + \frac{\partial^2}{\partial y^2}\left[\beta(y)\, S_{12}(x,y)\right] \approx N^2\left[\Delta_{ij}^{\beta} - 2(\beta_i+\beta_j)s_{ij}\right] \tag{6.31}$$

where Δ_{ij}^{β} is defined by

$$\Delta_{ij}^{\beta} = \beta_{i-1}\, s_{i-1\, j} + \beta_{i+1}\, s_{i+1\, j} + \beta_{j-1}\, s_{i\, j-1} + \beta_{j+1}\, s_{i\, j+1} \tag{6.32}$$

The forcing term in Eq. (6.27) can be approximated by

$$q_U(x)\eta(x)\,\delta(x-y) \approx N\, q_{U_i}\eta_i\,\delta_{ij} \tag{6.33}$$

and δ_{ij} is the discrete Kroneker delta function. Finally, the integral term is replaced with a summation, leading to

$$\begin{aligned}\int_0^1 \frac{\eta(x)\beta(z)^2}{r(z)} S_{12}(x,z)S_{12}(z,y)\,dz &\approx \frac{1}{N}\sum_{k=0}^{N}\frac{\eta_k\beta_k^2}{r_k}\, s_{ik}\, s_{kj} \\ &= \frac{1}{N}\left[I_{ij} + \left(\frac{\eta_i\beta_i^2}{r_i}s_{ii} + \frac{\eta_j\beta_i^2}{r_j}s_{jj}\right)\left(1 - \frac{1}{2}\delta_{ij}\right) s_{ij}\right]\end{aligned} \tag{6.34}$$

where

$$I_{ij} = \sum_{\substack{k=0 \\ k\neq i \\ k\neq j}}^{N} \frac{\eta_k \beta_k^2}{r_k} s_{ik}\, s_{kj} \tag{6.35}$$

Note that, in Eqs. (6.31) and (6.34), the terms involving s_{ij} have been isolated from terms involving neighboring points. Collecting the approximate expressions, we have, for the finite difference equation

$$N^2\Delta_{ij}^{\beta} - 2N^2(\beta_i+\beta_j)s_{ij} = N\, q_{U_i}\eta_i\,\delta_{ij} - \frac{1}{N}I_{ij} - \frac{1}{N}\left(\frac{\eta_i\beta_i^2}{r_i}s_{ii} + \frac{\eta_j\beta_j^2}{r_j}s_{jj}\right)\left(1 - \tfrac{1}{2}\delta_{ij}\right)s_{ij} \tag{6.36}$$

Thus, given an initial estimate for the solution at each mesh point, s_{ij}^0, the entire mesh is successively iterated according to the rule

$$s_{ij}^{n+1} = s_{ij}^n - \omega e_{ij}^n, \quad 0<\omega<2 \tag{6.37}$$

In this last equation, e_{ij}^n represents the residual error at each mesh point at the n-th iteration. An expression for this error is obtained by solving Eq. (6.36) for s_{ij}, which yields

$$e_{ij} = s_{ij} - \frac{N^2\Delta_{ij}^{\beta} + \frac{1}{N}I_{ij} - N\, q_{U_i}\eta_i\,\delta_{ij}}{2N^2(\beta_i+\beta_j) - \frac{1}{N}\left(\frac{\eta_i\beta_i^2}{r_i}s_{ii} + \frac{\eta_j\beta_j^2}{r_j}s_{jj}\right)\left(1 - \tfrac{1}{2}\delta_{ij}\right)} \tag{6.38}$$

Also, ω is a relaxation parameter, and can be adjusted to maximize the rate of convergence towards a solution, as discussed in Press (1986).

The condition for a converged solution is given by

$$\left|e_{ij}^n\right| < \varepsilon, \quad \forall\, i,j \tag{6.39}$$

where ε is some small positive constant. The relaxation method is guaranteed to converge when r approaches infinity (In this case, Eq. (6.27) reduces to Poisson's equation), and tests have shown that convergence is maintained over a wide range of values of q_U and r, provided ω is adjusted accordingly.

In Fig. 6-1, the gain surfaces for various q_U/r are shown for the case of constant section properties. The effect of the boundaries can be seen by observing the gain surface near (x,y)=(0,0) and (x,y)=(1,1). Qualitatively, the influence of the boundary conditions extends over a smaller domain as the control authority is increased (i.e., as the quantity r/q_U becomes smaller). A quantitative analysis indicates that the extent of this "boundary layer" is roughly proportional to $(r/q_U)^{1/4}$. This makes sense physically. As the control authority is increased (r decreasing), the system is able to suppress the majority of a disturbance before the energy reaches and reflects off the boundary. Thus, near the center of the beam, the controller models the beam as if it were infinite in length.

6.2.3.2 Solution of the Second Riccati Equation

Equation (6.28) does not have a well-behaved solution, since it requires that the integral of $S_{22}(x,y)$ cancel the delta function. We therefore make the following substitution:

$$S_{22}(x,y) = \tilde{S}_{22}(x,y) + \frac{\eta(x)}{\eta(x)\beta(x)^2}\, g(x)\, \delta(x-y) \tag{6.40}$$

where

$$g(x) = \sqrt{\frac{\eta(x)\beta(x)}{r(x)}\left[\eta(x)^2 q_U(x) + q_T(x)\right]} \tag{6.41}$$

This is equivalent to identifying a collocated component in the velocity feedback kernel. Equation (6.28) then becomes

$$\int_0^1 \frac{\eta(z)\beta(z)^2}{r(z)}\, \tilde{S}_{22}(x,z)\tilde{S}_{22}(z,y)\, dz + [g(x)+g(y)]\, \tilde{S}_{22}(x,y) - c(x,y) = 0 \tag{6.42}$$

where the known forcing term is given by

$$c(x,y) = \frac{\partial^2}{\partial x^2}\left[\eta(x)\, S_{12}(x,y)\right] + \frac{\partial^2}{\partial y^2}\left[\eta(y)\, S_{12}(x,y)\right] - q_U(x)\, \frac{\eta(x)^2}{\beta(x)}\, \delta(x-y) \tag{6.43}$$

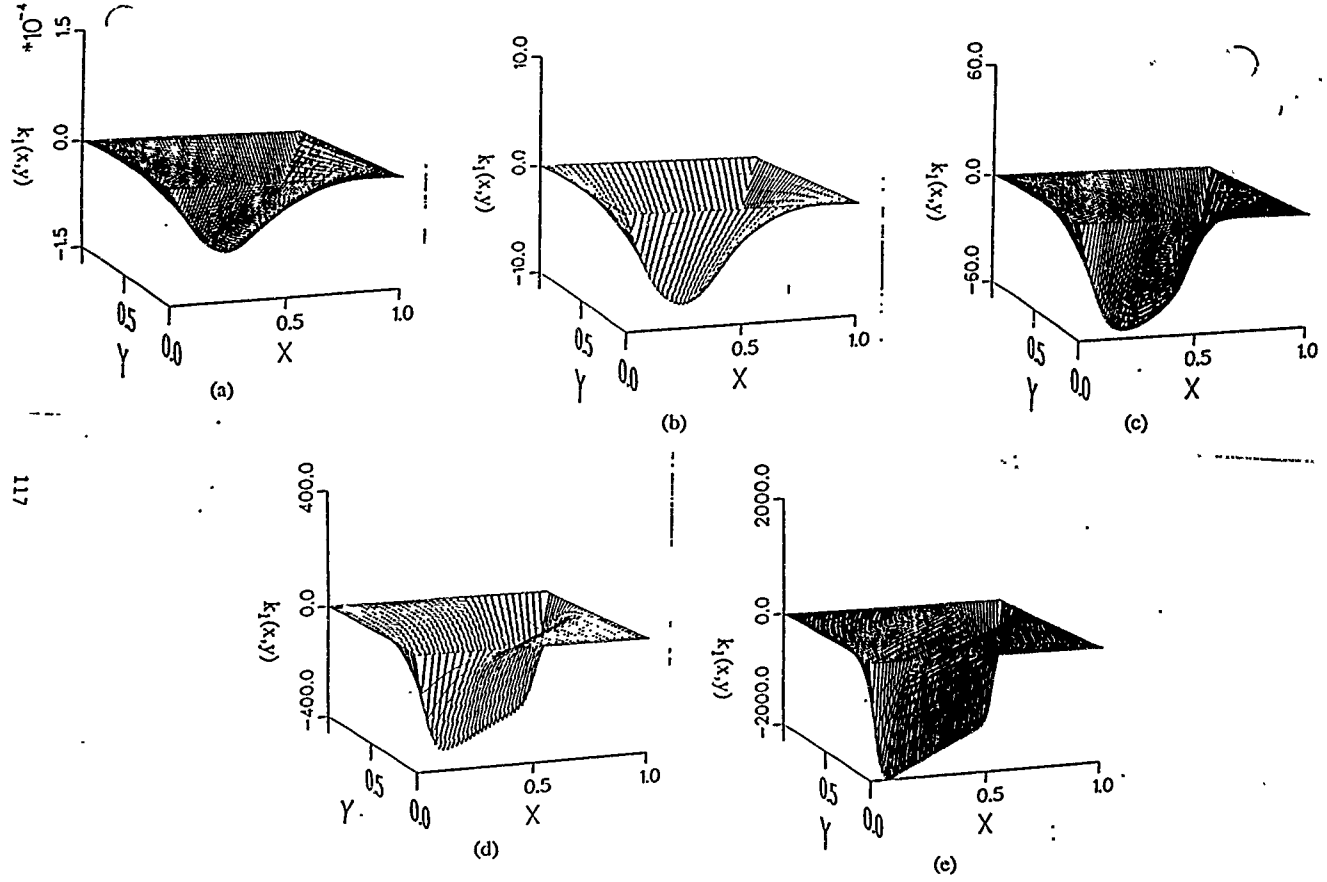

Fig. 6-1: Curvature feedback kernels for uniform beam: (a) $r/q_U=10^3$, (b) $r/q_U=10^{-2}$, (c) $r/q_U=10^{-3}$, (d) $r/q_U=10^{-4}$, (e) $r/q_U=10^{-5}$.

It is easy to show that $c(x,y)$ is continuous (assuming $\eta(x)$ and $\beta(x)$ are continuous), as the partial differentiation terms produce delta functions that exactly cancel the term involving $\delta(x-y)$.

The solution algorithm for S_{22} is straightforward. Upon discretizing in the spatial dimension, Eq. (6.42) becomes

$$\tilde{S}_{22}R^{-1}\tilde{S}_{22} + \tilde{S}_{22}G + G\tilde{S}_{22} - C = 0 \tag{6.44}$$

where

$$\tilde{S}_{22} = \left[\tilde{S}_{22}(x_i,y_j)\right] \tag{6.45a}$$

$$C = \left[c(x_i,y_j)\right] \tag{6.45b}$$

$$G = \text{diag}\left[g(x_i)\right] \tag{6.45c}$$

$$R = \text{diag}\left[N\frac{r(x_i)}{\eta(x_i)\beta(x_i)^2}\right] \tag{6.45d}$$

and N is the number of mesh points between x=0 and x=1. The matrix equation is solved by completing the square. After pre- and post-multiplying by $R^{-1/2}$, Eq. (6.44) can be factored as

$$\left[R^{-1/2}\tilde{S}_{22}R^{-1/2} + G\right]^2 = R^{-1/2}CR^{-1/2} + G^2 \tag{6.46}$$

The right hand side of Eq. (6.46) is symmetric and positive semidefinite. It therefore has the eigenvector decomposition

$$R^{-1/2}CR^{-1/2} + G^2 = W\Lambda W^T \tag{6.47}$$

where Λ is a diagonal matrix with non-negative entries. Finally, substituting Eq. (6.47) in Eq. (6.46) and solving for $\tilde{S}_{22}$ gives

$$\tilde{S}_{22} = R^{1/2}\left[W\Lambda^{1/2}W^T - G\right]R^{1/2} \tag{6.48}$$

Typical $\tilde{k}_2(x,y)$ surfaces are shown in Fig. 6-2 ($\tilde{k}_2(x,y)$ is just $k_2(x,y)$ without the delta function corresponding to the collocated feedback component). Finally, Fig. 6-3 shows the feedback gain kernels associated with a tapered beam.

6.2.4 The Case of Curvature Actuation

For the sake of simplicity, we will assume constant section properties and weighting functions for this case. This makes it possible to obtain an analytical expression for the feedback gains. (Note that, for force actuation, a numerical solution procedure is required even in the case of constant section properties and weightings.)

The feedback gains, expressed in terms of the solutions to the Riccati equations, become

$$k_1(x,y) = \frac{1}{r}\frac{\partial^2}{\partial x^2} S_{12}(x,y), \quad k_2(x,y) = \frac{1}{r}\frac{\partial^2}{\partial x^2} S_{22}(x,y) \qquad (6.49a,b)$$

and the functional Riccati equations themselves become

$$\frac{\partial^2}{\partial x^2} S_{12}(x,y) + \frac{\partial^2}{\partial y^2} S_{12}(x,y) = q_U \delta(x-y) - \frac{1}{r}\int_0^1 S_{12}(x,z)\frac{\partial^4}{\partial z^4} S_{12}(z,y)\, dz \qquad (6.50a)$$

$$\frac{\partial^2}{\partial x^2} S_{12}(x,y) + \frac{\partial^2}{\partial y^2} S_{12}(x,y) + q_T \delta(x-y) - \frac{1}{r}\int_0^1 S_{22}(x,z)\frac{\partial^4}{\partial z^4} S_{22}(z,y)\, dz = 0 \qquad (6.50b)$$

Integrating by parts and invoking the homogeneous boundary conditions yields

$$\frac{\partial^2}{\partial x^2} S_{12}(x,y) + \frac{\partial^2}{\partial y^2} S_{12}(x,y) = q_U \delta(x-y) - \frac{1}{r}\int_0^1 \frac{\partial^2}{\partial z^2} S_{12}(x,z)\frac{\partial^2}{\partial z^2} S_{12}(z,y)\, dz \qquad (6.51a)$$

$$\frac{\partial^2}{\partial x^2} S_{12}(x,y) + \frac{\partial^2}{\partial y^2} S_{12}(x,y) + q_T \delta(x-y) - \frac{1}{r}\int_0^1 \frac{\partial^2}{\partial z^2} S_{22}(x,z)\frac{\partial^2}{\partial z^2} S_{22}(z,y)\, dz = 0 \qquad (6.51b)$$

Furthermore, introducing Eqs. (6.49a,b) and exploiting the symmetry of S(x,y) yields

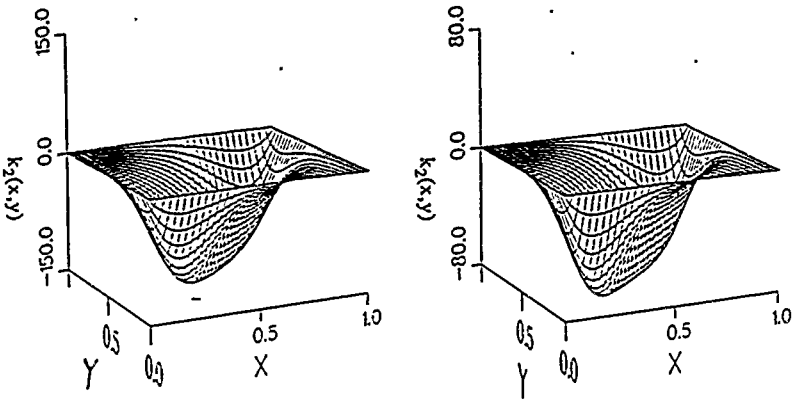

Fig 6-2: Velocity feedback kernels for uniform beam: (a) $r/q_U=10^{-4}$ and $q_T=0$, (b) $r/q_U=10^{-4}$ and $q_T=q_U$.

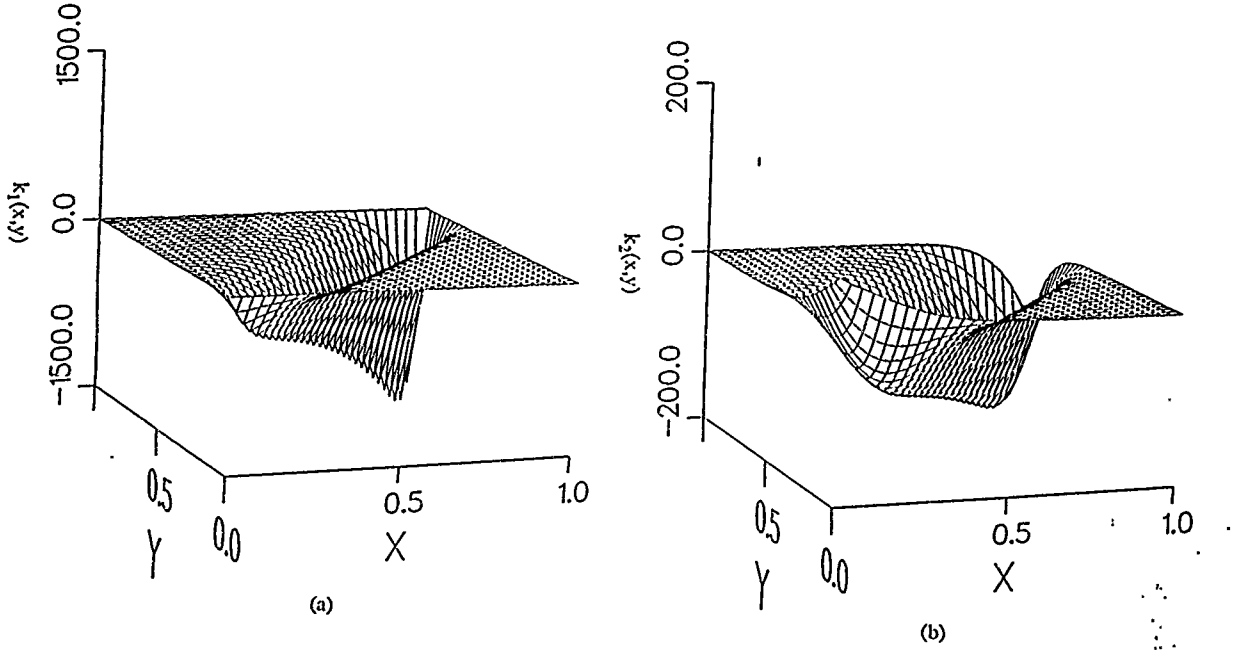

Fig 6-3: Feedback gains for tapered beam (Beam diameter varies linearly from 1.0 at x=0 to 0.75 at x=1): (a) Curvature feedback kernel, (b) Velocity feedback kernel.

$$2r k_{12}(x,y) = q_U \delta(x-y) - r \int_0^1 k_{12}(x,z) k_{12}(z,y)\, dz \tag{6.52a}$$

$$r \int_0^1 k_{22}(x,z) k_{22}(z,y)\, dz = 2r k_{12}(x,y) + q_T \delta(x-y) \tag{6.52b}$$

It can easily be shown that the generalized functions

$$k_1(x,y) = \left[\sqrt{1 + \frac{q_U}{r}} - 1 \right] \delta(x-y) \tag{6.53a}$$

$$k_2(x,y) = \sqrt{\frac{q_T}{r} + 2 \left[\sqrt{1 + \frac{q_U}{r}} - 1 \right]}\ \delta(x-y) \tag{6.53b}$$

solve the Riccati equations. The optimal control is therefore purely collocated, even though the controller has access to the state vector over the entire spatial domain.

6.2.5 Closed-Loop Simulation Results

The closed-loop simulations of a uniform beam with a sinusoidal initial condition and various control and state weightings are shown in Fig. 6-4. As expected, the response of the system becomes faster with increasing control authority. In Fig. 6-5, the response of the system to a center-span transverse impulse is shown. This figure can be compared with the open-loop case, shown in Fig. 5-3. In this case, most of the disturbance has been suppressed before it reflects from the boundaries, and the first mode of vibration is never established. This is characteristic of high-gain control systems, which provide high levels of damping augmentation. For these systems, the energy in the propagating wave is effectively absorbed as it progresses towards the boundaries of the system.

In order to compare the performance of the optimal distributed controller with the performance of discrete controllers, finite element models of the beam system were developed. These models have as state variables the same quantities that are used in the distributed model (i.e., curvature and velocity), but are only available at discrete points along the structure. Similarly, the control inputs are available at a finite number of stations along the beam. These models were used

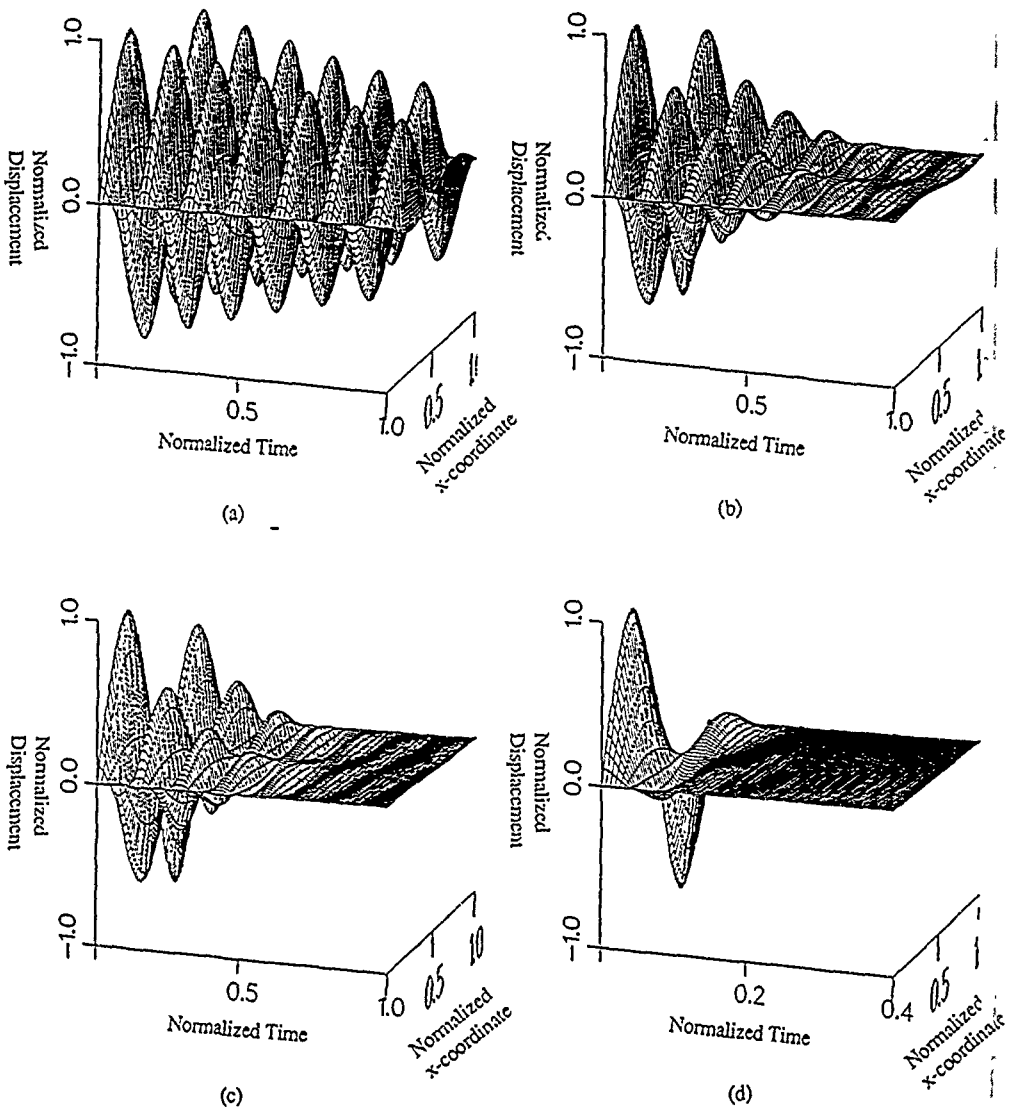

Fig 6-4: Closed-loop simulation of uniform beam with $v_0(x)=\sin(2\pi x)$: (a) $r/q_U=10^{-2}$ and $q_T=q_U$, (b) $r/q_U=10^{-3}$ and $q_T=q_U$, (c) $r/q_U=5\times10^{-4}$ and $q_T=q_U$, (d) $r/q_U=10^{-4}$ and $q_T=q_U$.

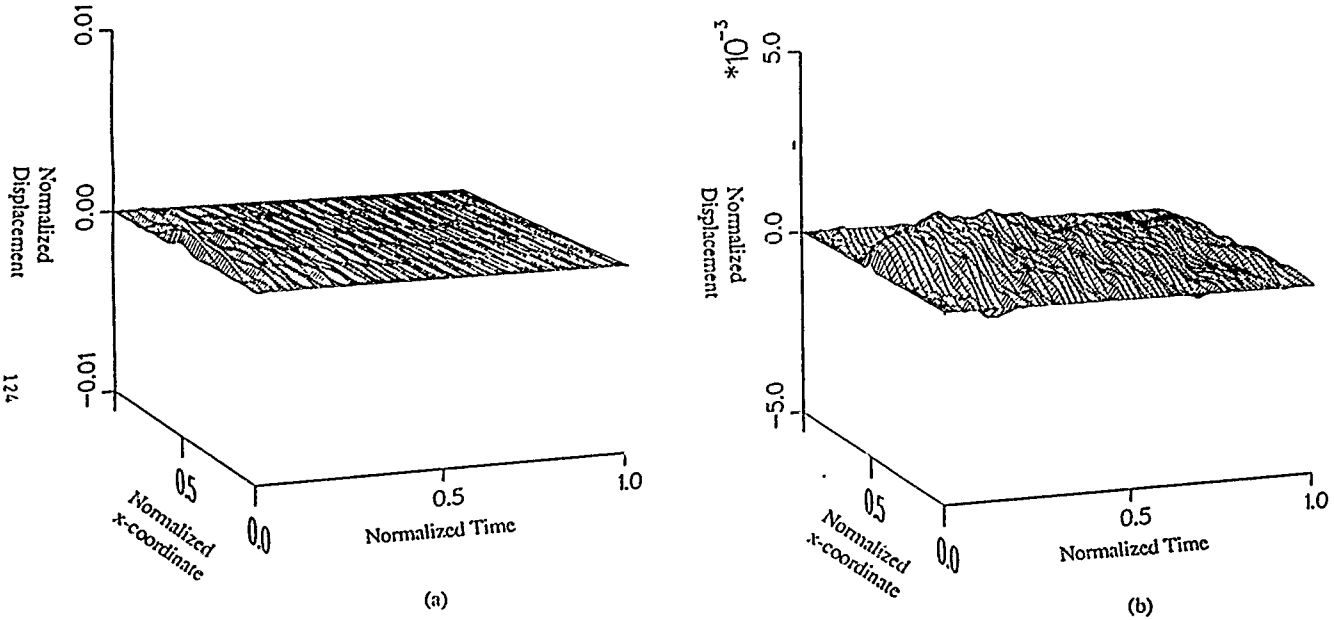

Fig. 6-5: Closed-loop simulation of uniform beam with unit impulse applied at center-span ($r/q_U=10^{-4}$ and $q_r=q_U$): (a) Long time scale, (b) Short time scale.

to develop full state LQR control laws for the discrete systems. Both the sinusoidal initial condition and the center-span impact cases were addressed. Table 6-1 summarizes the results of the study. In all cases, the optimal cost required to return the system to rest approaches the optimal distributed cost as the discretization becomes finer. (Details on determining the optimal cost for the distributed controller can be found in Appendix D.) This is convincing evidence that the distributed control formulation indeed converges upon an optimal solution.

6.3 Distributed Control of an Infinite Beam

In this section, we validate the results for the optimal control of finite beams by considering an infinite beam system. Most of the formulation presented in this section is based on recent work by deLuis (1989). The basic idea is to work in the spatial frequency-domain, using the spatially transformed dynamics of the beam system. This reduces the distributed control problem to a family of conventional optimal control problems, parametrized by the spatial frequency variable. The infinite model requires that the section properties and cost weightings be spatially constant, so that the spatial transform is possible. In his work, deLuis relies on functional analysis arguments to justify the form of the control law. In contrast, the approach presented here is somewhat more straightforward and intuitively satisfying.

6.3.1 Spatially Transformed Dynamics and Cost Functional

Because the beam is of infinite extent, we can take the spatial Fourier transform of (5.1). The resulting equation of motion, expressed in terms of t and the spatial frequency, ξ, is then

$$\dot{\hat{x}}(\xi,t) = A(\xi)\hat{x}(\xi,t) + b\hat{u}(\xi,t) \tag{6.54}$$

where $A(\xi)$ is obtained from Eq. (5.12a):

$$A(\xi) = \begin{bmatrix} 0 & -\xi^2 \\ \xi^2 & 0 \end{bmatrix} \tag{6.55}$$

	Weightings			Lumped Parameter Formulation			Distributed Formulation
	q_U	q_T	r	8 elements	16 elements	32 elements	
J_d	1	1	10^{-4}	13.68	13.28	13.19	13.15
	1	1	10^{-3}	22.02	21.72	21.65	21.64
	1	1	10^{-2}	56.79	56.67	56.64	56.63
	10	1	10^{-2}	158.48	156.62	156.18	156.13
J_v	1	1	10^{-4}	6.50×10^{-3}	6.81×10^{-3}	6.94×10^{-3}	7.07×10^{-3}
	1	1	10^{-3}	2.16×10^{-2}	2.24×10^{-2}	2.21×10^{-2}	2.24×10^{-2}
	1	1	10^{-2}	6.99×10^{-2}	7.03×10^{-2}	7.05×10^{-2}	7.07×10^{-2}
	10	1	10^{-2}	0.153	0.160	0.163	0.166

Table 6-1: Comparison between optimal costs for distributed control and conventional lumped-parameter control. In the table, J_d corresponds to an initial displacement field $v_0(x)=\sin(2\pi x)$, and J_d corresponds to an initial unit impulsive disturbance applied at the center-span of the beam.

The transformed state variable and the transformed control input are, in general, complex-valued. However, because A(ξ) and b are purely real for this system, the real and imaginary dynamics decouple, giving

$$\dot{\hat{x}}_r(\xi,t) = A(\xi)\hat{x}_r(\xi,t) + b\hat{u}_r(\xi,t), \quad \dot{\hat{x}}_i(\xi,t) = A(\xi)\hat{x}_i(\xi,t) + b\hat{u}_i(\xi,t) \qquad (6.56a,b)$$

Thus, for each value of ξ, we are left with two identical real-valued systems for which an optimal control solution is desired.

The cost functional to be minimized is quadratic in the normalized variables. For distributed control, we must integrate over the entire (infinite) domain. The cost functional is thus

$$J = \frac{1}{2}\int_0^{\infty}\int_{-\infty}^{\infty}\left\{q_U\left[\frac{\partial^2 w}{\partial x^2}\right]^2 + q_T\left[\frac{\partial w}{\partial t}\right]^2 + r f_u^2\right\} dx\, dt \qquad (6.57)$$

In this last expression, which is analogous to Eq. (6.21), q_U and q_T weigh potential and kinetic energy, respectively, while r weighs control effort. Equation (6.57) can be written

$$J = \frac{1}{2}\int_0^{\infty} J_\xi(t)\, dt \qquad (6.58)$$

where

$$J_\xi(t) = \int_{-\infty}^{\infty}\left[y(x,t)^T y(x,t) + r\, u(x,t)^2\right] dx \qquad (6.59)$$

and the following definitions have been made:

$$y(x,t) = Q^{1/2}x(x,t), \quad Q = \begin{bmatrix} q_U & 0 \\ 0 & q_T \end{bmatrix} \qquad (6.60a,b)$$

By making use of Parseval's theorem, we can write

$$J_\xi(t) = \frac{1}{2\pi}\int_{-\infty}^{\infty}\left[\hat{x}(\xi,t)^H Q\hat{x}(\xi,t) + r\,|\hat{u}(\xi,t)|^2\right] d\xi \qquad (6.61)$$

where the superscript (^{H}) represents the complex conjugate transpose operation. Now, interchanging the order of integration in (6.58) yields

$$J = \frac{1}{4\pi} \int_{-\infty}^{\infty} J_t(\xi)\, d\xi \tag{6.62}$$

where

$$J_t(\xi) = \int_0^{\infty} \left[\hat{x}(\xi,t)^H Q \hat{x}(\xi,t) + r\, |\hat{u}(\xi,t)|^2 \right] dt \tag{6.63}$$

At this point, the following observation can be made: J is minimized if and only if $J_t(\xi)$ is minimized for every value of ξ. We must now express $\hat{x}(\xi,t)$ and $\hat{u}(\xi,t)$ in terms of their real and imaginary parts. Because Q and r are purely real, the (imaginary) cross-terms cancel in (6.63), and we are left with

$$\begin{aligned} J_t(\xi) = & \int_0^{\infty} \left[\hat{x}_r(\xi,t)^H Q \hat{x}_r(\xi,t) + r\, \hat{u}_r(\xi,t)^2 \right] dt \\ & + \int_0^{\infty} \left[\hat{x}_i(\xi,t)^H Q \hat{x}_i(\xi,t) + r\, \hat{u}_i(\xi,t)^2 \right] dt \end{aligned} \tag{6.64}$$

6.3.2 Optimal Control Solution

For each value of ξ, we have two identical dynamic systems given by Eqs. (6.56a,b) and two identical cost functionals given by Eq. (6.64). Therefore, the control laws relating $\hat{u}_r$ to $\hat{x}_r$ and $\hat{u}_i$ to $\hat{x}_i$ will be identical, and can be combined into the single equation

$$\hat{u}(\xi,t) = -\hat{k}(\xi)^T \hat{x}(\xi,t) \tag{6.65}$$

where the transformed gain vector, $\hat{k}(\xi)$, is a real function of the spatial frequency. Taking the inverse transform of this equation yields

$$u(x,t) = -\int_{-\infty}^{\infty} k(x-y)^T x(y,t)\, dy \qquad (6.66)$$

Thus, the integration kernel k(x-y) can be though of as a weighting from the sensed state at a location y to the control actuation at a location x. Classical LQR theory gives, as the optimal solution

$$\hat{k}(\xi)^T = \left[\hat{k}_1(\xi)\ \hat{k}_2(\xi)\right] = \frac{1}{r} b^T S(\xi) \qquad (6.67)$$

where $S(\xi)$ solves the control algebraic Riccati equation

$$A(\xi)^T S(\xi) + S(\xi)A(\xi) + Q - \frac{1}{r} S(\xi) b b^T S(\xi) = 0 \qquad (6.68)$$

Substituting the known parameters $A(\xi)$, b, Q and r and solving for the elements of S gives

$$S_{11}(\xi) = r\xi^2 \sqrt{1+\lambda_U} \sqrt{\lambda_T + 2\left[\sqrt{1+\lambda_U} - 1\right]} \qquad (6.69a)$$

$$S_{12}(\xi) = -r\xi^2 \left[\sqrt{1+\lambda_U} - 1\right] \qquad (6.69b)$$

$$S_{22}(\xi) = r\xi^2 \sqrt{\lambda_T + 2\left[\sqrt{1+\lambda_U} - 1\right]} \qquad (6.69c)$$

where

$$\lambda_U = \frac{q_U}{r\xi^4}, \quad \lambda_T = \frac{q_T}{r\xi^4} \qquad (6.70a,b)$$

Note that the entire behavior of the solution is parametrized by the dimensionless groupings, λ_U and λ_T. Since ξ has the units of inverse length, we can infer that $(r/q_U)^{1/4}$ and $(r/q_T)^{1/4}$ represent nondimensional distances.

Substituting Eq. (6.69b) in Eq. (6.67), we obtain, for the feedback gain relating curvature to force,

$$k_1(x) = (q_U/r)^{3/4} f_1\left[(q_U/r)^{1/4} x\right] \qquad (6.71)$$

where $f_1(\cdot)$ is the inverse transform of $\hat{f}_1(\cdot)$, given by

$$\hat{f}_1(\xi) = -\left[\sqrt{\xi^4 + 1} - \xi^2\right] \tag{6.72}$$

A plot of $f_1(\cdot)$ is shown in Fig. 6-6. Some qualitative features of the feedback gain become apparent upon examination of Eq. (6.71). First, the magnitude of the feedback varies as $(q_U/r)^{3/4}$, so that increased curvature penalty and reduced control penality both increase the feedback gain, as expected. Second, the argument of $f_1(\cdot)$ indicates that the control becomes more localized with increasing state penalty and increasing control authority. This makes sense in terms of the nondimensional lengths described above. High control authority suggests that a disturbance can be suppressed quickly, before the majority of the energy travels very far along the beam, whereas low authority requires a longer time interval (and hence greater distance) to suppress the disturbance. These features are also observed for the finite beam system described in Section 6.2. In fact, cross sections of the finite beam gain kernels, taken near the center of the surface, have the approximate shape of the gain kernel for the infinite beam system, and the approximation gets better with increasing control authority. A quantitative analysis indicates that this is the case when $r/q_U < 10^{-3}$.

In computing $k_2(x)$, the velocity to force feedback term, an interesting feature emerges. The Riccati solution, $S_{22}(\xi)$, does not go to zero as ξ approaches infinity. As a result, the inverse transform of $\hat{k}_2(\xi)$ will include a delta function. In order to make the inverse transform continuous, this bias term is subtracted from $\hat{k}_2(\xi)$, and a delta function with magnitude equal to this bias is added to $k_2(x)$ after inversion. Thus, the velocity feedback gain kernel is expressed as

$$k_2(x) = (q_U/r)^{3/4}\, f_2\left[(q_U/r)^{1/4}x\,;\, q_T/q_U\right] + \sqrt{\frac{q_U}{r} + \frac{q_T}{r}}\,\delta(x) \tag{6.73}$$

where

$$\hat{f}_2(\xi\,;\gamma) = \sqrt{\gamma - 2k^2\,\hat{f}_1(\xi)} - \sqrt{\gamma + 1} \tag{6.74}$$

This corresponds exactly with the introduction of a collocated velocity feedback term for the finite beam system. Indeed, the magnitude of the collocated gain agrees with the finite case, with the assumption of constant section properties and weightings. Note that the velocity feedback term is parametrized by the same nondimensional length as $k_1(x)$, but an additional parameter, the ratio

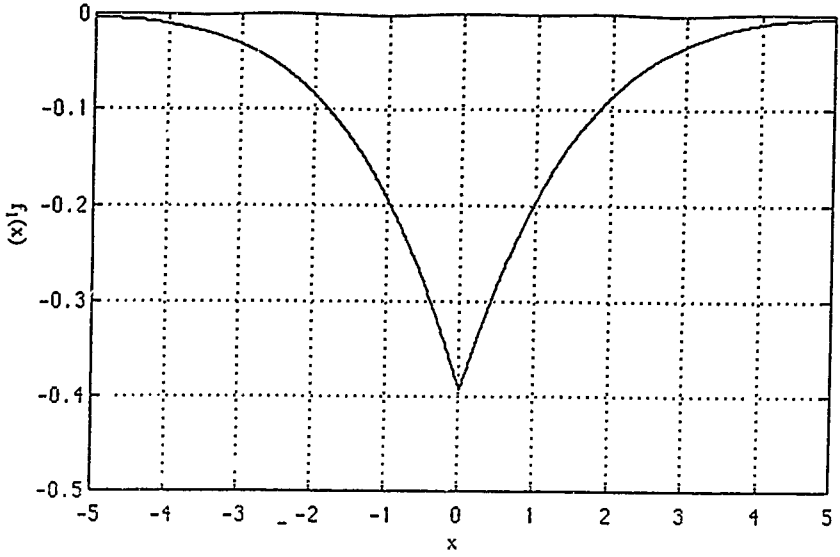

Fig. 6-6: Normalized curvature feedback gain kernel for infinite beam.

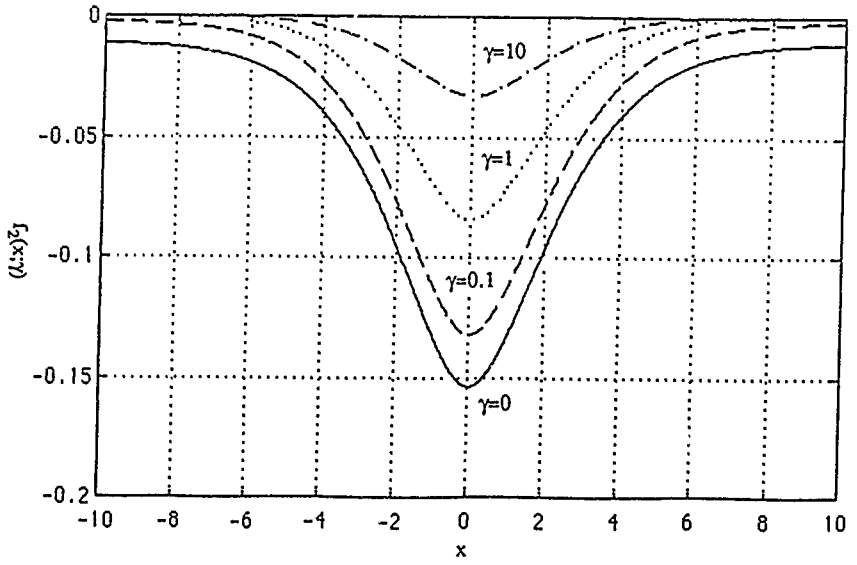

Fig. 6-7: Normalized velocity feedback gain kernel for infinite beam.

between kinetic and potential energy penalties, is also present. Plots of $f_2(\cdot\,;\gamma)$, shown for various γ, are shown in Fig. 6-7. Once again, cross sections of the velocity feedback gain kernel for the finite beam case agree quite well with the infinite beam kernel.

6.3.3 The Case of Curvature Actuation

We now study the case where a distributed actuator capable of inducing curvature in a continuous manner represents the control input. Such is the limiting case of a beam with many embedded piezoelectric actuators distributed along its span. For this system, the equation of motion is modified to

$$\frac{\partial^4}{\partial x^4} v(x,t) + \frac{\partial^2}{\partial t^2} v(x,t) = \frac{\partial^2}{\partial x^2} m_c(x,t) \tag{6.75}$$

where $m_c(x,t)$ represents the net action of the distributed piezoelectrics. By making the new definitions

$$u(x,t) = m_c(x,t), \quad b(\xi) = \begin{bmatrix} 0 \\ -\xi^2 \end{bmatrix} \tag{6.76a,b}$$

the transformed equation of motion becomes

$$\dot{\hat{x}}(\xi,t) = A(\xi)\hat{x}(\xi,t) + b(\xi)\hat{u}(\xi,t) \tag{6.77}$$

This equation is identical to Eq. (6.54) except that b is now a function of ξ. This subtle difference has a profound effect on the control law. Following the same procedure as in the previous subsection leads to expressions for the transformed gain kernels which are independant of ξ:

$$\hat{k}_1 = \sqrt{1 + \frac{qu}{r}} - 1, \quad \hat{k}_2 = \sqrt{\frac{qr}{r} + 2\,\hat{k}_1} \tag{6.78a,b}$$

As a result, we have

$$k_1(x) = \hat{k}_1\,\delta'(\cdot), \quad k_2(x) = \hat{k}_2\,\delta(x) \tag{6.79a,b}$$

The optimal control is therefore purely collocated, even though the controller has access to the state vector over the entire spatial domain. This result is quantitatively identical to the finite beam case presented in Section 6.2.5, regardless of the state and control effort penalties.

6.4 Discussion

It becomes clear that the choice of actuator for the Bernoulli-Euler beam system has a profound effect on the optimal control law. With a distributed force actuator, the curvature feedback is purely distributed (becoming more localized with increasing control authority), while the velocity feedback has both collocated and distributed components. For a finite beam, a nondimensional length, which depends on the state and control effort penalties, indicates the extent to which the boundary conditions imposed on the finite beam affect the optimal control solution. Numerical examples for finite beam systems support this claim.

For a beam with a distributed curvature actuator (a more realistic and implementable situation), both the curvature and velocity feedback gains are purely collocated, regardless of the nondimensional length parameter. As a result, the boundary conditions do not affect the optimal control solution for this type of actuation. The next logical step in this analysis would be to study the effect of replacing the distributed actuator with a set of discrete controls, which better reflects a physically realizable controlled structure. It would be interesting to observe whether or not the optimal feedback gains are still collocated for a set of discrete embedded piezoelectric actuators.

At present, no claims can be made concerning the robustness of the distributed controller. A quantitative robustness analysis would help determine the sensitivity of the performance of the system to errors in the structural model. Also, the assumption of a truly distributed controller is rather restrictive. Any implementable system will consist of a finite set of sensors and actuators. Consequently, the theory must be extended to account for discrete sensing and actuation. It may be possible to extend the optimal output feedback approach discussed by Levine (1971) or the optimal projection approach developed by Bernstein (1986) in a manner amenable to the discrete sensing/actuation problem.

Another future research topic is the determination of optimal distributed control laws for arbitrary boundary conditions. Such a development was attempted by Tzafestas (1970), but has found extremely limited application. For example, the optimal distributed control of a cantilevered beam was addressed by Bailey (1984) using Tzafestas' formulation, with the conclusion that the boundary conditions could not be posed in the specific mathematical form required by the formulation. Clearly, the problem lies in dealing with the boundary conditions which arise when determining the adjoint operators in Eqs. (6.6a-c). These boundary terms result in additional necessary conditions for optimality, expressed in terms of ordinary differential equations. Currently, no general formulation exists which includes these extra conditions. The ability to handle general boundary conditions would make it possible to develop control laws for multiple element structures, such as space frames and trusses.

Another possible application of distributed control theory is in the active control of two-dimensional structures, such as mirror surfaces and shell structures. However, numerical solutions for plates and membrane models require extensive computational capabilities, and therefore represent an ambitious undertaking.

7. HYBRID MODELLING AND CONTROL APPROACH FOR HAC/LAC DESIGN

It remains to develop a control strategy that utilizes the best aspects of both the TEM and direct modelling methodologies. For example, the distributed control solutions obtained through the direct model could form the basis for a LAC design. The resulting model of the controlled structure could then be transformed, and a HAC controller could be designed by posing the problem in the standard form, as described in Section 4.2. Finally, command prefiltering of control inputs for slew maneuvers would be determined using the open-loop optimal control theory discussed in Section 4.1. The exactness of the theory makes it more attractive than modal-based approaches, such as the work of Singer (1990). The entire hierarchically controlled system would then have the general form shown in Fig. 7-1.

Inherent in this objective is a general unification of the two modelling approaches, which has not been achieved to date. Such a unification would be a profound improvement in the ability to develop exact control models for large flexible structures. Analytic TEM solutions do exist, however, for some specific controlled structural elements. Consider, for example, the Bernoulli-Euler beam with curvature feedback. The dynamics equation, expressed in dimensional form, is

$$EI\frac{\partial^4}{\partial x^4}v(x,t) + \rho A\frac{\partial^2}{\partial t^2}v(x,t) = \frac{\partial^2}{\partial x^2}m_u(x,t) \tag{7.1}$$

The optimal distributed controller is collocated in this case, with the normalized feedback law given by

$$m_u(x,t) = -k_1\frac{\partial^2}{\partial x^2}v(x,t) - k_2\frac{\partial}{\partial t}v(x,t) \tag{7.2}$$

where k_1 and k_2 are determined via Eqs. (6.53a,b). Converting this feedback law into dimensional form yields

$$m_u(x,t) = -k_1 EI\frac{\partial^2}{\partial x^2}v(x,t) - k_2\sqrt{\rho AEI}\frac{\partial}{\partial t}v(x,t) \tag{7.3}$$

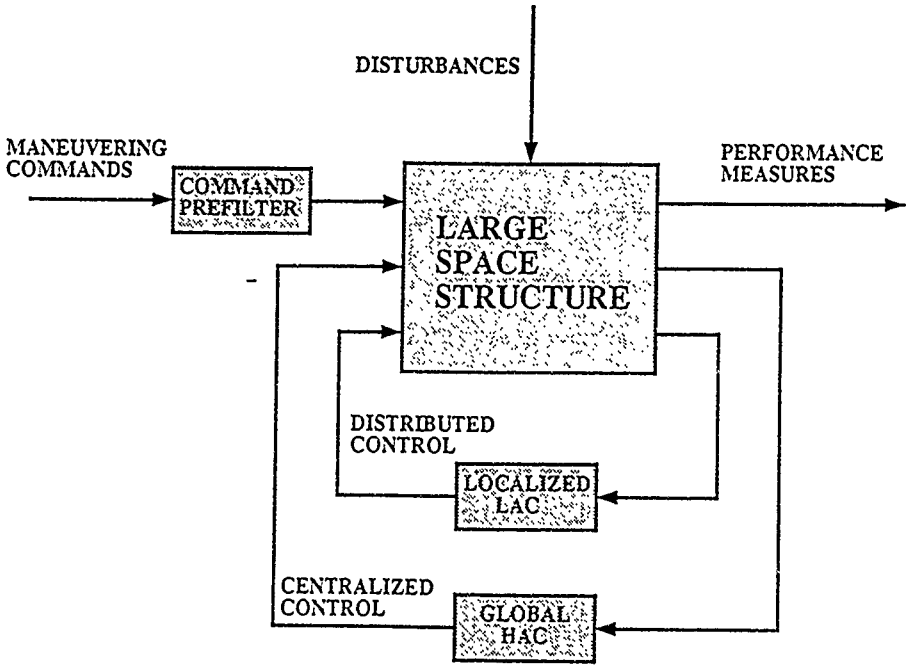

Fig. 7.1: Schematic of the complete HAC/LAC control architecture

and substituting this expression in the dynamics equation produces the equation of motion for the controlled structural element. It is given by

$$EI\,(1+k_1)\,\frac{\partial^4}{\partial x^4}v(x,t) + k_2\sqrt{\rho AEI}\,\frac{\partial^3}{\partial x^2\partial t}v(x,t) + \rho A\frac{\partial^2}{\partial t^2}v(x,t) = 0 \tag{7.4}$$

It is now possible to transform the closed-loop dynamics into the frequency-domain. Assuming zero initial conditions, we have

$$(1+k_1)\,\frac{\partial^4}{\partial x^4}\bar{v}(x,s) - j\,k_2\,\alpha^2\frac{\partial^2}{\partial x^2}\bar{v}(x,s) + \alpha^4\bar{v}(x,s) = 0 \tag{7.5}$$

where

$$\alpha^4 = -\frac{\rho A}{EI}\,s^2 \tag{7.6}$$

The homogeneous solution vector is then given by

$$v_H(x,s)^T = \left[e^{\alpha_1 x}\;\; e^{-\alpha_1 x}\;\; e^{j\alpha_2 x}\;\; e^{-j\alpha_2 x}\right] \tag{7.7}$$

with

$$\alpha_1 = \sqrt{\frac{\sqrt{1+k_1\cdot\left[\frac{k_2}{2}\right]^2} + j\,\frac{k_2}{2}}{1+k_1}}\;\alpha$$

$$\alpha_2 = \sqrt{\frac{\sqrt{1+k_1\cdot\left[\frac{k_2}{2}\right]^2} - j\,\frac{k_2}{2}}{1+k_1}}\;\alpha \tag{7.8a,b}$$

The expression for the internal state vector in terms of $\bar{v}(x,s)$ remains unchanged, and is given by Eq. (2.60). The same can be said for the generalized boundary displacements and forces. The homogeneous solution vector can then be used to derive analytical expressions for the dynamic stiffness and interpolation matrices, which will be slightly more complex than the matrices corresponding to the uncontrolled beam.

Unfortunately, if the feedback is indeed distributed rather than purely collocated, Eq. (7.5) becomes an integral equation. A general solution is therefore not available. However, the form of

the gain kernels for a particular problem (e.g., beam with force feedback) may lead to some form of analytical solution, or, at least, an accurate approximate solution. Whether or not these classes of controlled structures lend themselves to analytical TEM models in the general case remains an unresolved issue.

8. CONCLUSIONS AND RECOMMENDATIONS

The mathematically exact TEM and direct structural modelling methods have been developed and demonstrated. By retaining the dynamics that describe the structural model over the entire frequency range, accurate behavioral predictions are available. For example, the wave-like propagation characteristics associated with impulsive disturbances are easily observed using either exact modelling approach. In addition, these models do not require modal analysis techniques, although modal information is available for TEM models of frame-like structures. Furthermore, the frequency-domain analysis incorporates general viscoelastic damping mechanisms in a very straightforward manner. Finally, the dramatic increase in computation speed of the TEM analysis technique over traditional finite element modelling has been demonstrated.

New control formulations were developed that take advantage of the information available via the exact modelling methods. An open-loop optimal control technique was demonstrated using TEM models, and was found to virtually eliminate the residual energy associated with the slewing of flexible structures. The only approximation made concerned the control inputs themselves, which were assumed to have limited bandwidth. The direct analysis technique provided the framework for a distributed control theory. Having been developed, the theory was applied to a simple Bernoulli-Euler beam system, and the feedback gain kernels were determined. These kernels agreed with previous results concerning the optimal distributed control of an infinite beam.

Several issues remain unresolved, and are recommended for future research. Although the TEM methodology has been developed for two-dimensional structures, it is incomplete in two respects. First, the selection of boundary points and their relation to element geometry and solution accuracy must be addressed. Second, a rigorous method of determining the set of basis solutions for the homogeneous solution vector must be developed. Clearly, these two goals are intimately tied, as the number of basis solutions required is directly related to the number of the boundary points used. Inherent in this analysis is a comparison between the TEM analysis and finite element models of two-dimensional structures.

The closed-loop control problem, expressed in the frequency-domain with TEM models, remains to be solved. Here, the lack of a finite state-space representation of the plant is the fundamental difficulty. It may be possible to extend the coprime factorization technique to general structural systems, or develop some other approach.

The distributed control solutions developed here must be extended to include other structural elements, such as Timoshenko beams and axial and torsional rods. Two-dimensional elements, which may represent deformable mirror surfaces or solar panels, must also be incorporated into the distributed control framework, although this extension presents a considerably more difficult computational challenge. Finally, the theory must be extended to apply to multi-element structures, which may include any of the elements mentioned. The ability to handle the complex boundary conditions that arise at element junctions is the primary difficulty here.

An evaluation of the robustness of the distributed controller to model uncertainty must also be undertaken. Discrepencies between the model and the actual physical structure, caused by tolerances in physical dimensions and material properties, structural joint dynamics, nonlinear material behavior and other unmodelled dynamics, usually result in performance degradation. A rigorous robustness evaluation would quantify the relation between modelling error and performance. Linked to this issue are implementation considerations. Because actuators and sensors are always discrete in nature, the distributed control solution represents only a limiting case as the number of individual actuators and sensors approaches infinity. For any implementable control design, then, the effect of utilizing a finite set of actuators and sensors must be addressed. Also relevant is a study of the effect of actuator and sensor dynamics and their relation to robust stability.

A combined direct/TEM control methodology for structural systems is not yet available. This hybrid technique would facilitate the development of hierarchical control schemes, such as HAC/LAC, without resorting to modal analysis and truncation. Consequently, the problems of control and observation spillover would be alleviated, at least from a mathematical perspective.

(Actual implementation issues must also be addressed, as mentioned above.) Consequently, a less conservative control design would be required, resulting in enhanced nominal performance.

APPENDIX A: HIGH FREQUENCY TEM ELEMENTS

This appendix presents the dynamic stiffness matrices for high frequency TEM elements. In particular, the Mindlin-Herrmann axial rod and the Timoshenko beam, both described in Sec. 2.3.6, are discussed.

A.1 Mindlin-Herrmann Rod

The dynamics of the Mindlin-Herrmann rod are characterized by the following set of differential equations:

$$-a^2(\lambda+2G)\frac{\partial^2}{\partial x^2}v_1(x,s) + \rho a^2 s^2 v_1(x,s) = 2a\lambda\frac{\partial}{\partial x}v_2(x,s) \tag{A.1a}$$

$$a^2\kappa^2 G\frac{\partial^2}{\partial x^2}v_2(x,s) - \left[8\kappa_1^2(\lambda+G) + \rho a^2 s^2\right]v_2(x,s) = 4a\kappa_1^2\lambda\frac{\partial}{\partial x}v_1(x,s) \tag{A.1b}$$

All symbols in these equations are defined in Sec. 2.3.6. These equations apply to a rod of circular cross-section only. The Lame constants are related to the modulus of elasticity and Poisson's ratio of the material according to

$$\lambda = \frac{E\nu}{(1+\nu)(1-2\nu)}, \quad G = \frac{E}{2(1+\nu)} \tag{A.2a,b}$$

We will assume that the radial deformation, v_2, is constrained at the boundaries of the element. This is the case when the element is embedded in a structural junction. We therefore have

$$v_2(0,s) = v_2(L,s) = 0 \tag{A.3}$$

With these constraints imposed, the stiffness matrix becomes 2-by-2, and can be expressed by

$$K(s) = \frac{\pi a^2 E}{\Delta(s)}\begin{bmatrix}\beta_1 s_1 c_2 - \beta_2 s_2 c_1 & -\beta_1 s_1 + \beta_2 s_2 \\ -\beta_1 s_1 + \beta_2 s_2 & \beta_1 s_1 c_2 - \beta_2 s_2 c_1\end{bmatrix} \tag{A.4}$$

where

$$\Delta(s) = \frac{(1+\nu)(1-2\nu)}{(1-\nu)}\left[\frac{2\beta_1\beta_2(1-c_1c_2) + (\beta_1^2+\beta_2^2)s_1s_2}{\beta_1(\alpha_2 a) - \beta_2(\alpha_1 a)}\right] \tag{A.5}$$

and the following trigonometric definitions have been made:

$$c_i = \cos(\alpha_i L) \qquad s_i = \sin(\alpha_i L) \tag{A.6a,b}$$

Also, β_1 and β_2 are given by

$$\beta_i = \frac{\left[\kappa^2(1+\nu)(1-2\nu)^2\rho a^2 s^2 - 16\kappa_1^2\nu^2 E\right](\alpha_i a) + \kappa^2(1-\nu)(1-2\nu)E(\alpha_i a)^3}{4(1-\nu)(1-2\nu)\rho a^2 s^2 + 16\kappa_1^2 E} \tag{A.7}$$

and the nondimensional parameters $\alpha_1 a$ and $\alpha_2 a$ are given by

$$(\alpha_i a)^2 = -\lambda_1\left[(1+\lambda_2\sigma) \pm \sqrt{(1+\lambda_2\sigma)^2 - \frac{2}{\lambda_1}(1+\lambda_3\sigma)\sigma}\right] \tag{A.8}$$

where

$$\lambda_1 = \frac{4\kappa_1^2(1+\nu)}{\kappa^2(1-\nu)} \qquad \lambda_2 = \frac{(1+\kappa^2)(1-2\nu)+1}{8\kappa_1^2}$$
$$\lambda_3 = \frac{(1+\nu)(1-2\nu)}{4\kappa_1^2} \qquad \sigma = \frac{\rho a^2 s^2}{E} \tag{A.9a-d}$$

The stiffness matrix can be shown to reduce to that of the simple axial rod either by setting $\nu=0$ or by taking the limit as the radius, a, approaches zero.

A.2 Timoshenko Beam

The dynamics of the Timoshenko beam can be expressed either as a system of two coupled partial differential equations or as the single equation

$$EI\frac{\partial^4}{\partial x^4}v(x,t) + \rho A\ddot{v}(x,t) - \rho I\left[1+\frac{Ek}{G}\right]\frac{\partial^2}{\partial x^2}\ddot{v}(x,t) + \frac{\rho^2 Ik}{G}\ddot{\ddot{v}}(x,t) = f_d(x,t) \tag{A.10}$$

Taking the Laplace transform of this equation yields

$$\frac{\partial^4}{\partial x^4}v(x,s) + 2p_1\alpha^2\frac{\partial^2}{\partial x^2}v(x,s) - \alpha^4 v(x,s) = \tilde{f}_d(x,s) \tag{A.11}$$

where the following parameters have been defined:

$$\alpha^4 = -\frac{\rho A s^2}{EI} \qquad k_1 = \frac{E}{G}\frac{k}{\kappa} \qquad r^2 = \frac{I}{A} \tag{A.12a-e}$$

$$p_1 = \tfrac{1}{2}(1+k_1)(\alpha r)^2 \qquad p_2^2 = 1 - k_1(\alpha r)^4$$

The homogeneous solution vector is then

$$v_H(x,s) = \begin{bmatrix} \cosh(\alpha\beta_1 x) \\ \sinh(\alpha\beta_1 x) \\ \cos(\alpha\beta_2 x) \\ \sin(\alpha\beta_2 x) \end{bmatrix} \tag{A.13}$$

where

$$\beta_1^2 = p_3 - p_1, \quad \beta_2^2 = p_3 + p_1 \tag{A.14a,b}$$

and

$$p_3^2 = p_1^2 + p_2^2 = 1 + \tfrac{1}{4}(1-k_1)^2(\alpha r)^4 \tag{A.15}$$

Due the the internal shearing allowed by the Timoshenko model, the expressions for the internal state vector in terms of the homogeneous solution become considerably more complex. They are:

$$u(x,s) = \begin{bmatrix} v(x,s) \\ \theta(x,s) \\ M(x,s) \\ S(x,s) \end{bmatrix} = \begin{bmatrix} 1 \\ \frac{1}{p_2^2}\left[(1+p_4^2)\frac{\partial}{\partial x} + \frac{p_4}{\alpha^2}\frac{\partial^3}{\partial x^3}\right] \\ EI\left[\frac{\partial^2}{\partial x^2} + p_4\alpha^2\right] \\ \frac{EI}{p_2^2}\left[\frac{\partial^3}{\partial x^3} + p_1\alpha^2\frac{\partial}{\partial x}\right] \end{bmatrix} v(x,s) \tag{A.16}$$

where

$$p_4 = k_1(\alpha r)^2 \tag{A.17}$$

The stiffness matrix then takes the form given by Eq. (2.66), with

$$
\begin{aligned}
K_1(s) &= \frac{p_2}{\alpha^3}(\beta_4\,\mathrm{sh} - \beta_3\,\mathrm{st}) \\
K_2(s) &= \frac{p_2}{\alpha^3}(\beta_3\,\mathrm{ch}\,\mathrm{st} - \beta_4\,\mathrm{sh}\,\mathrm{ct}) \\
K_3(s) &= \frac{1}{\alpha^2}(\mathrm{ch} - \mathrm{ct}) \\
K_4(s) &= \frac{1}{p_3\alpha^2}\left[\frac{p_2^2+p_1 p_4}{p_2}\mathrm{sh}\,\mathrm{st} + (p_1-p_4)(1-\mathrm{ch}\,\mathrm{ct})\right] \\
K_5(s) &= \frac{1}{\alpha}(\beta_3\,\mathrm{sh} + \beta_4\,\mathrm{st}) \\
K_6(s) &= \frac{1}{\alpha}(\beta_4\,\mathrm{ch}\,\mathrm{st} + \beta_3\,\mathrm{sh}\,\mathrm{ct}) \\
\Delta(s) &= \frac{1}{p_3\alpha^4}\left[1 - \mathrm{ch}\,\mathrm{ct} - \frac{1}{2}\left(\frac{\beta_3}{\beta_4} - \frac{\beta_4}{\beta_3}\right)\mathrm{sh}\,\mathrm{st}\right]
\end{aligned}
\qquad \text{(A.18ag)}
$$

The trigonometric quantities must also be modified to

$$
\begin{aligned}
\mathrm{ch} &= \cosh(\alpha\beta_1 L) \\
\mathrm{sh} &= \sinh(\alpha\beta_1 L) \\
\mathrm{ct} &= \cos(\alpha\beta_2 L) \\
\mathrm{st} &= \sin(\alpha\beta_2 L)
\end{aligned}
\qquad \text{(A.19a-d)}
$$

where

$$
\beta_3 = \frac{\beta_1^2 + p_4}{\beta_1}, \quad \beta_4 = \frac{\beta_2^2 + p_4}{\beta_2} \qquad \text{(A.20a,b)}
$$

The stiffness matrix for the Bernoulli-Euler beam is recovered by setting the characteristic radius, r, to zero. Then, $p_1=p_4=0$, $p_2=p_3=1$, and $\beta_1=\beta_2=\beta_3=\beta_4=1$.

APPENDIX B: SIMULATION OF BEAM WITH CURVATURE ACTUATION

In this appendix, we extend the results of Section 5.1.2.3 to the case of a beam with a distributed curvature actuator. The modified equation of motion, expressed in the time-domian, is

$$\frac{\partial^2}{\partial x^2}\left[\eta(x)\frac{\partial^2}{\partial x^2}v(x,t)\right] + \frac{1}{\beta(x)}\frac{\partial^2}{\partial t^2}v(x,t) = \frac{\partial^2}{\partial x^2}m_u(x,t) + f_n(x,t) \tag{B.1}$$

which becomes, after Laplace transformation

$$\frac{\partial^2}{\partial x^2}\left[\eta(x)\frac{\partial^2}{\partial x^2}\bar{v}(x,s)\right] + \frac{1}{\beta(x)}\left[s^2\bar{v}(x,s) - s\,v_0(x) - \dot{v}_0(x)\right] = \frac{\partial^2}{\partial x^2}\bar{m}_u(x,s) + \bar{f}_n(x,s) \tag{B.2}$$

The assumed linear feedback control law is

$$m_u(x,t) = -\int_0^1 \left[k_1(x,y)\,\eta(y)\frac{\partial^2}{\partial y^2}v(y,t) + k_2(x,y)\frac{\partial}{\partial t}v(y,t)\right] dy \tag{B.3}$$

which transforms into

$$\bar{m}_u(x,s) = -\int_0^1 \left[k_1(x,y)\,\eta(y)\frac{\partial^2}{\partial y^2}\bar{v}(y,s) + k_2(x,y)\,s\,\bar{v}(y,s)\right] dy + \int_0^1 \left[k_2(x,y)\,v_0(y)\right] dy \tag{B.4}$$

Substituting this expression into Eq. (B.2) leads to

$$\frac{\partial^2}{\partial x^2}\left[\eta(x)\frac{\partial^2}{\partial x^2}\bar{v}(x,s)\right] + \frac{s^2}{\beta(x)}\bar{v}(x,s) + \frac{\partial^2}{\partial x^2}\left[\int_0^1 \left[k_1(x,y)\,\eta(y)\frac{\partial^2}{\partial y^2}\bar{v}(y,s) + s\,k_2(x,y)\,\bar{v}(y,s)\right] dy\right]$$
$$= \bar{f}_n(x,s) + \frac{1}{\beta(x)}\left[\dot{v}_0(x) + s\,v_0(x)\right] + \frac{\partial^2}{\partial x^2}\left[\int_0^1 k_2(x,y)\,v_0(y)\,dy\right] \tag{B.5}$$

Employing the same discretization technique used in Section 5.1.2.3, we obtain, for the finite-difference equation

$$\left[\frac{N^4}{s^2}DHD + s^2B + \frac{1}{N}DK(s)\right]\bar{v}(s) = \bar{f}_n(s) + \bar{f}_l(s) + N^2D\,\bar{f}_c(s) \quad \text{(B.6)}$$

All terms in this last equation are as defined in Section 5.1.2.3.

APPENDIX C: SIMULATION OF A TIMOSHENKO BEAM

In this appendix, we discuss the direct simulation of a Timoshenko beam. For simplicity, we will assumed that the initial conditions are zero and that the section properties are constant, although other situations can be treated in a manner similar to the Bernoulli-Euler beam model. The dimensional form of the equation of motion is

$$EI\frac{\partial^4}{\partial x_d^4}v_d(x_d,t_d) + \rho A\frac{\partial^2}{\partial t_d^2}v_d(x_d,t_d) - \rho I\left[1+\frac{Ek}{G}\right]\frac{\partial^4}{\partial x_d^2\partial t_d^2}v_d(x_d,t_d) + \frac{\rho^2 Ik}{G}\frac{\partial^4}{\partial t_d^4}v_d(x_d,t_d) = f_d(x,t) \qquad (C.1)$$

which can be normalized (using the same groupings as in Section 5.1.2.1) to

$$\frac{\partial^4}{\partial x^4}v(x,t) + \frac{\partial^2}{\partial t^2}v(x,t) - \alpha_I\left[1+\alpha_E\right]\frac{\partial^4}{\partial x^2\partial t^2}v(x,t) + \alpha_I^2\alpha_E\frac{\partial^4}{\partial t^4}v(x,t) = f(x,t) \qquad (C.2)$$

where

$$\alpha_I = \frac{I}{AL^2}, \quad \alpha_E = \frac{Ek}{G} \qquad (C.3a,b)$$

Taking the Laplace transform (neglecting initial conditions) yields

$$\frac{\partial^4}{\partial x^4}\tilde{v}(x,s) - \alpha_I\left[1+\alpha_E\right]s^2\frac{\partial^2}{\partial x^2}\tilde{v}(x,s) + s^2\tilde{v}(x,s) + \alpha_I^2\alpha_E s^4\tilde{v}(x,s) = \tilde{f}(x,s) \qquad (C.4)$$

Finally, the spatial discretization yields

$$\left[N^4 D^2 + s^2\left(I - \alpha_I(1+\alpha_E)N^2 D\right) + \alpha_I^2\alpha_E s^4 I\right]\tilde{v}(s) = \tilde{f}(s) \qquad (C.5)$$

APPENDIX D: OPTIMAL COSTS FOR DISTRIBUTED CONTROL SYSTEMS

This appendix discusses the computation of the optimal cost required to bring a distributed system to rest from an arbitrary initial condition using a distributed controller. We will restrict attention to the force actuation case, and we will assume uniform cross section properties. The formulation is analogous to the discrete case, for which the optimal cost is expressed by

$$J^* = \frac{1}{2} x_0^T S x_0 \tag{D.1}$$

where x_0 is the initial condition on the state vector and S is the Riccati matrix. Wang (1964) shows that, for the distributed case, the optimal cost has the form

$$J^* = \frac{1}{2} \int_0^1 \int_0^1 x_0(x)^T S(x,y) x_0(y)\, dx\, dy \tag{D.2}$$

where $x_0(x)$ is the distributed initial condition and S(x,y) is the Riccati matrix function associated with Eq. (6 19). Thus, for the case of an initial displacement, $v_0(x)=\sin(2\pi x)$, the optimal cost is

$$J^* = \frac{1}{2} \int_0^1 \int_0^1 \frac{\partial^2}{\partial x^2} v_0(x)\; S_{11}(x,y)\; \frac{\partial^2}{\partial x^2} v_0(y)\, dx\, dy$$

$$= 8\pi^4 \int_0^1 \int_0^1 \sin(2\pi x)\; S_{11}(x,y)\; \sin(2\pi y)\, dx\, dy \tag{D.3}$$

The Riccati equations for $S_{11}(x,y)$ follow directly from Eq. (6.25). For constant section properties, they are given by

$$\frac{\partial^2}{\partial x^2} S_{11}(x,y) - \frac{\partial^2}{\partial y^2} S_{22}(x,y) - \frac{1}{r}\int_0^1 S_{22}(x,z) S_{12}(z,y)\, dz = 0 \qquad \text{(D.4a)}$$

$$-\frac{\partial^2}{\partial x^2} S_{22}(x,y) + \frac{\partial^2}{\partial y^2} S_{11}(x,y) - \frac{1}{r}\int_0^1 S_{22}(x,z) S_{12}(z,y)\, dz = 0 \qquad \text{(D.4b)}$$

Adding these two equations yields

$$\nabla^2 S_{11}(x,y) = \nabla^2 S_{22}(x,y) + \frac{1}{r}\int_0^1 \left[S_{22}(x,z) S_{12}(z,y) + S_{12}(x,z) S_{22}(z,y) \right] dz \qquad \text{(D.5)}$$

Thus, S_{11} is computed using a simple relaxation algorithm. For the case of an initial velocity, $\dot{v}_0(x)=\delta(x-1/2)$, which is equivalent to a center-span impulse, the cost is simply

$$J^* = \frac{1}{2}\int_0^1\int_0^1 \dot{v}_0(x)\, S_{22}(x,y)\, \dot{v}_0(y)\, dx\, dy = \frac{1}{2} S_{22}(1/2,1/2) \qquad \text{(D.6)}$$

REFERENCES

Aubrun, J.N., 1980, "Theory of the Control of Structures by Low-Authority Controllers," *AIAA J. Guidance, Control and Dynamics*, V5, #3, pp. 444-451.

Bagley, R.L., and Torvik, P.J., 1983, "Fractional Calculus - A Different Approach to the Analysis of Viscoelastically Damped Structures," *AIAA Journal*, V21, #5, pp. 741-748.

Bailey, T.L., 1984, "Distributed-Parameter Vibration Control of a Cantilever Beam Using a Distributed-Parameter Actuator," M.S. Thesis, Massachusetts Institute of Technology, Cambridge, MA.

Balas, M.J., 1978, "Feedback Control of Flexible Systems," *IEEE Trans. Automatic Control*, V AC-23, #4, pp. 673-679.

Balas, M.J., 1982, "Toward a More Practical Control Theory for Distributed Parameter Systems," *Control and Dynamic Systems: Advances in Theory and Applications*, V18, Academic Press, N.Y., pp. 361-421.

Bernstein, D.S., and Hyland, D.C., 1986, "The Optimal Projection Equations for Finite-Dimensional Fixed-Order Dynamic Compensation of Infinite-Dimensional Systems," *SIAM J. Control and Optimization*, V24, #1, pp. 122 151.

Bernstein, D.S., and Hyland, D.C., 1990, "Optimal Projection Approach to Robust Fixed-Structure Control Design," *Mechanics and Control of Large Flexible Structures*, J.L. Junkins, ed , AIAA, Washington, D.C., pp. 237-293.

Breakwell, J.A., 1964, "Optimal Control of Distributed Systems," *J. of the Astronautical Sciences*, V29, #4, pp. 343-372.

Brogan, W.L., 1968, "Optimal Control Theory Applied to Systems Described by Partial Differential Equations," *Advances in Control Systems*, V6, Academic Press, N.Y., pp. 221-316.

Butkovskii, A.G. and Lerner, A.Y., 1960, *Automation Remote Control*, V21, p. 472.

Chun, H.M., Turner, J.D., and Frisch, H.P., 1991, "A Recursive Order-N Formulation for DISCOS with Topological Loops and Intermittent Surface Contact," Paper AAS 91-454, AAS/AIAA Astrodynamics Specialist Conference, Durango, Colorado, August 19-22.

Cooley, J.W., Lewis, P.A.W., and Welch, P.D., 1970, "The Fast Fourier Transform Algorithm: Programming Considerations in the Calculation of Sine, Cosine and Laplace Transforms," *J. Sound and Vibration*, V12, #3, pp. 315-337.

Davies, B., and Martin, B., 1979, "Numerical Inversion of the Laplace Transform: a Survey and Comparison of Methods," *J. Computational Physics*, V33, pp. 1-32.

deLuis, J., 1989, "Design and Implementation of Optimal Controllers for Intelligent Structures Using Infinite Order Structural Models," Ph.D. Thesis, Massachusetts Institute of Technology, Cambridge, MA.

Doyle, J.C., et al, 1989, "State-Space Solutions to Standard H2 and H∞ Control Problems," *IEEE Trans. Automatic Control*, V AC-34, #8, pp. 831-847.

Francis, B.A., 1987, *A Course in H∞ Control Theory*, Springer-Verlag, New York, NY.

Gibson, J S., 1979, "The Riccati Integral Equations for Optimal Control Problems on Hilbert Spaces," *SIAM J. Control and Optimization*, V17, #4, p. 537-565.

Gupta, N.K., Lyons, M.G., Aubrun, J.N., and Margulies, G., 1981, "Modelling, Control and System Identification Methods for Flexible Structures," NATO document, AGARDograph-AG-260.

Hughes, P.C., and MacTavish, D.J., 1989, "Dynamics Modelling of Viscoelastic Space Structures," *Proc. ESTEC Workshop on Modal Representation of Flexible Structures by Continuum Methods*, Noordwijk, The Netherlands, June 15-16, pp. 193-215.

Juang, J.N. and Dwyer, T.A.W., 1983, "First Order Solution of the Optimal Regulator Problem for a Distributed Parameter Elastic System," *J. of the Astronautical Sciences*, V31, #3, pp. 429-439.

Kosut, R.L., 1970, "Suboptimal Control of Linear Time-Invariant Systems Subject to Control Structure Constraints," *IEEE Trans. Automatic Control*, V AC-15, #5, pp. 557-563.

Kulla, P.H., 1990, *Dynamic Stiffness of Rectangular Plates*, Final Report, ESTEC Contract 7814/88/NL/JG(SC), RESSULT, Research and Consulting.

Lanczos, 1957, *Applied Analysis*, Putman, London.

Levine, W.S., Johnson, T.L., and Athans, M., 1971, "Optimal Limited State Variable Feedback Controllers for Linear Systems," *IEEE Trans. Automatic Control*, V AC-16, #6, pp.785-793.

Lions, J.L., 1971, *Optimal Control of Systems Governed by Partial Differential Equations*, Springer-Verlag, N.Y..

Lupi, V.D., Chun, H.M., and Turner, J.D., 1990, "Transform Methods for Precision Continuum and Control Models of Flexible Space Structures," *Proc. AIAA/AAS Astrodynamics Conf.*, Portland, OR, August 20-22, pp. 680-689.

Lupi, V., Chun, H., and Turner, J., 1991a, "Distributed Control and Simulation of a Bernoulli-Euler Beam," submitted to the *J. Guidance, Control and Dynamics*.

Lupi, V.D., Chun, H.M., and Turner, J.D., 1991b, "Dynamic Stiffness Formulation for Plane Stress Elements using a Frequency Dependent Stress Function," to appear in the *J. Appl. Mech.*

MacMartin, D.G., and Hall, S.R., 1990, "An H∞ Power Flow Approach to Control of Uncertain Structures," *Proc. American Controls Conference*, San Diego, CA, May 23-25, pp. 3073-3080.

Miller, D.W., and Hall, S.R., 1991, "Experimental Results Using Active Control of Travelling Wave Power Flow," *AIAA J. Guidance, Control and Dynamics*, V14, #2, pp. 350-358.

Nowacki, W., 1963, *Dynamics of Elastic Systems*, John Wiley & Sons, Inc., N.Y.

Piché, R.A., 1986a, "Analysis of Structural Control Problems Using Frequency-Domain Continuum Methods," PhD Thesis, Univ. of Waterloo, Waterloo, Ontario, pp. 48-52.

Piché, R.A., 1986b, "Analysis of Structural Control Problems Using Frequency-Domain Continuum Methods," PhD Thesis, Univ. of Waterloo, Waterloo, Ontario, pp. 197-214.

Plunkett, R., and Lee, C.T., 1970, "Length Optimization for Constrained Viscoelastic Layer Damping," *J. Acoustical Society of America*; V48, #1, pp. 150-161.

Press, W.H., Flannery, B.P., Teukolsky, S.A., and Vetterling, W.T., 1986, *Numerical Recipes*, Cambridge Univ. Press, N.Y.

Richtmyer, R.D., 1957, *Difference Methods for Initial Value Problems*, Wiley (Inter-Science), N.Y.

Schaechter, D.B., 1982, "Estimation of Distributed Parameter Systems," *J. Guidance and Control*, V5, #1, pp. 22-26.

Singer, N.C., and Seering, W.P., 1990, "Preshaping Command Inputs to Reduce System Vibration," *J. Dynamic Systems, Measurement and Control*, V112, pp. 76-82.

Skaar, S.B., 1984, "Closed Form Optimal Control Solutions for Continuous Linear Elastic Systems," *Journal of the Astronautical Sciences*, V32, #4, pp. 447-461.

Taylor, L.W., and Balakrishnon, A.V., 1986, "A Mathematical Problem and a Spacecraft Control Laboratory Experiment (SCOLE) Used to Evaluate Control Laws for Flexible Spacecraft .... NASA/IEEE Design Challenge," NASA Technical Memorandum 89075, Nov. 17-18, pp. 386-412.

Tzafestas, S.G. and Nightingale, J.M., 1970, "Optimal Distributed Parameter Control Using Classical Variational Calculus," *Int. J. Control*, V12, #4, pp. 593-608.

Wang, P.C., 1964, "Control of Distributed Parameter Systems," *Advances in Control Systems*, V1, Academic Press, N.Y., pp. 75-172.

Weeks, W.T., 1966, "Numerical Inversion of Laplace Transforms Using Laguerre Functions," *J. of the Assoc. for Comp. Mach.*, V13, #3, pp. 419-426.

Wilcox, D.J., 1978, "Numerical Laplace Transform and Inversion," *Int. J. Elec. Eng. Education*, V15; pp. 246-265.

Williams, F.W., and Wittrick, W.H., "Exact Buckling and Frequency Calculations Surveyed," *J. Structural Engineering*, V109, #1, pp. 169-187.

Wing, O., 1967, "An Efficient Method of Numerical Inversion of Laplace Trransforms," *Computing*, V2, #2, pp. 153-166.

Wittrick, W.H. and Williams, F.W., 1971, "A General Algorithm for Computing Natural Frequencies of Elastic Structures," *Quarterly Journal of Mechanics and Applied Mathematics*, V24, #3, pp. 263-284.

Yousuff, A., and Skelton, R.E., 1984, "Controller Reduction by Component Cost Analysis," *IEEE Trans. Automatic Control*, V AC-29, #6, pp. 520-530.

Zambettakis, I., Duaphin-Tanguy, G., and Rotella, F., 1989, "An Analytical Approach of Optimal Control for Multi-Scale Distributed Parameter Systems," *IFAC Control of Distributed Parameter Systems*, Perpignan, France, pp. 295-301.